ISTANBUL TECHNICAL UNIVERSITY ★ GRADUATE SCHOOL

MODELLING AND ANALYSIS OF GYROSCOPIC EFFECTS IN UNDAMPED ROTATING SYSTEMS

M.Sc. THESIS

Abdülsamet ERKAN

Department of Mechanical Engineering

Machine Dynamics, Vibrations and Acoustics Programme

MAY 2023

ISTANBUL TECHNICAL UNIVERSITY ★ GRADUATE SCHOOL

MODELLING AND ANALYSIS OF GYROSCOPIC EFFECTS IN UNDAMPED ROTATING SYSTEMS

M.Sc. THESIS

Abdülsamet ERKAN
(503201402)

Department of Mechanical Engineering

Machine Dynamics, Vibrations and Acoustics Programme

Thesis Advisor: Prof. Dr. Kenan Yüce ŞANLITÜRK
Thesis Co-Advisor: Prof. Dr. Hasan KÖRÜK

MAY 2023

İSTANBUL TEKNİK ÜNİVERSİTESİ ★ LİSANSÜSTÜ EĞİTİM ENSTİTÜSÜ

DÖNEN SÖNÜMSÜZ SİSTEMLERDE JİROSKOPİK ETKİLERİN MODELLENMESİ VE ANALİZİ

YÜKSEK LİSANS TEZİ

Abdülsamet ERKAN
(503201402)

Makina Mühendisliği Anabilim Dalı

Makina Dinamiği, Titreşim ve Akustik Programı

Tez Danışmanı: Prof. Dr. Kenan Yüce ŞANLITÜRK
Eş Danışman: Prof. Dr. Hasan KÖRÜK

MAYIS 2023

Abdülsamet ERKAN, a M.Sc. student of ITU Graduate School student ID 503201402 successfully defended the thesis entitled “MODELLING AND ANALYSIS OF GYROSCOPIC EFFECTS IN UNDAMPED ROTATING SYSTEMS”, which he prepared after fulfilling the requirements specified in the associated legislations, before the jury whose signatures are below.

Thesis Advisor : **Prof. Dr. Kenan Yüce ŞANLITÜRK** ....
Istanbul Technical University

Co-advisor : **Prof. Dr. Hasan KÖRÜK** ....
MEF University

Jury Members : **Prof. Dr. Vahit MERMERTAŞ** ....
Istanbul Technical University

Prof. Dr. Erdinç ALTUĞ ....
Istanbul Technical University

Prof. Dr. Orhan ÇAKAR ....
Firat University

Date of Submission : 08 May 2023

Date of Defense : 29 May 2023

Dedicated to my dearest mom and dad,

FOREWORD

I would like to express my deepest gratitude to my advisors Prof. Dr. Kenan Yüce Şanlıtürk and Prof. Dr. Hasan Körük. This long and hard journey has been a precious experience for me with their unique support, valuable advice, endless patience and understanding. It was an honour and a privilege for me to work with them. Additionally, I am thankful to them for introducing me to the fascinating world of rotor dynamics.

I present my heartfelt thanks to my beloved family and dedicate this study to them. Their unwavering support, love and faith in me have always been an inspiration and motivation throughout my life, and I am deeply grateful for their sacrifices, patience, and understanding.

May 2023

Abdülsamet ERKAN

(Mechanical Engineer)

TABLE OF CONTENTS

Page

ABBREVIATIONS

FEM	**:** Finite element method
FEA	**:** Finite element analysis
DOF	**:** Degree of freedom
RotFE	**:** Rotor dynamics toolbox
RPM	**:** Revolutions per minute
ND	**:** Nodal diameter
NC	**:** Nodal circle
MAC	**:** Modal assurance criterion

SYMBOLS

$\boldsymbol{\Omega}$	: Rotational speed
$\vec{\boldsymbol{\Omega}}, \{\boldsymbol{\Omega}\}$	: Rotational speed vectors
$[\boldsymbol{S}]$	: Rotational speed matrix
$\boldsymbol{XYZ}$	: Global coordinate system
$\boldsymbol{x_s y_s z_s}$	: Stationary coordinate system
$\boldsymbol{x_r y_r z_r}$	: Rotating coordinate system
$\boldsymbol{x_d y_d z_d}$	: Dynamic coordinate system
$\boldsymbol{\overline{x}\overline{y}\overline{z}}$	: Local coordinate system
$\boldsymbol{x_0 y_0 z_0}$	: Coordinate system on a cross-section along the beam element
$\boldsymbol{x_1 y_1 z_1}$	: Coordinate system after the first angular deformation
$\boldsymbol{x_2 y_2 z_2}$	: Coordinate system after the second angular deformation
$\boldsymbol{x_3 y_3 z_3}$	: Coordinate system after the third angular deformation
$\boldsymbol{\rho}, \boldsymbol{m}, \boldsymbol{V}$	: Density, mass and volume
$\boldsymbol{\phi}$	: Transverse shear effect parameter
$\boldsymbol{\kappa}$	: Shear correction factor
$\boldsymbol{E}, \boldsymbol{G}$	: Young’s and shear modulus
$\boldsymbol{A}$	: Area
$\boldsymbol{l}$	: Length of beam element
$\boldsymbol{I_p}$	: Polar area moment of inertia
$\boldsymbol{I_x}, \boldsymbol{I_y}, \boldsymbol{I_d}$	: Area moments of inertia (in the symmetric case $I_d = I_x = I_y$)
$\boldsymbol{H}, \vec{\boldsymbol{H}}$	: Angular momentum and angular momentum vector
$\boldsymbol{J_p}$	: Polar mass moment of inertia
$\boldsymbol{J_x}, \boldsymbol{J_y}, \boldsymbol{J_d}$	: Mass moments of inertia (in the symmetric case $J_d = J_x = J_y$)
$\boldsymbol{u}, \boldsymbol{v}, \boldsymbol{w}$	: Translational deformations
$\boldsymbol{\theta}, \boldsymbol{\psi}, \boldsymbol{\varphi}$	: Angular deformations
$\boldsymbol{M_x}, \boldsymbol{M_y}$	: Gyroscopic moments around x_s and y_s axes
$\vec{\boldsymbol{r}}$	: Position vector with respect to rotating reference frame
$\{\boldsymbol{R}\}$	: Position vector with respect to stationary reference frame

$\{\boldsymbol{R_0}\}$	: Position of rotating reference frame with respect to stationary reference frame
$\{\boldsymbol{r_0}\}$	: Position vector of point P_0 with respect to the rotating coordinate system
$\{\boldsymbol{u_r}\}$	: Elastic deformation vector defined in rotating reference frame
$\vec{\boldsymbol{v}}_{\boldsymbol{s}}$	: Velocity vector with respect to stationary reference frame
$\vec{\boldsymbol{v}}_{\boldsymbol{r}}$	: Velocity vector with respect to rotating reference frame
$\vec{\boldsymbol{v}}_{\boldsymbol{tan}}$	: Tangential velocity vector
$\vec{\boldsymbol{a}}_{\boldsymbol{s}}$	: Acceleration vector with respect to stationary reference frame
$\vec{\boldsymbol{a}}_{\boldsymbol{r}}$	: Acceleration vector with respect to rotating reference frame
$\vec{\boldsymbol{F}}_{\boldsymbol{s}}$	: Forces in stationary reference frame
$\vec{\boldsymbol{F}}_{\boldsymbol{cor,1}}, \vec{\boldsymbol{F}}_{\boldsymbol{cor,2}}$	: Coriolis force vectors generated by the first and second quadrants
$\vec{\boldsymbol{F}}_{\boldsymbol{cor,3}}, \vec{\boldsymbol{F}}_{\boldsymbol{cor,4}}$	: Coriolis force vectors generated by the third and fourth quadrants
$[\boldsymbol{N}]$	: Shape function matrix
$\{\boldsymbol{q_r}\}$	: Generalised coordinates in rotating reference frame
$\{\boldsymbol{q_s}\}$	: Generalised coordinates in stationary reference frame
$\{\boldsymbol{\varepsilon}\}$	: Strain vector
$[\boldsymbol{B}]$	: Matrix containing the shape functions' space derivatives
$\{\boldsymbol{\sigma}\}$	: Stress vector
$[\boldsymbol{E}]$	: Constitutive matrix
$\boldsymbol{U}, \boldsymbol{T}$	: Potential and kinetic energies
$[\boldsymbol{M}]$	: Mass matrix
$[\boldsymbol{G}]$	: Gyroscopic matrix
$[\boldsymbol{K}]$	: Structural stiffness matrix
$[\boldsymbol{K_{soft}}]$	: Spin softening matrix
$[\widehat{\boldsymbol{K}}]$	: General stiffness matrix
$\boldsymbol{f_{rot}}, \boldsymbol{f_{stat}}$	: Frequency (Hz) in rotating and stationary reference frames
$\boldsymbol{\zeta}$	: Dimensionless coordinate
$\boldsymbol{\xi}, \boldsymbol{\eta}, \boldsymbol{\zeta}$	: Natural coordinates

LIST OF TABLES

Page

LIST OF FIGURES

Page

MODELLING AND ANALYSIS OF GYROSCOPIC EFFECTS IN UNDAMPED ROTATING SYSTEMS

SUMMARY

The gyroscopic effect has always been an interesting phenomenon in the field of rotor dynamics owing to its unique and complicated results on the dynamics of rotating systems. The finite element method is commonly used in this field to model and analyse this effect. This method is based on developing discrete mathematical models of rotating finite elements and using them to discretise rotating structures. Structures with complex geometries are usually discretised using finite solid or shell elements while simpler systems composing of flexible shaft and rigid discs or isolated blades are discretised using finite beam elements. Despite the accuracy provided by solid/shell elements for complex structures, the requirement of significant modelling and computational effort becomes a drawback for this modelling technique. On the contrary, for simpler structures, beam elements provide satisfactorily accurate results with relatively less effort put into the modelling and computation stages. Using these relatively simpler models, the gyroscopic effects generated by the flexible rotating structures can be modelled and the outcomes of this phenomenon on the dynamics of a rotor can be investigated effectively.

In this thesis, it is aimed to include the gyroscopic effects in the models of rotating flexible shaft-disc-blade systems and analyse the results using finite beam elements. Besides the conventional beam element model of rotating shafts and blades, a flexible disc structure in the form of a so-called spiderweb is proposed. By doing so, a fully flexible rotating shaft-disc-blade system's dynamics under the gyroscopic influence is examined with relatively less degrees of freedom. Moreover, the effects of disc and blade flexibility on the dynamics are discussed using the proposed disc model. Considering the lack of capabilities of some popular computer programs for modelling the gyroscopic effects of rotating beam elements, it is also aimed to contribute to this field with the models presented throughout this thesis.

A comprehensive literature survey summarises the development of the rotor dynamics field over the years and reveals modern studies' focal points in the dynamics of rotating systems and the methods they employ. Furthermore, the place and the importance of the gyroscopic effects and finite element method in the literature is emphasised.

The gyroscopic effect is caused by the gyroscopic moments in stationary reference frame, or the Coriolis forces in rotating reference frame. Although at first glance they seem different, they are directly related to each other over the Coriolis acceleration. It is noticed that the relation between these two cases is not sufficiently explained in the the rotor dynamics literature, therefore, the generation of the gyroscopic moments and the Coriolis forces, as well as the relation between these two is explained and clarified in some detail in the second chapter of the thesis.

The gyroscopic effect's distinctive feature is its ability to generate complicated results on the dynamic behaviour of rotating objects. The gyroscopic effect is a speed-dependent phenomenon and causes the system's dynamics to change with changing rotational speed. This leads to the natural frequencies of the system to become speed-dependent as well. Some mode shapes, can also be highly influenced by the gyroscopic effects. Therefore, the gyroscopic effects necessitate to carry out the analyses at a range of rotational speeds. The gyroscopic effect introduces complexity to the mode shapes of rotating systems, which in return manifests itself as whirling motion of shafts and occurrence of travelling waves on discs. With these radical changes in the dynamics of rotors, the gyroscopic effect is accepted to be crucial to be accounted for in modelling and analysis of rotating structures.

In the modelling stage, first, the conventionel model of flexible shaft-rigid disc system is presented. The flexible shaft is discretised using Timoshenko beam elements with 8 degrees of freedom. The dynamics of these elements, as well as the rigid disc's, are expressed in stationary reference frame while taking the gyroscopic effects caused by the gyroscopic moments into account. Later, a more general Timoshenko beam element with 12 degrees of freedom is presented. This element is used to discretise flexible shaft-disc-blade system. Due to the nonaxissymmetric geometry of the system, the modelling is carried out in rotating reference frame. Therefore, the gyroscopic effect is taken into account by modelling the Coriolis forces. Owing to the orientation difference between a shaft and a blade with respect to the axis of rotation, separate beam element models are presented and used for modelling shafts and blades. Although the formulation of structural stiffness and mass matrices are the same, the gyroscopic and spin softening matrices differ between the shaft and the blade elements.

In order to account for the disc flexibility, a special disc model in the form of a so-called spiderweb is presented. This structure is composed of radial and connecting elements, both of which use the same mathematical model with the blade elements. Finally, an 8-noded isoparametric hexahedral solid element and the derivation of its matrices are presented.

With the models developed, a flexibe shaft-rigid disc system's dynamics is analysed first. The free vibration problem of the system is solved at different rotational speeds, and the natural frequencies and mode shapes are predicted. The gyroscopic effect is observed to vary with the order of the shaft's bending vibrations. As expected, depending on the location of the disc on the shaft, some modes experience strong gyroscopic effect generated by the disc. It is seen that the natural frequencies split almost linearly with increasing rotational speed, and there, naturally, occurs no shaft-disc interactions because of the disc's rigidity.

With the intention to investigate the gyroscopic effects in rotors, flexible shaft-flexible disc system, flexible shaft-disc-blade system and flexible bladed disc systems are also analysed. In these models, the so-called spiderweb disc is used to model a flexible disc, and the blades are intentionally oriented perpendicular to the disc in order to enchance the gyroscopic coupling in rotating reference frame. The natural frequencies in rotating reference frame and the mode shapes of the systems are predicted at different rotational speeds. Accordingly, Campbell diagrams are utilised to present the natural frequencies as a function of rotational speed. When the blades are attached, it is seen that the system dynamics gets tremendously complicated. The complex mode shapes of the shaft and the disc are presented by visualising the vibration patterns of the nodes on the bodies in various modes. It is seen that the spiderweb disc is capable of exhibiting the occurance of travelling waves on the disc.

Taking the disc's flexibility into account is found to be essential in order to be able to predict shaft-disc interactions and the so-called veering phenomenon in several mode shapes of different systems. Moreover, with the proposed model, a merging type of instability is predicted in a flexible shaft-disc-blade system.

Following the analyses of rotor models using beam finite elements, a solid bladed disc model is developed using 8-noded solid elements. The results of this model are used to predict how a solid bladed disc system behaves under the rotational effects. Then, the results are compared with those corresponding to previous systems modelled using beam elements. It is found that both types of models yield quite similar results in terms of the frequency splits caused by the gyroscopic effect, spin softening effect in blade dominated modes and the occurance of travelling waves on the disc.

This thesis investigated the complicated and interesing nature of the gyroscopic effects in rotating systems using various models based on the finite element approach. Besides the gyroscopic effect's generation mechanism, the relationship between the gyroscopic moments in stationary reference frame and the Coriolis forces in rotating reference frame are explained in some detail. By proposing a spiderweb disc structure discretised using finite beam elements, a cost-effective model of flexible shaft-disc-blade system is obtained. It is concluded that this system can provide accurate results and insight into the dynamics of rotating simplified shaft-disc-blade systems which can be highly influenced by rotational effects such as the gyroscopic effects.

DÖNEN SÖNÜMSÜZ SİSTEMLERDE JİROSKOPİK ETKİLERİN MODELLENMESİ VE ANALİZİ

ÖZET

Jiroskopik etkiler, sistemlerde dönüşten meydana gelen bir fenomen olarak, kendine has oluşum mekanizması ve sistemlerin dinamiğinde meydana getirdiği karmaşık sonuçlar sebebiyle rotor dinamiği alanında üzerinde durulan konulardan biri olmuştur. Jiroskopik etkilerin modellenmesinde ve analizinde sonlu elemanlar yöntemi ise sıklıkla kullanılan etkili bir yöntemdir. Sonlu elemanlar yöntemiyle, dönen sonlu elemanların matematik modelleri oluşturulur ve bu elemanlar dönen sistemlerin ayrıklaştırılmasında kullanılır. Literatürde, kompleks geometriye sahip dönen yapılar katı ve kabuk elemanlar kullanılarak ayrıklaştırılırken, esnek şaft-rijit disk veya tekil kanatçık gibi çok daha basit yapılar için ise kiriş elemanlar tercih edilmektedir. Katı ve kabuk elemanlarla modelleme, kompleks yapılar için oldukça doğru sonuçlar sunsa da bunun karşılığında modelleme ve hesaplama adımlarında oldukça fazla emek ve zaman gerektirmektedir. Ayrıca bu işlemleri gerçekleştirecek bilgisayarların da hafıza bakımından yeterli kapasiteye sahip olmaları gerektiği aşikardır. Buna karşın kiriş elemanlı modelleme, görece daha az serbestlik derecesiyle basitleştirilmiş dönen sistemleri modelleme imkanı sunması sayesinde rotor dinamiği analizlerinde azımsanamaz kolaylıklar sağlamaktadır. Bu basitleştirilmiş modeller kullanılarak dönen esnek yapılar tarafından üretilen jiroskopik etkilerin rotorun dinamiğinde meydana getirdiği sonuçları incemek mümkündür.

Bu tez çalışmasında, literatürde sıklıkla incelenen esnek şaft-disk-kanatçık sistemlerinde jiroskopik etkilerin sonlu kiriş elemanlar kullanılarak modellenmesi ve analizi hedeflenmiştir. Bu amaç doğrultusunda, geleneksel kiriş elemanlı şaft ve kanatçık modellerinin sunulmasının yanı sıra, esnek bir diskin kiriş elemanlar kullanılarak bir örümcek ağı yapısında modellenmesi önerilmiştir. Bu sayede, tamamen esnek olan döner bir şaft-disk-kanatçık sisteminin jiroskopik etkiler altındaki dinamik davranışının görece daha az serbestlik derecesiyle incelenmesi sağlanmıştır. Bu incelemenin yanında esnek disk ve kanatçıkların da rotorun dinamiğindeki rolü gözler önüne serilmiştir. Ayrıca, ilgili bazı popüler bilgisayar programlarının, dönen kiriş elemanların jiroskopik etkilerini modelleme kabiliyetlerindeki kısıtlar göz önüne alındığında, çalışma boyunca sunulacak modellerle bu altyapının da geliştirilmesi amaçlanmıştır.

Çalışma içerisinde sunulan kapsamlı bir literatür taramasıyla, rotor dinamiği alanının yıllar boyunca gelişimi özetlenmiş ve modern çalışmaların dönen sistemlerin dinamiğindeki odak noktaları ve çözüme ulaşmak için uyguladıkları yöntemler aktarılmıştır. Bunun yanı sıra, rotor dinamiği alanında jiroskopik etkilerin ve sonlu elemanlar yönteminin yeri ve önemi de vurgulanmıştır.

Çalışmada öncelikle jiroskopik etkilerin oluşumu açıklanmıştır. Jiroskopik etkiler, sabit koordinat sisteminde jiroskopik momentlerin bir sonucu olarak meydana gelmektedirler. Dönen koordinat sisteminde ise jiroskopik etkiler Coriolis

kuvvetlerinin oluşumundan meydana gelmektedir. Literatürdeki birçok kaynak, sistemleri yalnızca tek bir referans koordinat sisteminde ele almışlardır. Bu sebeple jiroskopik momentler ve Coriolis kuvvetleri arasındaki ilişkiden rotor dinamiği literatüründe pek de bahsedilmediği kanısına varılmıştır. Bu çalışmada, Coriolis ivmesi üzerinden, jiroskopik momentlerin ve Coriolis kuvvetlerinin oluşum mekanizmaları türetilerek bu iki fenomenin birbiriyle olan ilişkisi açıklığa kavuşturulmuştur. Böylece, ele alınan sistemlerin dinamik davranışlarının her iki referans koordinat sisteminde daha anlamlı bir şekilde incelenebilmesi hedeflenmiştir.

Jiroskopik etkilerin dönen sistemlerin analizinde hesaba katılması, meydana getirdiği sonuçlar sebebiyle büyük önem arz etmektedir. Bu önemli sonuçlarından biri jiroskopik etkinin doğrudan rotorun dönüş hızına bağlı olmasıdır. Artan dönüş hızıyla daha etkin hale gelen jiroskopik etki, sistemlerin bazı modlarının frekanslarını çok belirgin şekilde değiştirebilmektedir. Dolayısıyla sistemlerin dinamiği de dönüş hızına bağlı olmaktadır ve çeşitli dönüş hızlarında analizlerin gerçekleştirilmesi zorunlu hale gelmektedir. Bu çalışmada dönen sistemlerin doğal frekanslarını dönüş hızının bir fonksiyonu olarak inceleyebilmek için Campbell diyagramları kullanılmıştır.

Jiroskopik etkiler yalnızca sistemin doğal frekanslarını değil aynı zamanda mod şekillerini de etkilemektedir. Döner bir sistemin mod şekilleri jiroskopik etkiyle birlikte kompleks hale gelir. Bu kompleks mod şekilleri şaftın dolanım (whirl) hareketi yapması olarak kendini gösterirken, disk üzerinde hareket eden dalgalar olarak belirir.

Dönen sistemlerde jiroskopik etkinin modellenmesi için kullanılan sonlu kiriş elemanlar, Timoshenko kiriş teorisi kapsamında ele alınmıştır. Öncelikle 8 serbestlik dereceli Timoshenko kiriş elemanlarıyla esnek bir şaft modellenerek literatürde uzun süredir var olan bir model olan esnek şaft-rijit disk sistemi oluşturulmuştur. Bu sistem sabit koordinat sisteminde incelenmiş ve dolayısıyla şaftın ve rijit diskin oluşturduğu jiroskopik momentler modele dahil edilmiştir.

Daha sonrasında ise 12 serbestlik dereceli sonlu kiriş eleman sunularak daha gelişmiş bir model olan esnek şaft-disk-kanatçık sisteminin elemanları modellenmiştir. Bu sistemin dönüş ekseni etrafında eksenel simetriye sahip olmaması sebebiyle tüm elemanlar dönen referans sisteminde ele alınmışlardır. Dolayısıyla bu modelde elemanların meydana getirdiği jiroskopik etkiler, Coriolis kuvvetlerinin oluşumu üzerinden modele dahil edilmiştir. Kiriş elemanlardan oluşan şaftın ve kanatçığın dönüş eksenine göre oryantasyonlarının farklı olması sebebiyle bu iki elemanı oluşturan kiriş elemanların jiroskopi ve dönüş kaynaklı esnekleşme matrisleri birbirlerinden farklılık göstermektedir.

Diskin de esnekliğini modellere dahil edebilmek üzere örümcek ağı şeklinde ve tamamen kiriş elemanlardan oluşan bir yapı önerilmiştir. Bu disk radyal ve bağlantı elemanları olarak isimlendirilen iki tip elemandan oluşmaktadır. Her iki tip elemanın modelinde de kanatçıklarla aynı matematik model kullanılmaktadır. Son olarak da izoparametrik 8 düğüm noktalı lineer bir katı eleman tanıtılmış ve ilgili matrislerinin türetilmesinden bahsedilmiştir.

Geliştirilen kabiliyetlerle öncelikle rotor dinamiğindeki en temel sistemlerden biri olan esnek şaft-rijit disk sisteminin dinamik davranışı analiz edilmiştir. Belirli dönüş hızlarında gerçekleştirilen analizlerle birlikte bir Campbell diyagramı oluşturulmuş ve çeşitli şaft eğilme modlarının artan hızla birlikte sabit koordinat sistemindeki doğal frekanslarının değişimi gözlemlenmiştir. Diyagram incelendiğinde artan eğilme modlarıyla birlikte jiroskopik etki kaynaklı frekans ayrılmalarının daha da arttığı tespit edilmiştir. Bunun yanında, böyle bir modelde rijit disk, ataletsel özellikleri sebebiyle, şafta kıyasla daha belirgin jiroskopik etkiler meydana getirebilmektedir. Aynı zamanda diskin konumu da bazı modların jiroskopik etkiden daha fazla etkilenmesine sebep olmaktadır. Bu durum, çalışma içerisinde bazı mod şekillerinin sunulmasıyla incelenmiştir. Frekansların artan hızla birlikte oldukça lineer bir şekilde değişmesi ve modlar arasında hiçbir etkileşimin tespit edilmemiş olması, rijit disk varsayımının oldukça basitleştirilmiş bir sistem meydana getirdiğini ortaya koymaktadır. Bu varsayım bazı sistemlerde oldukça isabetli sonuçlar verse de kimi mühendislik uygulamalarında kullanılan daha esnek ve hafif disklerin dinamik davranışlarını ve esnek şaft-esnek disk etkileşimlerini modellemekte yetersiz kalabilmektedir.

Esnek bir diskin dönen bir sistemin dinamiğindeki rolünü anlamak için bu tezde önerilen örümcek ağı yapısındaki esnek disk kullanılmıştır. Önceki modeldeki rijit diskle aynı kütleye ve geometrik özelliklere sahip bir esnek disk oluşturularak ataletsel özellikleri denkleştirilmiştir. Tamamen kiriş elemanlardan oluşan esnek şaft-esnek disk sistemi belirli dönüş hızlarında analiz edilmiş ve bir Campbell diyagramı dönen koordinat sisteminde elde edilmiştir. Diskin de esnek olarak ele alınmasıyla artık modlar yalnızca şaft eğilme modları olmaktan çıkmış, yalın disk modları ve şaft-disk modları da gözlemlenir hale gelmiştir.

Doğal frekanslar incelendiğinde, dönen koordinat sisteminde, şaftın belirgin titreşimler gerçekleştirdiği modlarda jiroskopik etki de belirginken, diskin baskın olduğu modlarda jiroskopik etki daha zayıf görülmüştür. Dönen koordinat sisteminde bu durumun Coriolis kuvvetlerinin oluşum mekanizmasıyla tutarlılık içinde olduğu görülmüştür. Problemin sonuçlarını bir de sabit koordinat sisteminde incelemek için bir transformasyon gerçekleştirilmiş ve jiroskopik moment kaynaklı jiroskopik etkiler bu referans çerçevesinde kısaca tekrar analiz edilmiştir.

Diskin esnek hale gelmesiyle birlikte modlar arasında etkileşimler de meydana gelmiştir. Literatürde sapma (veering) ismiyle anılan fenomen, etkileşime giren modlar arasında mod şekillerinin takas edilmesine ve doğal frekansların artış/azalış trendinin radikal biçimde değişmesine sebep olmaktadır. Örümcek ağı yapısındaki esnek disk, jiroskopik etkinin yanı sıra, rotor dinamiğinde karşılaşılan böylesine karmaşık bir fenomeni de modelleyebilme kabiliyeti göstermiştir.

Dönen sistemlerin en önemli elemanlarından biri olan kanatçıklar, önceki sisteme eklenerek tamamen sonlu kiriş elemanlardan oluşan esnek bir şaft-disk-kanatçık sistemi elde edilmiştir. Genellikle, uygulamalarda radyal olarak konumlandırılan kanatçıklar, jiroskopik etkiyi daha da belirgin hale getirmek amacıyla diske dik olarak yerleştirilmişlerdir. Tekrardan belirli hızlarda özdeğer problemi çözümlenmiş ve sistemin çeşitli modlarının frekanslarının değişen hızla birlikte değişimini gösteren Campbell diyagramı dönen koordinat sisteminde elde edilmiştir. Kanatçıkların da eklenmesiyle birlikte sistemin dinamik davranışının çok daha karmaşık hale geldiği görülmüştür. Esnek şaftın ve diskin rotorun dinamiği üzerindeki etkilerine ek olarak, kanatçıkların varlığı dönen koordinat sistemindeki dönüş kaynaklı esnekleşme (spin softening) etkilerini çok daha baskın hale getirmiştir. Bu durum kanatçıkların baskın olduğu modlarda, modların doğal frekanslarının artan hızla birlikte belirgin bir şekilde düşmesiyle kendini göstermektedir.

Esnek kanatçıkların dahil edilmesiyle çok daha karmaşık hale gelen sistemin dinamiğinde, modlar arasındaki etkileşimlerin tespiti oldukça zorlaşmıştır. Bunun için her bir mod şekli dikkatle incelenmiş ve artan dönüş hızıyla birlikte doğal frekansların değişimi takip edilmiştir. Bu analizler sonucunda da çeşitli modlar arasında sapma etkileşimlerin varlığı belirlenmiştir. Buna ek olarak, tez kapsamında incelenen tüm sistemlerde sönüm yok sayılmasına rağmen, bu dönen sistemde, belirli bir hız aralığında bir instabilite bölgesi tespit edilmiştir. Bu instabilite tipinde etkileşime giren iki modun, instabilite bölgesinde aynı doğal frekanslara ve mod şekillerine sahip oldukları görülmüştür. Sistemin dönüş hızı bu instabilite bölgesinin dışına çıktığında ise modlar tekrardan birbirlerinden ayrı hale gelmişlerdir.

Esnek diskin düğüm çizgisi sayısı birden büyük olan modlarının esnek şaftın modlarıyla birleşmemesi, bu modlarda şaftın belirgin bir rolü olmadığını göstermektedir. Bu bilgiye dayanarak, kanatçıklı diski şaftan ayrı ele alıp dinamiği ayrıca analiz edilmiştir. Bu model, jiroskopik etkinin neden olduğu hareket eden dalganın davranışının incelenmesinde kullanılmıştır. Disk üzerindeki düğüm noktalarının bir titreşim periyodundaki titreşim şekilleri incelenerek hareket eden dalganın yön tespiti yapılmış ve modun ileri veya geri mod olduğuna karar verilmiştir. Son olarak, çalışma içerisinde sunulan katı eleman modeliyle benzer bir kanatçıklı disk modeli oluşturularak, katı elemanlı ve kiriş elemanlı modellerin dinamik davranışlarının birbirleriyle olan benzerlikleri irdelenmiştir. Yapılan karşılaştırma, her iki modelin de jiroskopik etkileri ve dönen kanatçıklı disklerin dinamik davranışlarını modelleme hususunda oldukça benzer sonuçlar verdiğini göstermiştir.

Bu çalışma dönen sistemlerde jiroskopik etkilerin karmaşık ve ilginç doğasını, sonlu elemanlar yaklaşımı temel alınmış çeşitli modellerle incelemiştir. Çalışma içerisinde, dönen sistemlerde jiroskopik etkilere sebep olan jiroskopik momentlerin ve Coriolis kuvvetlerinin oluşum mekanizması sunulmuştur. Bunun yanında, bu ikisi arasındaki ilişki de açıklanarak, elde edilen sonuçların sabit ve dönen koordinat sistemlerinde anlamlı bir şekilde incelenebilmesi sağlanmıştır. Örümcek ağı yapısındaki bir disk modeli teklif edilerek tamamen kiriş elemanlardan oluşan basitleştirilmiş bir esnek şaft-disk-kanatçık sistemi oluşturulmuştur. Bu model sayesinde, çok daha az emek ve zaman harcanarak jiroskopik etkinin dönen sistemler üzerinde meydana getirdiği karmaşık sonuçların incelenebilmesi sağlanmıştır. Çalışmadan elde edilen sonuçlar, teklif edilen modelin, dönen sistemlerin dinamiğini modellemede ve jiroskopik etkininin sonuçlarının incelenebilmesini sağlamada oldukça kabiliyetli olduğunu göstermiştir.

1. INTRODUCTION

The industrial revolution has led to the development of machines in which the power transmission is performed via mechanical elements. These elements are generally rotating elements. Vibration problems have become much more apparent over the years as machines have become larger, more complex, and the speeds of the rotating elements in these machines have tremendously increased. These vibrations may cause not only issues related to the operational performance but also result in a destructive situation that may harm itself and the environment. In the past, some researchers focused on understanding the dynamic behaviour of these rotating parts which can be the source of excessive vibration in different situations and made calculations for designs to keep the vibrations under an acceptable limit. Towards the end of the 19th century, some researchers laid the foundations of this field that is known today as rotor dynamics.

Compared to a stationary structure, a rotating structure retains complicated dynamic behaviour due to some additional effects seen only for rotating bodies. Gyroscopic effect is one of these effects that can be generated in a system that is not stationary but rotating and therefore has an angular momentum around an axis.

Although studies included only the shaft as a rotating element in the past, throughout the years with the development of rotor systems, bladed discs were included in the models for some other purposes. However, these elements changed the dynamics of a rotating system, and it became difficult to accurately model the system using the basic assumptions. In addition to the inertial effects, considering the gyroscopic effects generated by these elements is an expensive process. However, it provides a more precise modelling of the dynamics of a rotating system.

1.1 Problem Definition

In the early studies of rotor dynamics, gyroscopic effects seemed to be ignored but as the systems developed and changed, its existence has begun to be felt. These systems can be exemplified in today's modern technologies such as gas turbines, aircraft engines, wind turbines, and pumps which are commonly known to contain huge rotating parts with high speed. For such systems, as it is explained in this study, ignoring gyroscopic effects may cause unacceptable errors in analysing the dynamic characteristics of the structure while rotating.

In order to eliminate the errors, early studies that considered the gyroscopic effect attached rigid discs to a rotating flexible shaft to simulate the huge rotors while still ignoring the blades. Despite the fact that this is a somewhat helpful simplification and assumption, it has rarely been a completely accurate model since the disc and blade flexibility alters the gyroscopic effects and the coupling between flexible bodies is not accounted for.

Today, one of the most practical methods that offers solutions to rotor dynamics problems is the finite element method (FEM). By using the FEM, a rotating system's dynamics considering the gyroscopic effect can be obtained at different rotational speeds. As widely known, this is done by dividing a system into many small finite elements such as beam, shell and solid elements. Very first FEM applications used beam elements to discretise flexible shafts. As the rotors get more complex in the means of flexible components, solid and shell elements are employed to accurately model flexible discs and blades. Accordingly, the degrees of freedom (DOF) in the problem increased dramatically and the solutions became costly in the means of modelling effort, computational time and memory for computers.

1.2 Literature Survey

A comprehensive literature survey has been conducted to reveal the development of studies over the years as well as the state of art studies in rotor dynamics literature.

1.2.1 Early history of rotor dynamics and flexible shaft-rigid disc models

In the literature, Rankine's study [1] in 1869 titled "On the centrifugal force of rotating shafts" is accepted to be the first study that gave birth to rotor dynamics. In this earliest study of rotor dynamics, Rankine has made calculations for "limiting speed" of a rotating shaft and was first to name the special motion that the shaft undergoes as "whirl" [2,3]. Although, with this study, Rankine has introduced the rotor dynamics field to the literature, according to [2,3], this study delayed the progress of rotor dynamics for 50 years. He incorrectly predicted that a rotating shaft has a limiting speed beyond which it is impossible to get a stabile operation otherwise, a destructive failure is expected. That is why he named this speed as limiting. In fact, it will take many years to understand by the researchers that this is not a limiting, but a “critical speed” and it is safe to operate beyond.

Dunkerley [4], changed the name of limit speed to critical speed [3,5]. In this study, Dunkerley stated that the critical speed is dependent on the bearings, geometry of the shaft, elastic modulus and the location and mass of the discs attached to the shaft. He predicted and measured the first critical speeds of different shaft models.

Jeffcott [6], studied a simple massless shaft model supported by two rigid bearings at each end with a disc attached to the shaft in the middle and showed that it is possible to operate beyond the critical speed. In fact, this model is an extended version by adding external damping of the one which had been developed by Föppl 26 years ago, but according to [3,7-9], this study was published in German, and it was not heard much by the rotor dynamics society.

Despite the fact that there were many assumptions made by Jeffcott to make the model of the system quite simple to analyse, the outcomes of the study were critically helpful in understanding the basics of rotor dynamics. Therefore, today, this rotor model is known as “Jeffcott rotor” in the honour of Henry H. Jeffcott.

Based on these early studies, the rotor dynamics literature is evolved into a wide field of dynamics in which the behaviour of various rotating systems is investigated.

Eshleman and Eubanks [10], stated that modelling shafts as lumped masses would not provide correct results at high rotational speeds and, hence proposed a continuous flexible shaft and a rigid disc. In this study, the effect of a rigid disc attached to a shaft on critical speeds is presented by changing the mass and radius of the disc. It was shown that the inertial features and the location of the disc on the shaft highly influences the critical speeds via gyroscopic effects.

Eshleman and Eubanks [11], discussed the effect of rotary inertia, shear strains, gyroscopic moments and external torque on the critical speeds of rotors by considering Euler-Bernoulli and Timoshenko beams. Using the Newton’s second law, equations of motion of these two different beams were obtained. Ignoring the shear strain and rotary inertia during bending causes the Euler-Bernoulli beam to have the same critical speed as the slenderness increases. Meanwhile, Timoshenko beams take shear strain and rotary inertia into account, and it was seen that the critical speeds decrease as the beam gets slenderer.

Nelson and McVaugh [12] developed a flexible shaft-rigid disc model including gyroscopic effects, rotary inertia and axial load. In order to apply FEM, they discretised the shaft by finite beam elements and using the appropriate shape functions energy expressions are obtained. From these expressions, mass, stiffness and gyroscopic matrices are computed. In this work the damping was ignored, and an unbalance was defined. This early work presented the equation of motion in both stationary and rotating reference frame by performing a transformation. Whirl speeds were found to be satisfactorily accurate by the authors. Most importantly, this study is a special work which implemented FEM to analyse rotating systems in the rotor dynamics field. Correspondingly, they pointed out the possible capabilities of this method in future rotor dynamic analyses.

Zorzi and Nelson [13], added damping to the previously proposed model [12] and analysed the damping effect on the stability of the shaft-disc system.

Nelson [14], modelled a flexible shaft using Timoshenko beam elements and attached a rigid disc. System's matrices are obtained by Hamilton principle. The author compared the critical speed results with those obtained in [11] and concluded that FEM gives slightly better results.

Ozguven and Ozkan [15] added damping to the system given in [14] and besides the whirl frequencies they investigated the stability and unbalance response under the effect of damping. It was concluded that it is a must to take shear deformations into account when dealing with dynamics of damped rotors.

Gasch [16], studied a flexible rotating shaft of a turbo-rotor. This flexible shaft is divided into many beam elements based on the Euler-Bernoulli beam theory. Matrices of the beam elements are obtained via principle of virtual work. In this work, external damping caused by bearings as well as the internal damping of shaft itself are included. Furthermore, since it is a turbo-rotor, many other complex effects such as fluid-film forces, aerodynamic cross-coupling from steam flow etc. are included in the model.

Sauer and Wolf [17], simply explained the generation of gyroscopic moments on a beam element rotating around its axis and provided the gyroscopic matrix for such an element by using principle of virtual work. Using this obtained gyroscopic matrix a pump rotor is analysed to investigate the effects of gyroscopic moments. It was shown that gyroscopic moments cause the double modes' natural frequencies of the non-rotating system to split into two different natural frequencies when the system is rotating. Furthermore, as the rotational speed increases these two natural frequencies gets away from each other meaning that one of them is increasing while the other decreases.

Yu et al. [18] (a publication produced from Yu's PhD thesis [19]) studied the dynamics of a rotating shaft using 3-D solid elements and compared the results with Timoshenko and Euler-Bernoulli beams. They concluded that the solid element modelling provides consistent results with both beam theories for slender shafts and only with Timoshenko beam theory for stubby shafts.

Nandi and Neogy [20] presented a general formulation for rotating shafts using solid elements in both stationary and rotating reference frames. The model presented is compared with different cases in the literature and its capabilities is investigated.

1.2.2 Flexible shaft-flexible disc models

Rigid disc assumption loses its accuracy for thin and less stiff discs. In order to understand the effect of disc flexibility on the dynamics of rotors, several studies dealt with flexible shaft-flexible disc systems.

Loewy and Khader [21] studied the coupling between flexible shaft and flexible disc based on the shaft rigidity while considering the gyroscopic effect. They concluded that shaft flexibility is an infusive feature on the dynamics of rotating systems.

Jacquet-Richardet et al. [22] investigated the dynamics of a rotating flexible shaft-bladed disc system using FEM under the influence of gyroscopic and centrifugal stiffening effects in rotating reference frame. Comparing the predicted results with the experimental ones, they emphasised the significance of shaft and disc flexibility. Although the system consists of a flexible bladed disc, influence of the blades is not discussed. Hence, this study is mentioned in this section.

Irretier et al. [23] studied the dynamics of flexible shaft-disc model using the FEM with cyclic symmetry approach since the tuned system is axisymmetric. Their aim was to analyse the coupling between flexible shaft and flexible disc by obtaining Campbell diagrams for different rotational speeds in rotating reference frame. Besides the coupling phenomenon, they emphasised the importance of the inclusion of the shaft into the model as the shaft modes induce a non-negligible gyroscopic effect in rotating reference frame. The results are compared with flexible shaft-rigid disc and rigid shaft-flexible disc systems. It was concluded that there occurs a strong coupling between shaft bending and disc one nodal diameter mode and this coupling is said to be enhancing the gyroscopic and centrifugal stiffening effect on natural frequencies.

Combescure and Lazarus [24] presented a refined finite element modelling for dynamic analysis of rotating systems. Initially, they investigated the capabilities of beam and solid elements of modelling rotating bodies such as a shaft, a ring, and a disc. Later, they analysed a more realistic system. What is so unique about this study is that this study performed analyses in both stationary and rotating reference frame for the simple bodies to reveal the link between these two frames. The explanation of the relation between Coriolis forces in rotating reference frame and the gyroscopic moments in stationary reference frame is extremely rare to find in the literature.

Heydari and Khorram [25] studied the dynamics of a flexible shaft-disc model in stationary reference frame. Similar to the previously mentioned studies, they are inspired by the effects of flexible thin discs on rotor's dynamics as the rigid disc assumption loses its validity. They included the centrifugal stiffening and gyroscopic effects and aimed to analyse shaft bending and disc transverse mode coupling using the assumed mode method. Since the aim is to analyse the coupling vibrations of the disc and the shaft, they only included shaft bending and disc one nodal diameter modes. They concluded that disc flexibility significantly affects the natural frequencies but stated that the amount of effect is dependent on two factors: disc's location on the shaft and aspect ratio of the disc which is the ratio of disc's thickness to its outer radius. Additionally, they studied the gyroscopic effect generated by the disc by changing the polar mass moment of inertia and the location on the shaft. This analysis showed that the gyroscopic effect has no significance if the disc is located on an antinode on the shaft in a specific bending mode shape as it only undergoes a translational motion perpendicular to the undeformed beam axis. On the other hand, the gyroscopic effect is stronger if the disc is located on a node and even more enhanced if the disc exhibits its own flexible tilting motion apart from the angular displacement of the shaft during shaft bending vibrations.

Zhao et al. [26] studied a flexible shaft-disc system in stationary reference frame considering the centrifugal and gyroscopic effects. The shaft and the disc are modelled according to the Euler-Bernoulli beam and Kirchhoff's Plate theories, respectively. In this study, it is proposed to put artificial springs between the disc and the shaft. This way, it is aimed to change coupling condition by changing the springs' stiffnesses. Additionally, bearings are modelled as springs and depending on their stiffnesses, the boundary conditions are changed.

1.2.3 Rotating flexible blade models

Besides the dynamics of flexible shafts and flexible discs, rotating flexible blades have a unique dynamic behaviour. Throughout the years, the significance of rotating blade dynamics has been realised and rotating blades have become a focus of interest among researchers in the literature. Blade alone studies are carried out to understand how a single rotating blade behaves under rotational effects such as centrifugal stiffening, spin softening and the gyroscopic effect.

Yokoyama [27], approached such a system with FEM. A rotating beam attached to a rotating rigid hub is discretized with Timoshenko beam elements including the centrifugal stiffening but neglecting the gyroscopic effects. Elemental matrices of a Timoshenko beam were obtained with Hamilton's principle and presented explicitly, however, as it is widely known it is quite straightforward to turn a Timoshenko beam element into an Euler-Bernoulli beam element by omitting rotary inertia and shear deformations. The author aimed to show the differences of these two beam theories for thick and thin beams. Additionally, effects of setting angle and hub radius were discussed. Bazoune, A. and Khulief, Y. A. [28] extended this formulation for tapered Timoshenko beam elements but still the gyroscopic effects were ignored.

Yoo and Shin [29] studied a rotating cantilever beam. In this study, the equations of motion were obtained via D'Alembert's principle. The authors used a newly introduced hybrid set of deformation which is named as "stretching" instead of conventional axial deformation and stated that this method is much simpler and consistent. They showed that the gyroscopic effects cause coupling between elastic displacements of a blade in different directions. Furthermore, in their analysis, this coupling resulted in a veering phenomenon between a stretching and a bending mode.

A similar work is done by Lin and Hsiao [30]. In this study, the authors aimed to investigate the effect of Coriolis forces on a rotating Timoshenko beam attached to a rigid hub. They concluded that Coriolis is negligible for certain cases. They also made calculations to present the effects of rotational speed, hub radius and slenderness ratio.

Chung and Yoo [31] have made a similar study with the one done by Yoo and Shin [29]. Firstly, they obtained 3 partial differential equations which are the governing equations of stretching, chordwise and flapwise vibrations using Hamilton's principle considering the hybrid set of deformation. At this point, they discretised the beam with beam elements in the context of FEM and analysed the natural frequencies of the system considering the gyroscopic effect.

Zohoor and Kakavand [32] have taken a simple rotating beam into consideration with gyroscopic, centrifugal stiffening and spin softening effects. They compared the natural frequencies of rotating Euler-Bernoulli and Timoshenko beams and concluded that for slender bodies both theories provide close results, however evident differences appear if the body is not slender but rather thick compared to its length.

Yang et al. [33] considered a rotating Timoshenko beam attached to a rigid hub and studied its dynamic with varying setting angle. However, unlike the other studies, torsional vibrations are added to the model and, axial vibrations are defined separately rather than defining stretching deformations. Equations of motion are obtained using Hamilton's Principle. Power series solution is used to obtain the results. Besides the bending mode shapes, elliptic modal motions due to the gyroscopic effect are illustrated.

Zeng et al. [34] considered a rotating pre-twisted beam element attached to a rigid hub with a stagger angle in order to study the effects of coupling between flapwise-chordwise-axial and torsional vibrations. This is done by taking 6 DOFs of a cross-section of the beam into account.

As a novel study on the gyroscopic effects on rotating bodies, Yang et al. [35] claim that rotational effects on rotating beams is not clear in the literature and this topic should be investigated. For this purpose, they took centrifugal stiffening, spin softening and gyroscopic effects into account for an Euler-Bernoulli beam. Unlike the previous studies, they used the conventional axial deformation as well as bending deformations. As it is widely known in the literature that the flapwise vibrations, also known as out-of-plane bending vibrations, are not directly affected by the gyroscopic effects when the setting angle is zero, hence they excluded the related modes to only investigate the gyroscopic, centrifugal stiffening and spin softening effects. To understand their roles on the dynamics, in-plane modes (chordwise and longitudinal) are analysed under the influence of these rotational effects individually.

Chen et al. [36] investigated the spin softening and centrifugal stiffening effects on a real wind turbine blade modelled with finite shell elements. The results showed that the centrifugal stiffening effect is more dominant than spin softening in the analysed flapwise, edgewise and torsional modes. Therefore, the natural frequencies increase with increasing rotational speed. It is seen that the spin softening effect is more detectable in edgewise bending modes than flapwise modes.

1.2.4 Bladed disc models

Although, single blade analysis give insight into dynamics of rotating blades under the influence of Coriolis forces in rotating reference frame, it is equally important to analyse dynamics of bladed flexible discs since disc flexibility has critically important effects on the natural frequencies of the system and may introduce blade-disc interactions. Correspondingly, there are many studies based on dynamics of rotating bladed discs.

Hsieh and Abel [37] presented a general formulation for rotating flexible bladed discs. In this study, distributed and lumped mass approaches are proposed to model centrifugal and Coriolis (gyroscopic) effects generated by a flexible disc and blades.

Genta [38] studied the stability of rotating array of blades. In this study, it is shown that blades can induce instability even though the system is undamped. In these instability regions, undamped system’s eigenvalues have non-zero real parts indicating the change in stability of the mode.

Nikolic et al. [39] (a publication produced from Nikolic’s PhD thesis [40]) studied the effect of Coriolis acceleration on a mistuned bladed disc both theoretically and experimentally. The blades are swept in the axial direction to enhance the coupling and, ultimately the gyroscopic effect.

Kan and Xu [41], and Xin and Wang [42] studied the effect of Coriolis forces on realistic mistuned bladed disc using the FEM. In reference [42] it is shown that the disc-blade coupling strengthens the gyroscopic effect and, in some modes the centrifugal stiffening can decrease the gyroscopic influence.

Ruffini [43] studied the Coriolis effects in bladed discs. In this dissertation, firstly, four different rotating systems are analysed with different FEM programs and the accuracy of frequency splits due to Coriolis (gyroscopic) effect is discussed. Then, a new case study has been modelled. In this case a thin disc with bent blades has been manufactured and a test rig has been built. The bladed disc is a special design. Blades are bent so that they lie normal to the disc surface in order to maximize the Coriolis effect hence, the frequency split of the double modes.

1.2.5 Shaft-disc-blade models

Huang and Ho [44] studied the shaft torsional and blade bending coupling in rotating reference frame. In this study the disc is assumed to be rigid.

Yang and Huang [45] investigated the effects of blade stagger angle and the stiffness of the bearings on the coupling between the shaft and the blades.

Ma et al. [46], aimed to develop a new dynamic model for a rotor-blade system and derived the equations of motion of the system using Hamilton’s principle taking torsional and lateral deformations of the shaft, gyroscopic, spin softening and centrifugal stiffening effects into account. It should be noted that the disc on which the blades are attached is assumed to be rigid. The beams are modelled based on the Timoshenko beam theory. Assumed mode method is utilised for solution. In order to validate the proposed model, an FE analysis is performed in Ansys. However, the researchers state that the existence of the blades violates the axisymmetry of the structure and thus, the gyroscopic effect of the blades is ignored, and only the inertial and stiffening effects are considered in stationary reference frame analysis. Researchers also stated that as the number of blades increases the coupling modes of the system increases thus, becoming a more complex system to analyse. This could be a very important inference as the modern rotor-blade systems have many blades mounted.

Chatelet et al. [47] studied the shaft-blade coupling in a flexible shaft-disc-blade system. It is stated that they employed global non-rotating mode shapes of shaft-disc-blade system to obtain the dynamics of first, a thin-walled composite shaft and secondly a more complex rotating pump system. The analysis of the complex system is performed in rotating reference frame due to the non axisymmetric features of the system. Meanwhile, cyclic-symmetry approach is utilised owing to the rotationally periodic geometry. Only the ND1 modes of the disc which are coupled with bending modes of the shaft are considered. Accordingly, a transformation from rotating to stationary reference frame is carried out. Results are obtained for three cases: flexible shaft-flexible blade, rigid blade-flexible shaft, and flexible blade-rigid shaft. These results showed that the blade-shaft coupling is only evident at low rotational speeds for forward modes, on the other hand, always significant in the whole rotational speed range for backward modes.

Similar to the work done by reference [46], She et al. [48] proposed a model where the disc and shaft is accepted to be flexible in order to investigate the coupled modes of vibrations of shaft-disc-blade system. It is stated that the flexible shaft-rigid disc modelling does not provide accurate results anymore due to the increased flexibility of the advanced rotating systems. Besides the importance of coupling between the disc and the other components, it is claimed that the disc flexibility directly affects important phenomena such as veering and merging. With a more flexible disc, these phenomena are more likely to occur in a rotating system.

She et al. [49], improved the previous model's [48] coupling modelling. As mentioned by Ma et al. [46], in this study FEM validation using Ansys is performed in stationary reference frame by ignoring the gyroscopic effects generated by blades due to the violation of axisymmetry. In this model, they introduced tuned and mistuned lacing wires between the flexible blades and systems with and without lacing wires are analysed in rotating reference frame.

Yang et al. [50] ignored the disc's flexibility in a shaft-disc-blade system in order to analyse the coupling between shaft and blades considering the gyroscopic effect.

Contact analyses of rotating structures are another focus of interest among researchers. Lesaffre et al. [51] investigated the dynamics of a shaft-disc-blade system under the gyroscopic, spin softening and centrifugal stiffening effects in rotating reference frame. Their aim was to study the contact between engine casing and the rotating structure. While doing that, they made comments about the dynamics of the system with changing rotational speed and detected several instability regions in the speed range of interest.

1.2.6 Rotor dynamics toolbox (RotFE)

RotFE is a free to use toolbox used in MATLAB prepared by Bucher I. [52]. A user can model a flexible shaft as series of beam elements and attach rigid discs and springs to it arbitrarily in order to investigate its dynamic behaviour in stationary reference frame.

Beam elements used in this program are based on the Timoshenko beam theory and they have 2 nodes at each end having 4 DOF at each node: 2 translational and 2 rotational. Torsional and axial vibrations are neglected.

RotFE computes the mass, stiffness, and gyroscopic matrices for each Timoshenko beam and assembles them into the global matrices. If required, user can add springs and rigid discs to any node on the shaft. Their effects are added to the related matrices. Additionally, unbalance and misalignment can be defined for the shaft.

After completing the model, an eigenvalue problem is set and by solving it, the natural frequencies are obtained. At this point, orbits of each mode can be visualized and if desired, a Campbell diagram can be plotted.

RotFE is an effective tool for understanding the gyroscopic effects generated by a shaft and rigid discs. The author of this thesis benefited too much from this tool at the beginning of the study and used it to validate the flexible shaft-rigid disc model that is covered in a further section.

This literature survey shows that in rotor dynamics, besides separate shaft, disc, and blade analyses, rotating bladed discs and shaft-disc-blade systems are analysed, frequently. Some of these studies utilised FEM while the others preferred different methods. Despite the fact that early studies usually used finite beam elements to discretise simple bodies, solid and shell elements are also preferred later on for more complex systems. Most of the studies take the gyroscopic effect, which is the main interest of this thesis, into account, however, it is possible to find studies that are neglecting it. Moreover, it is seen that the some of these studies mainly worked on other topics in rotor dynamics such as coupling vibrations, forced response analysis, effects of bearings, etc. while only considering the gyroscopic effect as a secondary phenomenon.

1.3 Objective and Scope of the Thesis

In this study, it is aimed to model rotating fully flexible disc-blade and shaft-disc-blade systems and analyse their dynamics under the gyroscopic effect. Unlike the studies in the literature, it is proposed to discretise the whole system with finite beam elements. This is achieved by modelling the flexible disc as a spiderweb-like structure. Thus, a simplified shaft-disc-blade system can be modelled and analysed with less modelling effort and computational time thanks to the relatively low number of DOF. This way, the influence of the gyroscopic effects and other phenomena on the dynamics of rotating shaft-disc-blade system is investigated. Throughout the study, the modelling of dynamics of rotating beam elements is explained in detail and the gyroscopic matrices are presented explicitly. This way it is intended to form a basis for future studies.

The scope of this thesis is as follows,

In the first chapter, an introduction to rotor dynamics is presented. Following the introduction, the problem is defined, and a literature survey is presented to have a comprehensive insight into the rotor dynamics studies.

In the second chapter, the generation of the gyroscopic effect in stationary and rotating reference frames is explained and its influence on the dynamics of a rotor is discussed. After that, dynamics of rotating flexible discs and blades considering the gyroscopic effects are explained. Finally, the FEM approach to rotor dynamics and solution of the complex eigenvalue problems are discussed.

In the third chapter, rotating flexible shafts, discs and blades are modelled using finite beam elements according to the FEM theory. Finally, the derivation of matrices of a rotating solid element is presented.

In the fourth chapter, rotating systems are modelled and solved based on the methodology given in the third chapter. Mode shapes are visualised in order to demonstrate the nodal diameters and travelling waves on the disc and whirling motion of shafts. Campbell diagrams and frequency split percentages are provided to investigate the change of natural frequencies under the gyroscopic influence. Veering phenomenon and merging type instabilities are explained.

In the fifth chapter, the results are summarised, the performance and the accuracy of the model are evaluated. Finally, suggestions for future work regarding the modelling of dynamics of flexible rotating bodies and how to further develop the models presented in this study are given.

2. THEORY

2.1 Generation of Gyroscopic Moments and Coriolis Forces

The gyroscopic effects in rotating systems are investigated in this thesis. The gyroscopic effects do not influence the dynamics of stationary systems, however, can be very significant in the dynamics of rotating systems, and in some cases, they may even produce unpredictable results. Modelling and analysis of rotating systems including the gyroscopic effects can become quite complicated when the flexibilities of the disc and blades need to be included in the model. In order to understand the dynamic behaviour of systems with flexible shaft/disc/blades, one needs to understand the mechanism of the generation of the gyroscopic effects in the first place.

It should be noted that the gyroscopic effects are the direct results of the so-called Coriolis acceleration [3,39,42]. In the literature, the term "gyroscopic effect" is mostly used when the shaft vibrations are considered [10,12,14,16] while the term "Coriolis effect" is used to address the same effect generated by the flexible blades [30,34]. However, it is also possible to encounter the use of opposite terminology in many other studies on rotor dynamics [32,33,35,47]. This can be explained by the fact that both of these effects originate from the Coriolis acceleration, and they cause the exact same results in the dynamics in both stationary and rotating reference frames. To be consistent in this thesis, these effects will always be referred to as gyroscopic effects regardless of the chosen reference frame unless stated otherwise.

2.1.1 Gyroscopic moments

Gyroscopic effects should not be ignored, especially in the field of modern rotor dynamics. In order to understand the generation of gyroscopic moments causing gyroscopic effects on the dynamics of a rotor, one needs to remember the basics of engineering mechanics.

A rotating body has angular momentum due to rotational speed and its mass moment of inertia. Referring to Figure 2.1(a), suppose that a disc is rotating with an angular velocity vector of $\Omega\vec{k}$ around z_s axis in stationary coordinate system $x_s y_s z_s$ where $\vec{\imath}$, $\vec{\jmath}$ and $\vec{k}$ are the unit vectors along x_s, y_s and z_s axes, respectively.

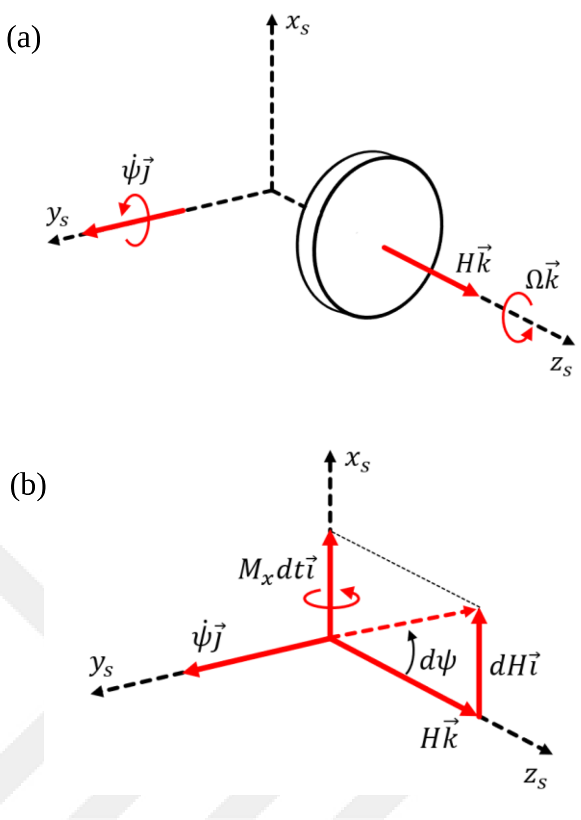

Figure 2.1 : (a) A rotating disc, (b) precession of the disc and the resultant change in angular momentum (adapted from [53]).

Here, the disc has an angular momentum, $\vec{H} = H\vec{k}$ where H can be expressed as

$$H = J_p\Omega \tag{2.1}$$

in which J_p is polar mass moment of inertia of the disc. If the system is not excited, the direction and magnitude of angular momentum is conserved. However, in rotor systems, a shaft vibrates due to several reasons, and it forces the mounted disc to change the direction of rotation. This motion that the disc undergoes is called precession. At this point, the generation of gyroscopic moments can be explained by referring to [3,53,54] as follows.

Let's assume that the disc precesses with an angular velocity of $\dot{\psi}$ around y_s axis for time dt while rotating as shown in Figure 2.1(b). Since the disc has an angular momentum around z_s axis, the precession causes the angular momentum vector to change the direction with an angle $d\psi = \dot{\psi}dt$. The change of angular momentum vector is expressed as $d\vec{H}$ and, according to the Newton's second law, the rate of change of angular momentum vector is equal to the net moment applied to the body as

$$\vec{M} = \dot{\vec{H}} = \frac{d\vec{H}}{dt} \tag{2.2}$$

Obviously, in Figure 2.1(b), the change of angular momentum, $d\vec{H}$, is in the positive x_s direction, thus the moment in equation (2.2) is said to occur in the same direction as well. Noting that $d\vec{H}$ sweeps an angle of $d\psi$ and using equation (2.2), a relation can be declared as [53]

$$\tan d\psi = \frac{\vec{M}dt}{\vec{H}} \rightarrow d\psi = \frac{\vec{M}dt}{J_p\vec{\Omega}} \tag{2.3}$$

Putting the vector forms aside, equation (2.3) can be rewritten as:

$$M_x = J_p\Omega\frac{d\psi}{dt} \tag{2.4}$$

By substituting $\dot{\psi} = {d\psi}/{dt}$ into equation (2.4), gyroscopic moment, M_x, around x_s axis generated due the precession around y_s axis is expressed as

$$M_x = J_p\Omega\dot{\psi} \tag{2.5}$$

The same process can be repeated for a precession of the disc with an angular velocity of $\dot{\theta}$ around x_s axis. This time, a gyroscopic moment will act around the y_s axis as

$$M_y = -J_p\Omega\dot{\theta} \tag{2.6}$$

where the negative sign indicates that the moment is along the negative y_s axis. In summary, precession of a rotating body changes the direction of angular momentum, and this causes gyroscopic moments acting on the body. This phenomenon could also be explained verbally: If a body, rotating around an axis, precesses around a second axis will experience a moment around a third axis [3]. Lastly, it should be noted that this mechanism is reversible meaning that if a rotating body is subjected to a moment perpendicular to the axis of rotation, then the body undergoes a precession around the third axis.

2.1.2 Coriolis forces

Expressions of Coriolis forces can be obtained first by applying Newton's second law to a rotating particle with mass m by referring to [40,42,53]. Here, the main objective is to express Newton's second law in rotating reference frame and obtain the forces acting on the system. There are two reference frames (Figure 2.2): rotating (x_r, y_r, z_r) and stationary reference frame (x_s, y_s, z_s).

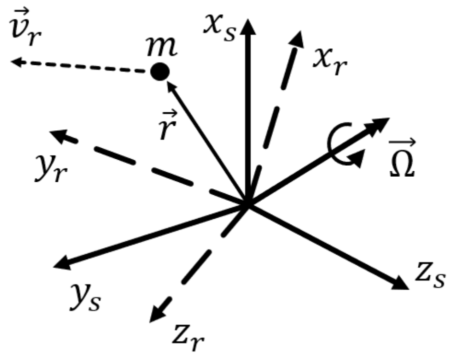

Figure 2.2 : A depiction of the moving mass in rotating and stationary reference frames.

Rotating reference frame has a relative rotational speed with respect to the stationary reference frame as $\vec{\Omega}$. The position vector of the mass with respect to the rotating reference frame's origin is expressed as $\vec{r}$. Assuming the rotating reference frame does not have a relative translational velocity with respect to the stationary reference frame and their origins are coinciding, the velocity, $\vec{v}_s$, of the mass with respect to the stationary reference frame can be expressed in terms of velocity, $\vec{v}_r$, and the position vector, $\vec{r}$, which are relative to rotating reference frame as

$$\vec{v}_s = \vec{v}_r + \vec{\Omega} \times \vec{r} \tag{2.7}$$

in which the second term on the right-hand side appears due to the rate of change of unit vectors of the rotating reference frame. Differentiating the expression above with respect to time and assuming a constant $\vec{\Omega}$ yields [40,55]

$$\vec{a}_s = \vec{a}_r + 2(\vec{\Omega} \times \vec{v}_r) + \vec{\Omega} \times (\vec{\Omega} \times \vec{r}) \tag{2.8}$$

where $\vec{a}_s$ and $\vec{a}_r$ represent the acceleration vectors with respect to stationary and rotating reference frames, respectively. Remembering the objective just mentioned, substituting equation (2.8) into Newton's second law in stationary reference frame which is in the form of

$$\vec{F}_s = m\vec{a}_s \tag{2.9}$$

yields the forces acting on the mass in rotating reference frame as [40,55]

$$\vec{F}_s - 2m(\vec{\Omega} \times \vec{v}_r) - m\vec{\Omega} \times (\vec{\Omega} \times \vec{r}) = m\vec{a}_r \tag{2.10}$$

It should be noted that the second term on the left-hand side of equation (2.10) is the Coriolis force and the third one is the so-called centrifugal force. The Coriolis force is obviously dependent on the rotational speed as well as the velocity of the mass with respect to the rotating reference frame. Furthermore, the cross product between these two vectors implies that there won't be any Coriolis force generated if these two vectors are parallel since the product will vanish. It can also be said that the Coriolis force will be maximum for velocity components that are perpendicular to the rotational speed vector. These inferences are critical and will be helpful to understand the gyroscopic effect generated by rotating blades.

2.1.3 Fictitious forces and the relation between the Coriolis forces and the gyroscopic moments

Although they may look different at first glance, there is an important relation between gyroscopic moments in stationary reference frame and Coriolis forces in rotating reference frame. The studies in the literature analyse their systems either in stationary or rotating reference frames. Consequently, they only deal with either gyroscopic moments or Coriolis forces. Nevertheless, the literature survey in this study revealed that none of the studies and textbooks, except for one [3], in rotor dynamics literature explained the relation between the Coriolis forces and gyroscopic moments. It is found appropriate here to shed light on this topic to better understand the gyroscopic effect phenomenon and easily correlate the results of both rotating and stationary reference frames.

Let us first recall the forces that appeared in rotating reference frame (equation (2.10)): the Coriolis force and the centrifugal force. Since they can only be observed in rotating reference frame, these two forces are categorised as fictitious forces (or pseudo forces) [56,57]. These forces are "artificially" introduced to ensure that Newton's second law is valid in rotating reference frame [57]. The reason behind this is explained here by referring to [57]. For this purpose, let's start with the centrifugal force because explaining the generation of the fictitious centrifugal force at first would be helpful to understand the need for introducing the Coriolis forces in rotating reference frame.

For a stationary observer, a mass that is rotating around an axis continuously experiences a centripetal (centre seeking) force in order to maintain its circular motion. Obviously, this force is always directed to the centre of rotation and dependent on the square of the rotational speed. In the perspective of Newton's second law (equation (2.9)), a centripetal force is applied to this mass and simultaneously, it accelerates due to the change of direction of its tangential velocity to maintain the circular motion. Therefore, for a stationary observer, everything seems to be meaningful. However, for a rotating observer, although the force can be observed via the $\vec{F}_s$ term in equation (2.10), the acceleration cannot be observed in rotating reference frame. In fact, the mass is observed to be stationary by the rotating observer. Clearly, there should be a force with an equal magnitude in the opposite direction to that of the centripetal force so that the net external force on the mass is zero. This force is the fictitious centrifugal force that only appears in rotating reference frame and is expressed in the second term in equation (2.10). This way, the Newton's second law's validity is ensured by introducing a force artificially.

It was stated that the Coriolis force is generated if a rotating mass exhibits a motion with a velocity with respect to rotating reference frame. If a review is conducted in stationary reference frame, it is seen that the magnitude of the tangential velocity changes due to the relative velocity, and the direction of the relative velocity vector changes due to the rotation of the mass. The total acceleration (except the centripetal acceleration) of the mass caused by the changes in both velocity vectors is equal to the Coriolis acceleration $2(\vec{\Omega} \times \vec{v}_r)$ in equation (2.8) [53,56]. The derivation of this expression and the centripetal acceleration is presented in page 389 in [53] and in page 36 in [56] with simple cases and not provided here for brevity. Interested readers are invited to refer to these textbooks.

Again, for a stationary observer, the rotating mass seems to experience an acceleration. The related force is transmitted to the rotating reference frame via the $\vec{F}_s$ term in equation (2.10). Although a force is observed to be applied to the mass, the rotating observer only witnesses that the mass undergoes a motion with a constant velocity. Once more, a fictitious force in the opposite direction with the same magnitude is needed to be introduced so that the net force applied on the nonaccelerating mass is zero and Newton's second law becomes valid in the rotating reference frame. This is the Coriolis force that appears to be the second term on the right-hand side of equation (2.10).

So far, the generation of the Coriolis force from another perspective is presented. Now, in order to establish the relation between the gyroscopic moments and the Coriolis forces, the system in Section 2.1.1 is taken into consideration. This time, instead of the change in the direction of the angular momentum, the motion of an infinitesimal mass, dm, on the disc during the precession is considered. It should be stated that the following explanation is adapted from references [3,58] to the current case here and the axisymmetry of the system is exploited.

Let's assume that an infinitesimal mass, dm, is located in the first quadrant as shown in Figure 2.3(a) where r and α are the two variables that describe its position. Since the disc has a rotational velocity $\vec{\Omega}$ around the positive z_s axis, the mass dm has a tangential velocity, $\vec{v}_{tan}$ and its components along the x_s and y_s axes. If the system undergoes a precession with an angular speed $\dot{\psi}$ around the positive y_s axis, the tangential velocity components appear as relative velocities as shown in Figure 2.3(b).

Now employing the second term on the right-hand side in equation (2.10), the Coriolis force, $d\vec{F}_{cor,1}$, generated by the mass dm in the first quadrant is expressed as

$$\begin{aligned} d\vec{F}_{cor,1} &= -2dm\left(\vec{\dot{\psi}} \times \vec{v}_{tan}\right) = -2dm\left(\dot{\psi}\vec{j}\right) \times \Omega r(-\sin\alpha\,\vec{\imath} + \cos\alpha\,\vec{j}) \\ &= -\left(2\Omega\dot{\psi}r\sin\alpha\right)dm\vec{k} \end{aligned} \tag{2.11}$$

If this analysis is repeated for the infinitesimal masses located in the other quadrants shown in Figure 2.3(a), the Coriolis forces generated by these masses are expressed as

$$\begin{gathered} d\vec{F}_{cor,3} = -d\vec{F}_{cor,1} \\ d\vec{F}_{cor,2} = -d\vec{F}_{cor,4} = -\left(2\Omega\dot{\psi}r\cos\alpha\right)dm\vec{k} \end{gathered} \tag{2.12}$$

where the numbers in the subscripts indicate the related quadrant generating the force.

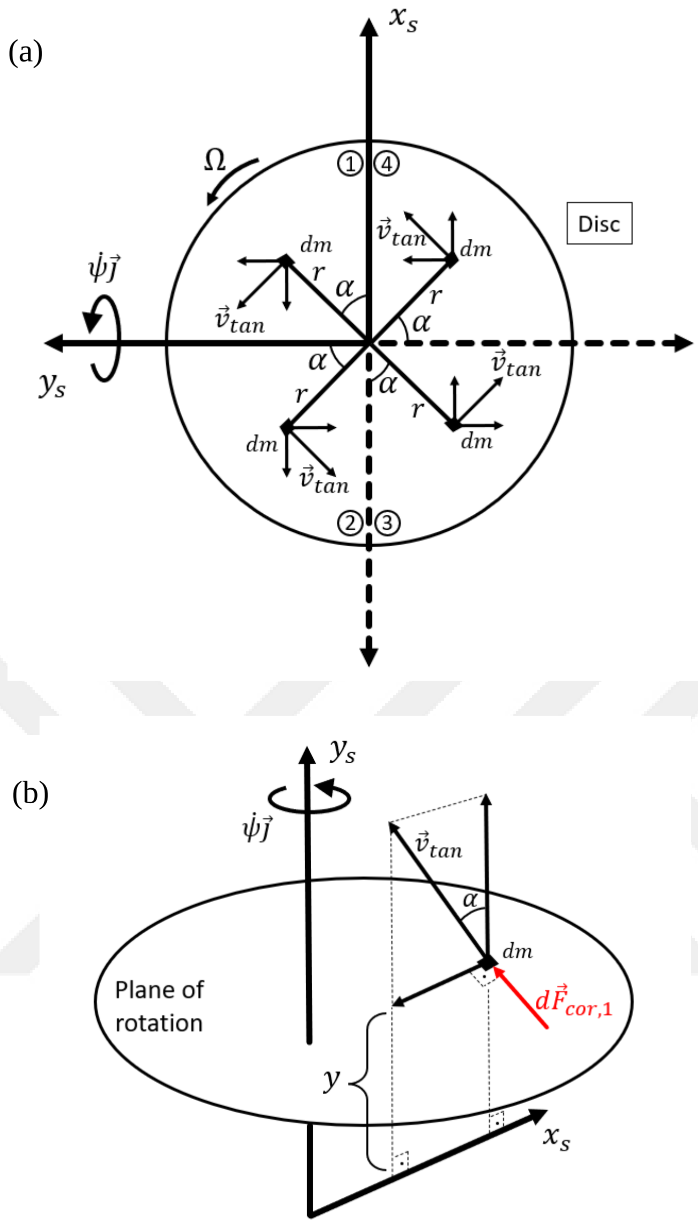

Figure 2.3 : (a) Depiction of the tangential velocity components of infinitesimal masses on the quadrants on the rotating disc during precession, (b) tangential velocity components of infinitesimal mass in the first quadrant and the generated Coriolis force.

Obviously, Coriolis forces at each quadrant generate a net moment around negative x_s axis as shown in Figure 2.4. In order to express the moments generated by each quadrant around the x_s axis, let's define variable y as the moment arm which is the distance between mass dm and the x_s axis. Obviously, $r \sin \alpha$ for the first and the third quadrant, and $r \cos \alpha$ for the second and the fourth quadrant are the moment arms for the forces in these quadrants (Figure 2.3a).

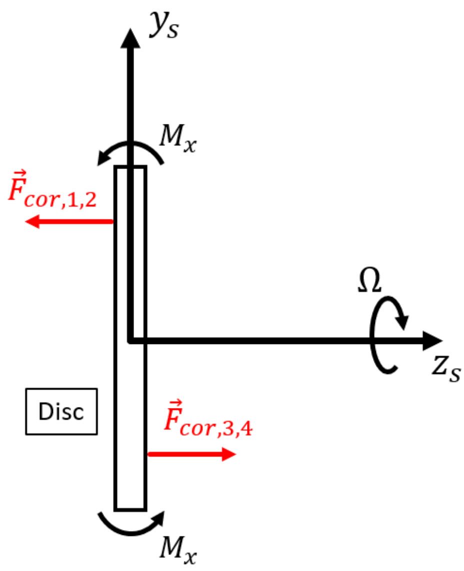

Figure 2.4 : The moment generated by the Coriolis forces on the disc.

Now, the moment generated by the first and the second quadrant around the x_s axis is expressed as

$$\vec{M}_{1,2} = \vec{M}_1 + \vec{M}_2 = \int [(y\vec{j}) \times d\vec{F}_{cor,1}] + \int [(y\vec{j}) \times d\vec{F}_{cor,2}] \tag{2.13}$$

where the integration is carried out over a single quadrant. Replacing y with $r \sin\alpha$ in $d\vec{F}_{cor,1}$ (equation (2.11)) and $r\cos\alpha$ in $d\vec{F}_{cor,2}$ (equation (2.12)) and performing the cross products yields

$$\vec{M}_{1,2} = -2\int 2\Omega\dot{\psi}y^2 dm\,\vec{\imath} = -2\Omega\dot{\psi}\int 2y^2 dm\,\vec{\imath} = -2\Omega\dot{\psi}\frac{J_x}{2}\vec{\imath} = -\Omega\dot{\psi}J_x\vec{\imath} \tag{2.14}$$

where J_x is the mass moment of inertia of the disc around the x_s axis. Performing the same computations for the other half of the disc, the moment generated is obtained as

$$\vec{M}_{3,4} = -2\int 2\Omega\dot{\psi}y^2 dm\,\vec{\imath} = -2\Omega\dot{\psi}\int 2y^2 dm\,\vec{\imath} = -2\Omega\dot{\psi}\frac{J_x}{2}\vec{\imath} = -\Omega\dot{\psi}J_x\vec{\imath} \tag{2.15}$$

The net moment applied on the disc generated by the Coriolis forces then becomes

$$\vec{M}_x = \vec{M}_{1,2} + \vec{M}_{3,4} = -2\Omega\dot{\psi}J_x\vec{\imath} = -\Omega\dot{\psi}J_p\vec{\imath} \tag{2.16}$$

where J_p is polar mass moment of inertia of the disc. Lastly, it should be stated that in the current case, the Coriolis forces do not cause a moment around y_s axis since the disc is symmetric [3,58]. Comparing equation (2.16) with equation (2.5), it is seen that both results are the same in magnitude but different in the directions. Naturally, as is expected, the Coriolis forces apply a net moment in the opposite direction to ensure that Newton's second law is valid in rotating reference frame [58]. The same procedure can also be applied to obtain the resultant moment due to a precession of the disc around x_s axis. It should be noted that the explanation given so far is intentionally carried out in rotating reference frame to emphasise the role of the fictitious Coriolis forces. However, the forces the causes the gyroscopic moments in stationary reference frame can also be directly obtained through the second acceleration term on the right-hand side in equation (2.8).

2.2 Results of Gyroscopic Effects on the Dynamics of a Rotor

So far, it is shown that the gyroscopic effect is generated by gyroscopic moments in stationary reference frame and Coriolis forces in rotating reference frame. It is worth remembering that in both cases the effect is dependent on the rotational speed of the rotor. From the FEM perspective, this implies that the gyroscopic matrix is also dependent on the rotational speed. Hence, as the modal characteristics of the system may change due to the change in rotational speed, for a detailed dynamic analysis, the problem should be solved at many different rotational speeds in a range.

The natural frequencies and mode shapes of a rotating body are predicted by solving the eigenvalue problem as shown later in this chapter. It is known that an axisymmetric rotor, such as a shaft with a circular cross-section or a disc, supported by isotropic bearings has double modes and each pair have exactly the same natural frequencies at rest [59]. In fact, this is the reason why these modes are called double modes. For example, double modes of a shaft are the bending modes that separately take place in two different planes which are perpendicular to each other. Meanwhile, a flexible disc's double modes are characterised as nodal diameter modes, and in these mode shapes, stationary nodal diameters appear on the disc. However, as the system starts rotating, shaft bending does not take place in a single plane anymore, but instead, the shaft traces an orbit around the undeformed shaft axis while rotating simultaneously. In other words, bending is not in-plane anymore. This special motion is called "whirling". If the shaft whirls in the same direction with rotation, then it is called the forward whirl and for opposite directions of whirl and rotation, this mode is called the backward whirl. For a rotating flexible disc, the nodal diameters are not stationary anymore, but they travel on the disc. This situation is the appearance of the so-called travelling waves. Similar to the shaft vibrations, depending on the direction of travelling waves, these modes are called forward and backward. This phenomenon arises due to the complex mode shapes introduced by the gyroscopic effect and its algebraic background is left to be explained in a forthcoming section.

At this point, it should be noted that the gyroscopic effect does not only introduce such special motions to rotor dynamics, but it also causes these double modes' natural frequencies to split into two new branches by increasing and decreasing the forward and backward mode's natural frequencies in stationary reference frame, respectively. On the other hand, in rotating reference frame, backward modes' frequencies increase while forward modes' frequencies decrease. This phenomenon is often referred to as "frequency split" in the literature [3,40,42,60]. As the rotational speed increases, frequency split tends to increase due to the speed-dependent gyroscopic effect. Nonetheless, this may not always be clearly visible as there might be other influencing factors in the system.

The variation of the natural frequencies of a rotating system necessitates a new type of data presentation to examine the speed-dependent dynamic behaviour of rotors. The so-called Campbell diagrams are used to visualise the relation between rotational speed and natural frequencies. A sample Campbell diagram in rotating reference frame is presented in Figure 2.5 where each line represents a mode. By examining the diagram, it can be said that the forward and backward whirl frequencies decouple as the rotational speed increases. This way, an analyst can easily track the natural frequencies of a system as a function of rotational speed. In order to obtain Campbell diagrams, the eigenvalue problem should be solved for a range of rotational speed and then the computed natural whirl frequencies are plotted. Similarly, if the Campbell diagram is to be obtained experimentally, the tests need to be carried at varying rotational speeds.

At this point, another important issue highlights the importance of Campbell diagrams. Frequency of various forces acting on a rotating system is a function of rotational speed. In a forced vibration situation, to ensure that the forced response of the system is not dangerous, one must refer to Campbell diagrams.

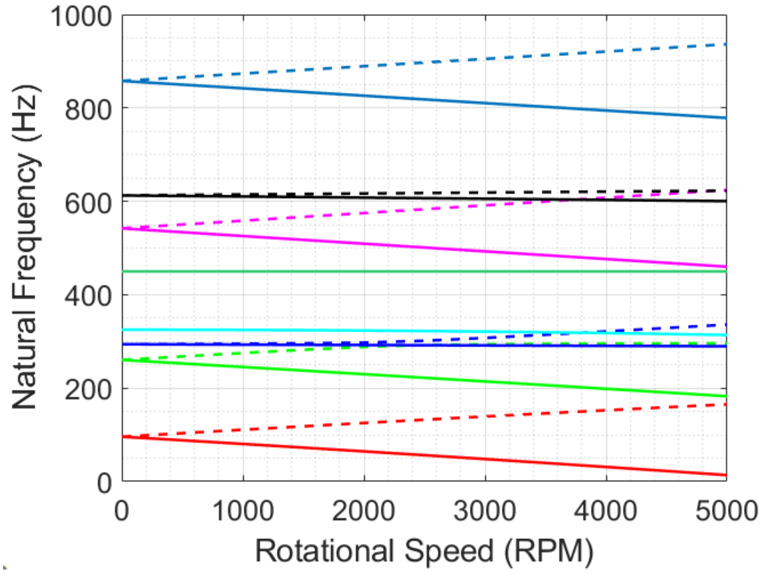

Figure 2.5 : A Campbell diagram example in rotating reference frame (solid lines: forward, dashed lines: backward).

The usage of Campbell diagrams for this topic can be embodied by a simple example as described in [9,54]: Assuming that an unbalance excitation is acting on a rotating system, the forcing frequency is equal to the rotational speed. For ensuring the safety of the system in operational conditions, a $\omega = \Omega$ line in Campbell diagram is drawn that passes through the origin, where ω is forcing frequency and Ω is the rotational speed. The speeds at the points where this line and natural frequencies intersect are known as critical speeds in a stationary reference frame analysis. As this terminology suggests, these points are critical since, from the basic knowledge of mechanical vibrations, matching forcing and natural frequencies may lead to excessive amplitudes of vibration. By saying “may” it is meant to be a possibility and therefore, further investigation is needed to analyse the forced response and decide whether it is critical or not. Consequently, in operational conditions, a system should be designed to avoid these critical speeds.

Veering is another phenomenon that is caused by the gyroscopic coupling [35]. In the case of veering, the modes’ frequencies that are expected to intersect, veer away [51,61-63]. This does not only change the trend of the increase/decrease of frequencies with rotational speed, but also most importantly, the mode shapes of the interacted modes are exchanged through veering [49,51]. In other words, a specific mode’s mode shapes at two different rotational speed may not be the same anymore. In the light of this information, it can be said that veering is an important phenomenon to be detected in a complex system and strict caution is required to accurately analyse systems with such behaviour.

As a conclusion to this section, it can be said that the gyroscopic effect is a unique phenomenon with its dependency on the rotational speed. Modern machines such as compressors and turbines are known to be lightweight and have high rotational speed due to required performance of the system. For such cases, evidently, the gyroscopic effect has significant influence on the dynamics of the system. Neglecting these effects may result in very significant errors between the predicted dynamic behaviour of theoretical model and the experimental results [7,64].

2.3 Dynamics of Rotating Discs and Blades

In engineering applications, shafts generally do not rotate alone. There are various applications where one or more bladed structures are mounted on them. In this way, with the power transmission through shafts, useful work is done by these structural components. For example, in an aircraft engine, the compressors are mounted on a shaft which rotates with a certain speed to pressurise the air entering the engine. In fact, to increase the efficiency, the air must be pressurised up to a certain level and this usually requires many stages of compressors in a row, each of which may have different geometries and different numbers of blades. These rotating elements have significant influence on the dynamics of the rotor. The influence of such structures is strong not only for aircraft engines, but also for many other engineering applications. Therefore, as shown in the literature survey, in addition to shafts, these structures are analysed and added to the models by researchers. Due to their complex properties, the dynamics of bladed discs are not straightforward to model hence, discs and thin rectangular cross-sectional blades are studied to understand their dynamic behaviours [44-46,48,49].

2.3.1 Dynamics of rotating discs

Discs with various diameters and thicknesses are used in practice. In the analyses of rotor dynamics, discs are mostly supported at their centres on the shaft. Early studies of rotor dynamics considered these discs as rigid. Therefore, only their inertial effects and gyroscopic effects generated by the precession are included. However, as the rotating structures become lightweight in modern engineering applications, this assumption loses its validity due to the dramatic change of natural frequencies and increasing interactions between shaft-disc and disc-blade vibrations [65]. This, ultimately, led the researchers to study bladed disc dynamics.

The mode shapes of a disc alone are defined by the numbers of nodal diameters (ND) and nodal circles (NC). It should be noted that if a disc is considered in free-free condition, there would be additional 6 rigid body modes. NDs are the nodal lines that lie along the diameter on the disc. NCs, as the name suggests, are the appearance of circular-shaped nodal lines on the disc. It should be reminded here that the vibrations at nodes/points located on these NDs and NCs are zero for that specific mode. Some mode shapes of an ordinary flexible disc are presented in Figure 2.6.

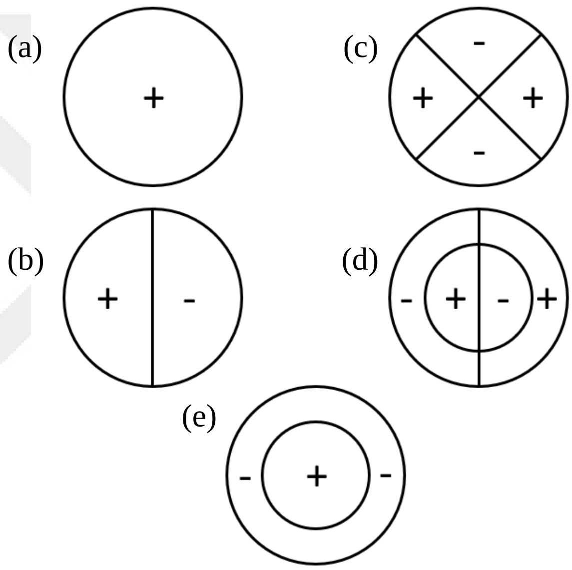

Figure 2.6 : Certain mode shapes of a flexible disc (ND, NC), (a) (0, 0), (b) (1,0), (c) (2,0), (d) (1,1), (e) (0,1) (adapted from [54]).

As shown in Figure 2.6, mode shapes may be composed of only NDs or NCs or both at the same time. The modes with non-zero NDs are called as double modes and have identical natural frequencies and shifted mode shapes. Many studies on rotor dynamics refer to the modes by their number of NDs without specifically mentioning the number of NCs [22,63,66,67]. This is due to changing characteristics of disc vibrations with increasing NDs. Torsional and umbrella modes are usually investigated in special cases.

In a specific vibration mode of a stationary disc, the NDs are stationary, meaning that only the nodes/points that are not located on the NDs exhibit vibrations. Additionally, all the points will reach their maximum at the same instant when the eigenvectors are real, as previously mentioned. However, this situation becomes more complicated when the disc rotates. The gyroscopic effect generated by the rotation introduces travelling waves, causing the NDs to rotate relative to the disc as well. As anticipated, a wave that is travelling on the disc causes the nodes to reach their maximum/minimum at different time instances respectively rather than simultaneously.

For a rotating disc, not only the number of NDs is important but also the direction of the travelling wave is of great interest. Since travelling waves were explained previously, it is appropriate not to repeat them here. However, it should be noted here that for a rotating disc, it is crucial to state whether a mode is forward or backward as well as the reference frame in which the analysis is carried out if a transformation between coordinate systems is necessary.

2.3.2 Dynamics of rotating blades

As previously outlined in the literature survey, there are many studies on the dynamics of a single rotating blade [27-35]. The studies based on the FEM procedure, discretised the blades mostly using beam elements. Additionally, the blades are clamped at one end and the other end is free to vibrate. The clamped end is said to be connected to a rigid hub which rotates around an axis that is perpendicular to the blade axis. Although the modelling is similar to that of the shafts, having the blades perpendicular to the axis of rotation causes the blade to have different dynamics than the shafts. This can be easily anticipated once the generation of the Coriolis forces is recalled. The Coriolis forces are generated by elastic deformations that are taking place in the plane of rotation. For blades with zero-stagger angle, these elastic deformations are known as longitudinal and chord-wise vibrations (or in-plane vibrations in general) [35]. Meanwhile, the Coriolis forces do not influence out-of-plane vibrations much and these mode shapes do not exhibit considerable frequency changes due to gyroscopic effects in rotating reference frame. In addition to the natural frequency change, the longitudinal and chord-wise modes are coupled via the Coriolis terms [30,32,35]. However, in real applications, blades are assembled with a stagger angle for operational purposes. Therefore, eventually, components of both chord-wise and flap-wise vibrations generate the Coriolis forces in the rotating reference frame. Besides, the so-called centrifugal stiffening can be much more influential than the gyroscopic effects [35] and the spin softening effect [36] for certain modes of blades. The blades in engineering applications are usually thin and located away from the axis of rotation and, therefore they are subjected to high centrifugal forces. The presence of static stress due to centrifugal forces along the blade stiffens the element and natural frequencies can increase tremendously at high rotational speeds. Therefore, centrifugal stiffening may overshadow the gyroscopic effect in most cases of rotating slender blades. Some studies are seen to be avoiding the huge effort required for modelling gyroscopic effects by simply neglecting them [27,28].

2.3.3 Coupled vibrations in rotors

So far, general information about the dynamic behaviour of rotating flexible discs and blades has been given, separately. However, for a rotor consisting of a shaft carrying a bladed disc, vibration modes of different components cannot always characterise the assembly modes. In other words, there may be interactions between these three components such that all the components can vibrate simultaneously. This type of vibration is known as coupled vibrations, and it is common for certain mode shapes of a rotating fully flexible shaft-disc-blade system. This is a clear indication that rigid disc assumption is not always valid as the coupling vibrations cannot be modelled.

The mode shapes in which a coupling between shaft and disc occurs only are ND0 and ND1 modes of the disc. These coupled mode shapes are itemised as follows [9,22,40,47,54,68,69]:

- The ND0 torsional vibration of the disc is coupled with the shaft and the blades by applying a net torsional moment, causing the shaft to twist and the blades to bend in the plane of rotation.
- The ND0 umbrella mode of a disc is coupled with the shaft and the blades again by applying a net axial force, causing the shaft to vibrate longitudinally and the blades to vibrate along the direction perpendicular to the plane of rotation.
- The ND1 modes of the disc are coupled with the shaft when bending moment and shearing force are exchanged between the disc and the shaft, resulting in shaft bending vibrations. Simultaneously, blades exhibit in-plane or out-of-plane bending vibrations.

These couplings are reversible, meaning that not only the discs but also the shaft or the blades can generate these coupling effects [68]. Modes having more than one NDs do not cause coupling [9,25,68] because the net bending moment and the shearing force applied by the disc/shaft is zero [40,69]. Therefore, if modes other than ND1 are to be investigated, researchers appear to neglect the shafts and focused only on the bladed disc as the shafts have no influence on these modes [40].

2.4 FEM Approach to Rotor Dynamics

As can be seen in the literature survey section, there are numerous studies on rotor dynamics. For the purpose of understanding the dynamic behaviour of rotating systems, some of these studies approach the problem using the FEM while others prefer to use different methods such as assumed mode method [46]. In this thesis, the FEM is employed to model and solve rotor dynamics problems.

FEM is an effective way of solving differential equations which govern the phenomena such as static stress-strain analyses of structures, dynamic analyses of bodies and analyses of heat and mass flow [54]. According to this method, the body that is to be analysed is divided into many small finite elements. Thus, this method is not only used for uniform and relatively simple shaped bodies, but also used for complex shaped bodies with nonuniform features. The important thing here is to obtain the relevant matrices of each element that forms the structure and then assemble the global matrices.

Fundamentally, dynamics of a rotating structure is similar to a nonrotating one, the difference being the effects generated by rotation. Rotation necessitates to perform extra computations to accurately model the dynamics of a rotating body. Consequently, the main objective in modelling a rotating system is to obtain matrices of rotational effects besides the mass and stiffness matrices for a rotor dynamic analysis. One of these effects is, undoubtedly, the gyroscopic effect.

Obviously, there are many different finite elements such as beam, shell and solid elements, which are commonly used in rotor dynamics. Beam elements are mostly utilised for discretising the flexible shafts and isolated rotating blade analyses while shell and solid elements are usually preferred for more complicated rotating systems containing flexible bladed discs. Nonetheless, in this section, it is aimed to present the FEM approach in rotor dynamics by deriving the expressions of governing matrices for a general finite element in stationary and rotating reference frames. This will provide a basic understanding of FEM approach to rotor dynamics.

2.4.1 Analysis in rotating reference frame

In rotor dynamics, modelling a system in a reference frame means that the displacement vector is expressed in that reference frame. A rotating body can be investigated in two reference frames: rotating and stationary. This situation is sometimes identified as an observer rotating with the rotating system and an observer that is stationary. Before performing a dynamic analysis, one must first decide in which frame of reference the dynamics of the rotating system should/can be formulated. For this purpose, the axisymmetry of the system should be examined in the first place.

Taking the individual blades into account in a rotating system supported by isotropic bearings, the axisymmetry is no longer valid and this makes it mandatory to follow the rotating reference frame approach to avoid time dependent terms in matrices [43,54,70]. In this section, this approach is explained by referring to textbooks and studies in the literature [9,37,42,43,71].

In rotor dynamic analyses, energy approach is a reliable and practical method that is commonly performed to obtain equations of motion of a rotating body. This method, as its name suggests, requires expressing the kinetic and potential energies in terms of generalised coordinates. In this case, the first step is to express the position of a small particle in a rotating body using the dynamic relations between coordinate systems. Depiction of a rotating body and reference axes are shown in Figure 2.7.

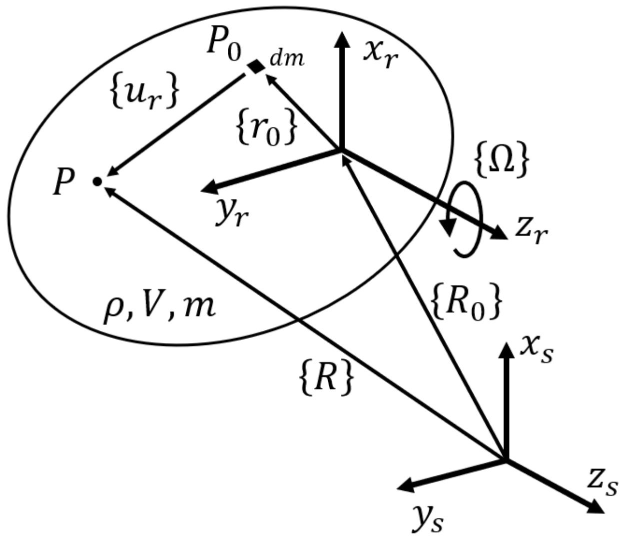

Figure 2.7 : Depiction of a rotating body and rotating and stationary reference frames.

In Figure 2.7, a stationary reference frame (x_s, y_s, z_s) and a rotating reference frame (x_r, y_r, z_r) are shown. The rotating coordinate system is fixed to the body and rotates with it. Let's assume that the flexible body with density ρ, volume V and mass m undergoes an elastic deformation and thus a particle with mass dm at point P_0 travels to point P. Noting that curly brackets are used to represent the vectors from now on, the position vector of point P in the deformed configuration with respect to stationary reference frame, $\{R\}$, is given as

$$\{R\} = \{R_0\} + \{r_0\} + \{u_r\} \tag{2.17}$$

where $\{R_0\}$ is the vector defining the position of rotating coordinate system with respect to the stationary coordinate system, $\{r_0\} = \{x_0, y_0, z_0\}^T$ is the position vector of point P_0 with respect to the rotating coordinate system, $\{u_r\} = \{u_r, v_r, w_r\}^T$ is the elastic deformation vector and subscript r represents that the deformation is defined in rotating reference frame. It should be declared that $\{R_0\}$ and $\{r_0\}$ contains constant terms. The body is assumed to be rotating with a constant rotational speed $\{\Omega\} = \{0,0,\Omega_z\}^T$ relative to the stationary system as shown in Figure 2.7. The absolute velocity of the particle can be obtained by taking the derivative of equation (2.17) with respect to time considering the rotation of unit vectors of rotating reference frame as done by [37,40,42,43,70] or utilising the transformation matrices to define vectors in different frames as done by [9,55,71]. In fact, both approaches lead to the same expression of velocity with respect to the stationary reference frame as

$$\{\dot{R}\} = \{v_P\} = \{\dot{u}_r\} + \{\Omega\} \times (\{r_0\} + \{u_r\}) \tag{2.18}$$

At this point, one might take one more derivative of equation (2.18) with respect to time and obtain the acceleration and then the forces applied on the mass dm in rotating reference frame as done by [20,42] to be used in principle of virtual work. However, in this study, kinetic and potential energy terms are used to obtain the governing matrices. For this purpose, kinetic energy, T, of the whole volume, is expressed as

$$T = \frac{1}{2}\int_V \rho \{v_P\}^T \{v_P\}\, dV \tag{2.19}$$

Before substituting the equation (2.18) into equation (2.19), the cross product in equation (2.18) is transformed into a scalar product by defining [37,43,70]

$$\{\Omega\}\times = [S] = \begin{bmatrix} 0 & -\Omega_z & \Omega_y \\ \Omega_z & 0 & -\Omega_x \\ -\Omega_y & \Omega_x & 0 \end{bmatrix} = \begin{bmatrix} 0 & -\Omega_z & 0 \\ \Omega_z & 0 & 0 \\ 0 & 0 & 0 \end{bmatrix} \tag{2.20}$$

With this definition substituting equation (2.18) into equation (2.19) and arranging the terms yields

$$\begin{aligned} T = \frac{1}{2}\int_V \rho[\{\dot{u}_r\}^T\{\dot{u}_r\} + 2\{\dot{u}_r\}^T[S](\{r_0\}+\{u_r\}) \\ + (\{r_0\}+\{u_r\})^T[S]^T[S](\{r_0\}+\{u_r\})]\, dV \end{aligned} \tag{2.21}$$

In the FEM perspective, assuming the rotating body is a general finite element as a whole, substituting the expression

$$\{u_r\} = [N]\{q_r\} \tag{2.22}$$

which relates the vector of generalised coordinates, $\{q_r\}$, to elastic displacement vector, $\{u_r\}$, via shape function matrix, $[N]$. Inserting this into equation (2.21) yields [9,37]

$$\begin{aligned} T = \frac{1}{2}\int_V \rho\{\dot{q}_r\}^T[N]^T[N]\{\dot{q}_r\}\, dV + \int_V \rho\{\dot{q}_r\}^T[N]^T[S]\{r_0\}\, dV \\ + \int_V \rho\{\dot{q}_r\}^T[N]^T[S][N]\{q_r\}\, dV + \frac{1}{2}\int_V \rho\{r_0\}^T[S]^T[S]\{r_0\}\, dV \\ + \frac{1}{2}\int_V \rho\{q_r\}^T[N]^T[S]^T[S][N]\{q_r\}\, dV \\ + \frac{1}{2}\int_V \rho\{r_0\}^T[S]^T[S][N]\{q_r\}\, dV \\ + \frac{1}{2}\int_V \rho\{q_r\}^T[N]^T[S]^T[S]\{r_0\}\, dV \end{aligned} \tag{2.23}$$

Potential energy of the rotating system is obtained similar to a non-rotating system. For this purpose

$$\{\varepsilon\} = [B]\{q_r\} \tag{2.24}$$

is defined where $\{\varepsilon\}$ is a vector containing the strain distribution in the element, $[B]$ is the matrix containing shape functions' space derivatives. Assuming that there is no pre-stress and pre-strain in the element [9], the stress vector, $\{\sigma\}$, of the element can be related to nodal displacement vector, $\{q_r\}$, as [72]

$$\{\sigma\} = [E]\{\varepsilon\} = [E][B]\{q_r\} \tag{2.25}$$

where $[E]$ is the constitutive matrix which is related to material properties of the finite element. From here, using equation (2.24) and (2.25), potential energy, U, of the element is expressed as

$$U = \frac{1}{2}\int_V \{\varepsilon^T\}\{\sigma\}dV = \frac{1}{2}\int_V q_r^T[B]^T[E][B]q_r dV \tag{2.26}$$

It should be restated here that, in this study, pre-stress and pre-strain caused by centrifugal stiffening and thermal effects are not included. If included, there should be extra terms in stress and strain vectors to accurately address those effects [9,55].

At this point, substituting the kinetic energy in equation (2.23) and potential energy equation (2.26) into Lagrange's equation of motion in the form

$$\frac{d}{dt}\left(\frac{\partial T}{\partial \dot{q}}\right) - \frac{\partial T}{\partial q} + \frac{\partial U}{\partial q} = Q \tag{2.27}$$

where q is a generalised coordinate (in this case q_r's) and Q is a generalised external force, yields the equation of motion of a rotating body in rotating reference frame as

$$[M]\{\ddot{q}_r\} + [G(\Omega)]\{\dot{q}_r\} + \left[[K] - \left[K_{soft}(\Omega)\right]\right]\{q_r\} = \{f(t)\} \tag{2.28}$$

where

$$[M] = \int_V \rho[N]^T[N]\,dV \tag{2.29}$$

is the mass matrix,

$$[G] = 2\int_V \rho[N]^T[S][N]\,dV \tag{2.30}$$

is the gyroscopic matrix which is clearly dependent on rotational speed due to $[S]$ matrix,

$$[K] = \int_V [B]^T [E][B] dV \tag{2.31}$$

is the structural stiffness matrix,

$$[K_{soft}] = \int_V \rho [N]^T [S]^T [S][N]\, dV \tag{2.32}$$

is the spin softening matrix generated by the change [40] in centrifugal force (the third term on the left-hand side in equation (2.10)) which is dependent on the square of the rotational speed. This matrix is responsible of decreasing the natural frequencies of the system [36,43,54,55], since it is added to the general stiffness matrix with a minus sign in front after the derivation $(-\frac{\partial T}{\partial q})$ in the Lagrange's equation (equation (2.27)) is performed. Obviously, once the kinetic energy equation (2.23) is substituted in the Lagrange's equation, the second and fourth integral disappears after the differentiations are performed [9]. Additionally, a constant term appears in the equation of motion once the sixth and seventh integral is differentiated with respect to the nodal displacement vector, however, the problem is assumed to be linear thus this constant term is neglected [9]. Obviously, in the case of free vibrations, the right-hand side of equation (2.28) becomes zero.

2.4.2 Analysis in stationary reference frame

If a system is axisymmetric such as a single flexible shaft or flexible shaft-disc system and supported by isotropic bearings, then the system can be modelled in stationary reference frame. Accordingly, in this section, a general finite element with an elastic displacement vector defined in stationary reference frame is taken into account. Throughout this section, the derivation is based on the one presented by [9].

As in the previous section, the aim here is also to express the velocity of a particle with mass *dm* on a rotating body. For this purpose, three reference frames are defined as shown in Figure 2.8: stationary, rotating, and dynamic. The stationary and the rotating ones are the same as the ones defined in the previous section. In addition to the stationary and rotating frames, the dynamic frame to be used here is a frame that is fixed to the rotating body and performs its small angular displacements θ and ψ around x_r and y_r axes, respectively.

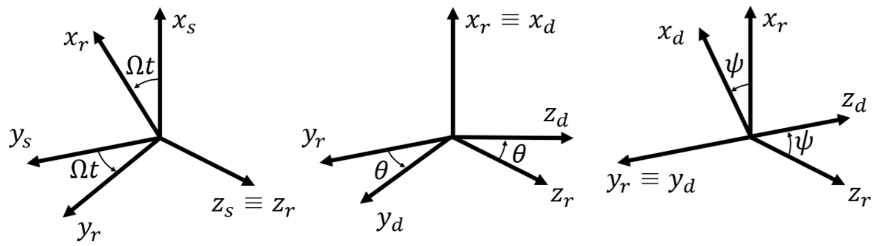

Figure 2.8 : Relative angular positions of stationary, rotating, and dynamic reference frames (adapted from [9]).

A vector defined in any reference frame can be translated to another frame by multiplying it with a transformation matrix that contains the relative angular displacements. That is to say, a vector defining the position of a particle at point P in the stationary reference frame should be expressed by a series of multiplication of vectors and matrices. This is surely a lengthy procedure and will not be provided here for brevity. Interested readers are invited to refer to [9,71] for more details. The velocity of point P, $\{v_P\}$, is expressed as [9]

$$\{v_P\} = \begin{Bmatrix} \dot{u}_i + y_i(\dot{\psi}\theta - \Omega) + \dot{\psi}(z_i + w_i + \psi x_i - \theta y_i) \\ \dot{v}_i - x_i(\dot{\psi}\theta - \Omega) - \dot{\theta}(z_i + w_i + \psi x_i - \theta y_i) \\ \dot{w}_i + \dot{\psi}x_i - \dot{\theta}y_i \end{Bmatrix} \tag{2.33}$$

where x_i, y_i and z_i represent the position of point P in stationary axes. Substituting the equation (2.33) into equation (2.19) yields

$$\begin{aligned} T = \frac{1}{2}\int_V \rho(\dot{u}_i^2 + \dot{v}_i^2 + \dot{w}_i^2)\, dV \\ - \Omega \int_V \rho\big[w_i(\dot{\theta}x_i + \dot{\psi}y_i) + x_i^2(\dot{\theta}\psi - \dot{\psi}\theta) \\ + x_i y_i(\dot{\psi}\psi - \dot{\theta}\theta)\big]\, dV + \frac{1}{2}\Omega^2 \int_V \rho(x_i^2 + y_i^2)\, dV \end{aligned} \tag{2.34}$$

Evidently, in this equation, the first integral is related to the mass matrix. The second integral is related to the gyroscopic behaviour of the system and although it looks complex, only the first term in the integral appears in the equation of motion [71]. Here, care must be given to the fact that despite the gyroscopic moments in stationary reference frame and the Coriolis forces in rotating reference frame have the same effects on a rotating system's dynamics as previously explained in this chapter, they are expressed by angular and translational generalised coordinates, respectively.

Finally, the third integral is apparently a constant term which will vanish once the equation of motion is obtained. For discretisation, the shape functions, nodal displacement and velocity vectors defined for the element in stationary reference frame are substituted into the kinetic energy expression above by defining [9]

$$\begin{aligned} \theta_i &= \frac{1}{2}\left(\frac{\partial u_i}{\partial z} - \frac{\partial w_i}{\partial x}\right) \\ \psi_i &= \frac{1}{2}\left(\frac{\partial w_i}{\partial y} - \frac{\partial v_i}{\partial z}\right) \end{aligned} \tag{2.35}$$

which relates the translational DOFs to angular DOFs. Potential energy of the system is the same as the one obtained in rotating reference frame owing to the axisymmetric body assumption [70,71]. In this case, applying the Lagrange's equation of motion in equation (2.27) by using the kinetic and potential energies, a flexible rotating body's equation of motion in stationary reference frame is expressed as

$$[M]\{\ddot{q}_s\} + [G(\Omega)]\{\dot{q}_s\} + [K]\{q_s\} = \{f(t)\} \tag{2.36}$$

For free vibration case, the right-hand side of equation (2.36) becomes zero.

2.4.3 Transformation of natural frequencies between reference frames

Until now, it has been shown that a rotating system could be analysed in either stationary reference frame or rotating reference frame depending on the properties of the system. Correspondingly, the natural frequencies are identified based on the reference frame in which the analysis is performed. Naturally, these frequencies numerically change when expressed with respect to another reference frame. Fortunately, it is possible to transform the natural frequencies from one reference frame to another easily by applying a procedure. This procedure is derived for this thesis after a comprehensive literature survey about this topic and applied as follows.

If the concerned mode is a shaft bending mode, then the transformation from rotating reference frame to stationary reference frame is performed by applying [19,54,68]

$$\begin{aligned} f_{stat} &= f_{rot} + \frac{\Omega}{60} \ \textit{for forward modes} \\ f_{stat} &= f_{rot} - \frac{\Omega}{60} \ \textit{for backward modes} \end{aligned} \tag{2.37}$$

where f_{stat} [Hz] and f_{rot} [Hz] are respectively the natural frequencies in stationary and rotating reference frames and Ω [RPM] is the rotational speed at which the natural frequencies are computed. It should be noted here that f_{stat} and f_{rot} are the absolute values of the natural frequencies.

Similarly, if the concerned mode is a disc mode, then the transformation is performed by applying [24,65,70,73]

$$\begin{aligned} f_{stat} &= f_{rot} + n\frac{\Omega}{60} \text{ for forward modes} \\ f_{stat} &= f_{rot} - n\frac{\Omega}{60} \text{ for backward modes} \end{aligned} \tag{2.38}$$

where n is the number of NDs occurring in the mode shape.

Now, one might question the procedure for the coupled modes of more complex systems such as flexible shaft-flexible disc systems. In that case, to carry out an accurate transformation, both components' mode shapes should be identified. Previously, it was stated that only the ND1 modes of a disc couple the shaft bending modes. Therefore, for such a coupled mode, equation (2.37) is applied. On the other hand, since the mode shapes with number of NDs greater than two are decoupled from the shaft modes, equation (2.38) is applied.

Interestingly, references [22,47,74,75] apply the equation (2.37), although their systems include flexible discs. At first glance, this might look like a discrepancy. However, all these studies state that they are only interested in shaft bending-disc ND1 modes therefore, there is no need to consider the equation (2.38).

Lastly, this procedure indicates that it is essential to detect whether a mode is a forward mode or a backward mode and the mode shapes of the components, before performing the transformation.

2.5 Eigenvalue Problem of a Rotor Under Gyroscopic Effects

Natural frequencies and mode shapes of a system can be computed by solving the eigenvalue problem. The equations of motion for an undamped gyroscopic rotating system without any external force can be expressed as

$$[M]\{\ddot{q}\} + [G(\Omega)]\{\dot{q}\} + [\widehat{K}]\{q\} = \{0\} \tag{2.39}$$

where $[M]$ is the symmetric mass matrix, $[G(\Omega)]$ is a speed dependent skew-symmetric gyroscopic matrix, $[\hat{K}]$ is a stiffness matrix and $\{q\}$, $\{\dot{q}\}$ and $\{\ddot{q}\}$ are the nodal displacement, velocity, and acceleration vectors, respectively. It should be noted that if the system is analysed in stationary reference frame, then the $[\hat{K}]$ consists only the structural stiffness matrix. Meanwhile for an analysis in rotating reference frame, this matrix is the sum of structural stiffness and spin softening matrices.

Due to the skew-symmetry introduced by the gyroscopic matrix, although the system is undamped, a straightforward solution cannot be obtained. Thus, a state-space solution should be conducted. Hence, the eigenvalue problem can be formulated by defining a new vector and two new matrices as [55]

$$[A] = \begin{bmatrix} [M] & [0] \\ [0] & [I] \end{bmatrix}, [B] = \begin{bmatrix} [G] & [\hat{K}] \\ -[I] & [0] \end{bmatrix}, \quad \{\Gamma\} = \begin{Bmatrix} \{\dot{q}\} \\ \{q\} \end{Bmatrix} \tag{2.40}$$

to form

$$[A]\{\dot{\Gamma}\} + [B]\{\Gamma\} = \{0\} \tag{2.41}$$

where, $[I]$ is an identity matrix and $\{0\}$ represents a zero vector. In the FEM, the dimensions of the matrices and vectors given in equation (2.39) are dependent on the number DOF of the system. For a system with n DOF, the dimensions of $[A]$ and $[B]$ are $2n$ by $2n$ and $\{\Gamma\}$ is $2n$ by 1. Solution of a damped gyroscopic system's state-space problem would normally provide $2n$ complex eigenvalues in the form of [54]

$$\begin{aligned} \lambda_i &= -\zeta_i\omega_i + j\omega_i\sqrt{1-\zeta_i^2} \;\; ; \; i = n+1, \dots, 2n \\ \lambda_i^* &= -\zeta_i\omega_i - j\omega_i\sqrt{1-\zeta_i^2} \;\; ; \; i = 1,2,3 \dots, n \end{aligned} \tag{2.42}$$

where ζ_i and ω_i are the i'th mode's damping ratio and natural frequency respectively. Besides the general role of damping in vibratory systems, in rotor dynamics, damping is also directly related to stability of the system. If the real part of an eigenvalue obtained from a state-space solution of a rotating system is positive, then this is an indication of the instability, and the related mode is said to be unstable [9]. Likewise, the mode is said to be stable if the real part of the related eigenvalue is negative. In our case, owing to the existence of skew-symmetric gyroscopic matrix and absence of damping, the solution of the eigenvalue problem in equation (2.41) provides purely complex $2n$ eigenvalues as the real parts in equation (2.42) vanishes.

Additionally, $2n$ by 1 left and right complex eigenvectors are obtained. According to equation (2.40) second half of the right eigenvectors are the complex mode shapes of the system. Imaginary part of these mode shapes signifies that the nodes on the body have a relative phase which indicates that each node will reach its maximum at different time instances during rotation [59]. Undoubtedly, this is an indication of travelling waves.

Last but not least, it should be remarked here that due to the existence of a speed-dependent matrix, the eigenvalue problem should be solved for different rotating speeds in a range. This means that rotor dynamics analyses are computationally much more expensive than those of non-rotating systems.

3. MODELLING OF ROTATING FLEXIBLE BODIES

3.1 Modelling With Beam Elements

Beam elements are the most commonly used finite elements in FEM for modelling rotating bodies such as shafts and blades. As shown in the literature survey in Section 1.2, early studies of rotor dynamics based on FEM mostly used finite beam elements as they provide accurate results with less computational effort for simple rotors.

In order to discretise a rotating body with finite beam elements, one must formulate a beam element based on a beam theory such as Euler-Bernoulli or Timoshenko. Hence, it is mandatory for a researcher to have complete knowledge of different beam theories. In this context, J. S. Rao states that “For a rotor dynamist, beam theory is the backbone of all analyses; all rotors were modelled as beams throughout the 20th century and only recently have we begun to understand solid model rotor dynamics” [2]. Therefore, before getting into the beam element modelling, two of the most popular beam theories in rotor dynamics are first explained here. Following the introduction of beam theories, the mathematical modelling of different rotating bodies using finite beam elements are presented in this section.

3.1.1 Finite beam element and beam theories

Modelling a flexible body with beam elements requires expressing the motion of each beam element mathematically. There are commonly used beam theories based on different assumptions. These beam theories have been used throughout the years to investigate the static and dynamic behaviours of beam-like structures such as shafts and blades. These are Euler-Bernoulli and Timoshenko beam theories. Apart from these two, Rayleigh beam theory is also applied to rotor dynamics [12]. Beam elements used in this thesis are based on Timoshenko beam theory, however, the differences between different theories are also explained and their advantages and disadvantages are discussed in the view of rotor dynamics.

For both Euler-Bernoulli and Timoshenko beam theories, the planar cross-section of the beam is assumed to be perpendicular to the neutral axis in the undeformed state.

After bending takes place, the cross-section of the beam is assumed to remain planar and oriented perpendicular to the deformed beam axis in the Euler-Bernoulli theory. However, the beam’s cross-sections are assumed to be planar but no longer perpendicular to the beam’s deformed axis in the Timoshenko beam theory. This distinction is the direct result of the assumption made about the shear strains on the cross-section. Euler-Bernoulli beam theory neglects the shear deformation, but the Timoshenko beam theory takes them into account [3,9,54,76]. For slender beams, which are said to be longer in length relative to their cross-sectional dimensions, both theories yield same results since the shear strains are so small compared to the normal strain. Meanwhile, for stub beams which are shorter in length compared to their cross-section, shear deformations are significant. Therefore, it can be said that the Timoshenko beam theory can provide accurate results for both slender and stub beams [19,32,54,77-80].

Another difference between these theories is the assumption on the rotary inertia which can be highly influential on the vibrations of structures. Euler-Bernoulli beam theory ignores the rotary inertia. Ignoring the rotary inertia for low frequencies of vibration can be acceptable. On the other hand, for higher frequencies, the inertial effects can become important [3], leading to inaccurate results in the simulations based on the Euler-Bernoulli beam theory, especially when the rotary inertia is non-negligible.

Although the Euler-Bernoulli beam theory simplifies the mathematical expressions for a beam element significantly, because of the aforementioned assumptions, it may lead to unacceptable results for certain cases. In general, Timoshenko beam theory yields more accurate results with the cost of a more complicated modelling. Consequently, one must choose an appropriate theory, wisely. In this study, a comprehensive modelling for rotating systems is aimed. Therefore, Timoshenko beam theory is adopted for all finite beam elements used in this thesis.

3.1.2 Flexible shaft-rigid disc system

As stated in Section 1.2.1, the very first rotor dynamic studies that approached the problem with FEM considered the shafts as flexible while the discs that are mounted on the shafts as rigid. This way, the inertias of the discs were incorporated into the model. Obviously, this is a substantial simplification of engineering applications. Nevertheless, this model presents a good understanding of the basics of rotating body dynamics. Hence, in this study, a flexible shaft-rigid disc system is modelled and investigated in the first place.

Since the structure studied in this section does not contain a non-axisymmetric part, the analysis is carried out in stationary reference frame, which is also usually used in the literature for this type of problems.

3.1.2.1 Timoshenko beam element with 8 DOFs

For the modelling of a flexible shaft, 8 DOF Timoshenko beam elements are used. This element is shown in Figure 3.1 where it is shown that there are two nodes at each end of the element, each node having two translational and two rotational DOFs, making a total of eight DOFs.

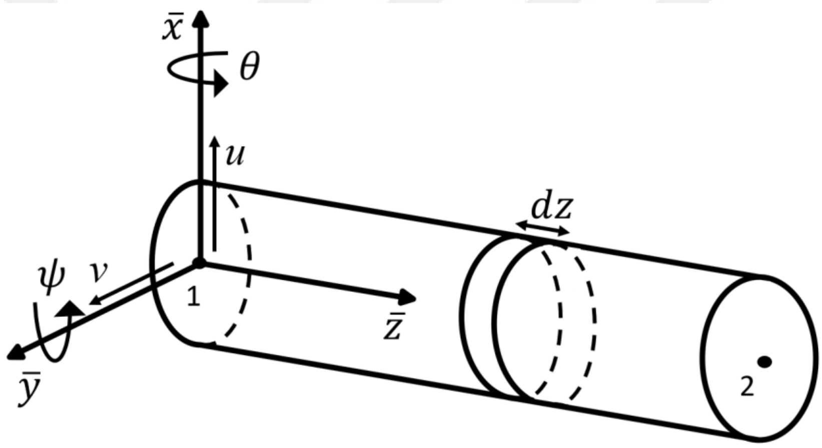

Figure 3.1 : 8 DOF Timoshenko beam element.

As it can be anticipated, only bending vibrations of the shaft can be studied using this element. Although it is straightforward to add axial and torsional DOFs, it is not much of a deal since gyroscopic effects are not generated by axial and torsional deformation for a shaft element in stationary reference frame. These DOFs are added to the model when dealing with more complex systems later in this thesis.

It is assumed that the $\bar{z}$ axis is coincident with the neutral axis of the beam element. Displacement vector of this element is expressed as

$$\{q\} = \{u_1, v_1, \theta_1, \psi_1, u_2, v_2, \theta_2, \psi_2\}^T \tag{3.1}$$

Using the nodal DOFs, the displacement of any point on the beam axis can be interpolated by using shape functions. For a Timoshenko beam, the derivation of the shape functions can be found in many textbooks [9,54,72] and articles [14,81]. Thus, only the shape functions are presented, and the complete derivation are not included here. The shape functions that will be used to relate nodal displacements to displacements along the element are given as [3,9,14,27]

$$
\begin{aligned}
&N_{1,1} = \frac{1+\phi(1-\zeta)-3\zeta^2+2\zeta^3}{1+\phi} \qquad N_{1,2} = l\zeta\frac{1+\frac{1}{2}\phi(1-\zeta)-2\zeta+\zeta^2}{1+\phi} \\
&N_{1,3} = \zeta\frac{\phi+3\zeta-2\zeta^2}{1+\phi} \qquad N_{1,4} = l\zeta\frac{-\frac{1}{2}\phi(1-\zeta)-\zeta+\zeta^2}{1+\phi} \\
&N_{2,1} = 6\zeta\frac{\zeta-1}{l(1+\phi)} \qquad N_{2,2} = \frac{1+\phi(1-\zeta)-4\zeta+3\zeta^2}{1+\phi} \\
&N_{2,3} = -6\zeta\frac{\zeta-1}{l(1+\phi)} \qquad N_{2,4} = \frac{\phi\zeta-2\zeta+3\zeta^2}{1+\phi}
\end{aligned}
\tag{3.2}
$$

In these expressions, $N_{1,i}$ is ith translational shape function, $N_{2,i}$ is ith rotational shape function, $\zeta = {}^{z}/_{l}$ is dimensionless coordinate along the beam axis and the transverse shear effect parameter [14,15,72]

$$\phi = \frac{12EI_d}{\kappa GAl^2} \tag{3.3}$$

where E, I_d, G, A and l are the Young's modulus of the material, diametral area moment of inertia, shear modulus of the material, area of the cross section and the length of the element, respectively. It should be noted that, since these elements are used to model a shaft, they are accepted to be axisymmetric around the neutral axis, hence the element is symmetric around both x and y axes. Therefore, $I_d = I_x = I_y$ relation is employed here. Finally, κ is the shear correction factor to account for the shear strain distribution on the cross section [76].

One last thing to note about the transverse shear effect parameter given in equation (3.3) is that, as the beam element gets slenderer, ϕ converges to zero and the Euler-Bernoulli beam's shape functions can be obtained. This summarizes the difference between Timoshenko and Euler-Bernoulli beams' shape functions.

From the shape functions given above, the displacements of points on the beam axis can be obtained by the relation [3,9]

$$\begin{Bmatrix} u \\ v \\ \theta \\ \psi \end{Bmatrix} = \begin{bmatrix} N_{11} & 0 & 0 & N_{12} & N_{13} & 0 & 0 & N_{14} \\ 0 & N_{11} & -N_{12} & 0 & 0 & N_{13} & -N_{14} & 0 \\ 0 & -N_{21} & N_{22} & 0 & 0 & -N_{23} & N_{24} & 0 \\ N_{21} & 0 & 0 & N_{22} & N_{23} & 0 & 0 & N_{24} \end{bmatrix} \begin{Bmatrix} u_1 \\ v_1 \\ \theta_1 \\ \psi_1 \\ u_2 \\ v_2 \\ \theta_2 \\ \psi_2 \end{Bmatrix} \tag{3.4}$$

$$= \begin{bmatrix} \{N_1\} \\ \{N_2\} \\ \{N_3\} \\ \{N_4\} \end{bmatrix} \{q\}$$

It should be noted that $\{N_i\}$ is the i'th row of the shape function matrix above.

3.1.2.2 Modelling of a flexible shaft

Following the introduction of the beam element; the mass, stiffness and gyroscopic matrices of the beam element can be obtained. In this section, these matrices are obtained through utilising the Lagrange's equation of motion which is based on the use of the potential and kinetic energy expressions of the beam element in stationary reference frame [3,9].

Potential energy, dU, of a portion with a differential length of dz in the Timoshenko beam element given in Figure 3.1 can be expressed as [9]

$$dU = \frac{1}{2} EI_d \left[\left(\frac{d\psi}{dz} \right)^2 + \left(\frac{d\theta}{dz} \right)^2 \right] dz + \frac{1}{2} GA\kappa (\gamma_{xz}^2 + \gamma_{yz}^2) dz \tag{3.5}$$

In this equation, it can be seen that the first term on the right-hand side corresponds to the potential energy of the portion due to bending deformation energy and the second term corresponds to the shear deformation energy. Subsequently, in equation (3.5), shear strains can be rewritten in terms of translational and rotational displacements by introducing [9]

$$\gamma_{xz} = \psi - \frac{du}{dz}, \quad \gamma_{yz} = -\theta - \frac{dv}{dz} \tag{3.6}$$

Using equation (3.4), introducing $dz = ld\zeta$ and taking integrals along the beam element leads to the potential energy, U, of the beam element similar to [9] as

$$
\begin{aligned}
U = \frac{EI_d}{2l}\int_0^1 \left[\{q\}^T \frac{d}{d\zeta}\{N_1\}^T \frac{d}{d\zeta}\{N_1\}\{q\} + \{q\}^T \frac{d}{d\zeta}\{N_2\}^T \frac{d}{d\zeta}\{N_2\}\{q\}\right] d\zeta \\
+ \frac{6EI_d}{\phi l}\int_0^1 \left[\left(\{N_4\}\{q\} - \frac{1}{l}\frac{d}{d\zeta}\{N_1\}\{q\}\right)^2 \right. \\
\left. + \left(-\{N_3\}\{q\} - \frac{1}{l}\frac{d}{d\zeta}\{N_2\}\{q\}\right)^2\right] d\zeta
\end{aligned}
\tag{3.7}
$$

Substituting equation (3.7) into Lagrange's equation of motion in equation (2.27), the structural stiffness matrix, $[K]$, is obtained as [14]

$$
[K] = \frac{EI_d}{l^3(1+\phi)}\begin{bmatrix}
12 & & & & & & & \\
0 & 12 & & & & & sym & \\
0 & -6l & (4+\phi)l^2 & & & & & \\
6l & 0 & 0 & (4+\phi)l^2 & & & & \\
-12 & 0 & 0 & -6l & 12 & & & \\
0 & -12 & 6l & 0 & 0 & 12 & & \\
0 & -6l & (2-\phi)l^2 & 0 & 0 & 6l & (4+\phi)l^2 & \\
6l & 0 & 0 & (2-\phi)l^2 & -6l & 0 & 0 & (4+\phi)l^2
\end{bmatrix}
\tag{3.8}
$$

For the same differential portion of beam element, by taking rotary inertia and gyroscopic effects into account, kinetic energy, dT, is expressed as [3,9]

$$
dT = \frac{1}{2}\rho A(\dot{u}^2 + \dot{v}^2)dz + \frac{1}{2}\rho I_d\left(\dot{\theta}^2 + \dot{\psi}^2\right)dz + \frac{1}{2}\rho I_p \Omega^2 dz + \rho I_p \Omega \dot{\theta}\psi dz
\tag{3.9}
$$

where the first term is translational kinetic energy, the second term is rotational kinetic energy, the third term is the kinetic energy caused by the rotation of the shaft and the last term is the kinetic energy caused by the gyroscopic moments. In equation (3.9), mass moments of inertia of the infinitesimal portion dJ_x and dJ_y around $\bar{x}$ and $\bar{y}$ axes are replaced with $\rho I_d dz$ which is valid for thin portions [54]. Similarly, the polar mass moment of inertia of the infinitesimal portion, dJ_p, can also be rewritten as $\rho I_p dz$ where I_d and I_p are the diametral and polar area moment of inertia of the infinitesimal portion.

As it is done for the differential potential energy expression, if one substitutes shape functions and displacement vectors into equation (3.9), defines $dz = ld\zeta, I_p = 2I_d$ and takes the integral along the beam element, kinetic energy of the whole element can be expressed as

$$
\begin{aligned}
T = \frac{1}{2}\rho A l \int_0^1 (\{\dot{q}\}^T [N_1]^T [N_1]\{\dot{q}\} + \{\dot{q}\}^T [N_2]^T [N_2]\{\dot{q}\}) d\zeta \\
+ \frac{1}{2}\rho I_d l \int_0^1 (\{\dot{q}\}^T [N_3]^T [N_3]\{\dot{q}\} + \{\dot{q}\}^T [N_4]^T [N_4]\{\dot{q}\}) d\zeta \\
+ \rho I_d l \Omega^2 + 2\rho I_d l \Omega \int_0^1 (\{\dot{q}\}^T [N_3]^T [N_4]\{q\}) d\zeta
\end{aligned}
\tag{3.10}
$$

Substituting equation (3.10) into the Lagrange's equations of motion (equation (2.27)) yields translational mass matrix, $[M_t]$, rotational mass matrix, $[M_r]$ and the gyroscopic matrix $[G]$ as [3,14]

$$
[M_t] = \frac{\rho A l}{420(1+\phi)^2}
\begin{bmatrix}
m_1 & & & & & & & \\
0 & m_1 & & & & & sym & \\
0 & -l m_2 & l^2 m_5 & & & & & \\
l m_2 & 0 & 0 & l^2 m_5 & & & & \\
m_3 & 0 & 0 & l m_4 & m_1 & & & \\
0 & m_3 & -l m_4 & 0 & 0 & m_1 & & \\
0 & l m_4 & -l^2 m_6 & 0 & 0 & l m_2 & l^2 m_5 & \\
-l m_4 & 0 & 0 & -l^2 m_6 & -l m_2 & 0 & 0 & l^2 m_5
\end{bmatrix}
\tag{3.11}
$$

$$
[M_r] = \frac{\rho I_d}{30 l(1+\phi)^2}
\begin{bmatrix}
m_7 & & & & & & & \\
0 & m_7 & & & & & sym & \\
0 & l m_8 & l^2 m_9 & & & & & \\
l m_8 & 0 & 0 & l^2 m_9 & & & & \\
-m_7 & 0 & 0 & l m_8 & m_7 & & & \\
0 & -m_7 & -l m_8 & 0 & 0 & m_7 & & \\
0 & l m_8 & -l^2 m_{10} & 0 & 0 & l m_8 & l^2 m_9 & \\
-l m_8 & 0 & 0 & -l^2 m_{10} & -l m_8 & 0 & 0 & l^2 m_9
\end{bmatrix}
\tag{3.12}
$$

$$
[G] = \frac{\rho I_d}{15 l(1+\phi)^2}
\begin{bmatrix}
0 & & & & & & & \\
-m_7 & 0 & & & & & skew & \\
l m_8 & 0 & 0 & & & & sym & \\
0 & l m_8 & -l^2 m_9 & 0 & & & & \\
0 & -m_7 & l m_8 & 0 & 0 & & & \\
m_7 & 0 & 0 & l m_8 & -m_7 & 0 & & \\
l m_8 & 0 & 0 & -l^2 m_{10} & -l m_8 & 0 & 0 & \\
0 & m_8 & l^2 m_{10} & 0 & 0 & -l m_8 & -l^2 m_9 & 0
\end{bmatrix}
\tag{3.13}
$$

where

$$m_1 = 156 + 294\phi + 140\phi^2 \qquad m_2 = 22 + 38.5\phi + 17.5\phi^2$$

$$m_3 = 54 + 126\phi + 70\phi^2 \qquad m_4 = 13 + 31.5\phi + 17.5\phi^2$$

$$m_5 = 4 + 7\phi + 3.5\phi^2 \qquad m_6 = 3 + 7\phi + 3.5\phi^2 \tag{3.14}$$

$$m_7 = 36 \qquad m_8 = 3 - 15\phi$$

$$m_9 = 4 + 5\phi + 10\phi^2 \qquad m_{10} = 1 + 5\phi - 5\phi^2$$

Global mass matrix of the element can be written as

$$[M] = [M_t] + [M_r] \tag{3.15}$$

Thus far, mass, stiffness and gyroscopic matrices for a Timoshenko beam element have been obtained. It is known that an elastic shaft can be divided into many small finite beam elements and for each element, the aforementioned matrices can be computed. Following this procedure, these matrices are assembled in a way considering the formation of the elements on the shaft to obtain the global matrices of the system.

3.1.2.3 Modelling of a rigid disc

In the previous section, the gyroscopic matrix of a flexible shaft was obtained. In engineering applications, the radius and cross-sections of shafts are much smaller than those of the discs attached on them. As stated before, higher polar mass moment of inertia results in higher gyroscopic moments acting on the system in the case of precession of the shaft. Hence, the effect of gyroscopic moments generated by discs attached to the shafts should also be considered in such situations. In this section, a rigid disc's effect on rotor dynamics is modelled and included in the finite element model.

Since the disc is considered rigid, it doesn't have deformation potential energy. In order to account for the gyroscopic moments acting on a rotating rigid disc, the kinetic energy, T_d, of the disc should be obtained. A rigid disc, having diametral mass moment of inertia J_d, polar mass moment of inertia J_p, mass m_d and rotating with the speed of Ω has a kinetic energy as (adapted from the equation (3.9) above)

$$T_d = \frac{1}{2} m_d (\dot{u}_i^2 + \dot{v}_i^2) + \frac{1}{2} J_d \left(\dot{\theta}_i^2 + \dot{\psi}_i^2\right) + \frac{1}{2} J_p \Omega^2 + J_p \Omega \dot{\theta}_i \psi_i \tag{3.16}$$

In this expression, subscript i indicates the i'th node on the shaft where the disc is mounted on. Now, referring to [54], the Lagrange's equations of motion is implemented to obtain mass and gyroscopic matrices of the disc and it yields

$$\begin{Bmatrix} \frac{d}{dt}\left(\frac{\partial T_d}{\partial \dot{u}_i}\right) - \frac{\partial T_d}{\partial u_i} \\ \vdots \\ \frac{d}{dt}\left(\frac{\partial T_d}{\partial \dot{\psi}_i}\right) - \frac{\partial T_d}{\partial \psi_i} \end{Bmatrix} = \begin{bmatrix} m_d & 0 & 0 & 0 \\ 0 & m_d & 0 & 0 \\ 0 & 0 & J_d & 0 \\ 0 & 0 & 0 & J_d \end{bmatrix} \begin{Bmatrix} \ddot{u}_i \\ \ddot{v}_i \\ \ddot{\theta}_i \\ \ddot{\psi}_i \end{Bmatrix} + \Omega \begin{bmatrix} 0 & 0 & 0 & 0 \\ 0 & 0 & 0 & 0 \\ 0 & 0 & 0 & J_p \\ 0 & 0 & -J_p & 0 \end{bmatrix} \begin{Bmatrix} \dot{u}_i \\ \dot{v}_i \\ \dot{\theta}_i \\ \dot{\psi}_i \end{Bmatrix} \tag{3.17}$$

Each term given in these matrices should be added to the relevant elements in the global mass and global gyroscopic matrices in order to account for the rigid discs' effect on rotor's dynamics.

3.1.3 Flexible shaft-disc-blade model

Rigid disc assumption offers easier modelling and decreases the computational time for solutions, tremendously. However, this assumption is no longer valid if the discs are thin and thus flexible, such as those in many engineering applications. In this case, the disc's and blades' flexibilities should be accounted for in the model. Therefore, in this section, the modelling of a flexible shaft-disc-blade system using beam elements is presented. Due to the presence of blades and the non-axisymmetric geometry of the proposed flexible disc, the rotating reference frame approach is embraced [43,54,70].

3.1.3.4 Timoshenko beam element with 12 DOFs

Comparing to the previous model, the DOFs of the element are increased from eight to twelve in order to be able to model the axial and torsional behaviour of the structure as well. Previously, the 8 DOF beam element was assumed to be axisymmetric since it was aimed to be used to analyse the shaft in the stationary reference frame. However, this time, the model includes blades that do not necessarily be circular cross-section. Therefore, a general beam element is presented here, which is to be used for shafts, discs, and blades. The beam formulated here does not necessarily have circular cross section. However, for visualisation purpose, the beam element is depicted with a circular cross-section in Figure 3.2.

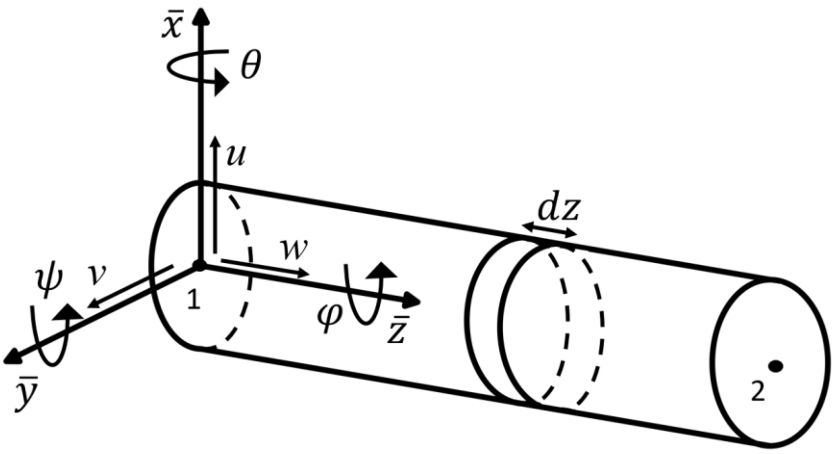

Figure 3.2 : 12 DOF Timoshenko beam element.

In Figure 3.2, there are 2 nodes at each end of the element and the DOFs are depicted on the local coordinate axes. Thus, the nodal displacement vector is expressed as

$$\{q\} = \{u_1, v_1, w_1, \theta_1, \psi_1, \varphi_1, u_2, v_2, w_2, \theta_2, \psi_2, \varphi_2\}^T \tag{3.18}$$

At any point on the element, displacements can be computed by [34]

$$\begin{Bmatrix} u \\ v \\ w \\ \theta \\ \psi \\ \varphi \end{Bmatrix} = \begin{bmatrix} N_{Tr,y,1} & 0 & 0 & 0 & N_{Tr,y,2} & 0 & N_{Tr,y,3} & 0 & 0 & 0 & N_{Tr,y,4} & 0 \\ 0 & N_{Tr,x,1} & 0 & N_{Tr,x,2} & 0 & 0 & 0 & N_{Tr,x,3} & 0 & N_{Tr,x,4} & 0 & 0 \\ 0 & 0 & N_{A,1} & 0 & 0 & 0 & 0 & 0 & N_{A,2} & 0 & 0 & 0 \\ 0 & N_{R,x,1} & 0 & N_{R,x,2} & 0 & 0 & 0 & N_{R,x,3} & 0 & N_{R,x,4} & 0 & 0 \\ N_{R,y,1} & 0 & 0 & 0 & N_{R,y,2} & 0 & N_{R,y,3} & 0 & 0 & 0 & N_{R,y,4} & 0 \\ 0 & 0 & 0 & 0 & 0 & N_{To,1} & 0 & 0 & 0 & 0 & 0 & N_{To,1} \end{bmatrix} \cdots$$

$$\cdots \begin{Bmatrix} u_1 \\ v_1 \\ w_1 \\ \theta_1 \\ \psi_1 \\ \varphi_1 \\ u_2 \\ v_2 \\ w_2 \\ \theta_2 \\ \psi_2 \\ \varphi_2 \end{Bmatrix} \tag{3.19}$$

where

$$N_{Tr,x,1} = \frac{1 + \phi_x(1-\zeta) - 3\zeta^2 + 2\zeta^3}{1 + \phi_x} \qquad N_{Tr,x,2} = -l\zeta \frac{1 + \frac{1}{2}\phi_x(1-\zeta) - 2\zeta + \zeta^2}{1 + \phi_x}$$

$$N_{Tr,x,3} = \zeta \frac{\phi_x + 3\zeta - 2\zeta^2}{1 + \phi_x} \qquad N_{Tr,x,4} = -l\zeta \frac{-\frac{1}{2}\phi_x(1-\zeta) - \zeta + \zeta^2}{1 + \phi_x} \tag{3.20}$$

$$N_{Tr,y,1} = \frac{1 + \phi_y(1-\zeta) - 3\zeta^2 + 2\zeta^3}{1+\phi_y} \quad N_{Tr,y,2} = l\zeta\frac{1 + \frac{1}{2}\phi_y(1-\zeta) - 2\zeta + \zeta^2}{1+\phi_y}$$

$$N_{Tr,y,3} = \zeta\frac{\phi_y + 3\zeta - 2\zeta^2}{1+\phi_y} \qquad N_{Tr,y,4} = l\zeta\frac{-\frac{1}{2}\phi_y(1-\zeta) - \zeta + \zeta^2}{1+\phi_y}$$

$$N_{R,x,1} = -6\zeta\frac{\zeta-1}{l(1+\phi_x)} \qquad N_{R,x,2} = \frac{1 + \phi_x(1-\zeta) - 4\zeta + 3\zeta^2}{1+\phi_x}$$

$$N_{R,x,3} = 6\zeta\frac{\zeta-1}{l(1+\phi_x)} \qquad N_{R,x,4} = \frac{\phi_x\zeta - 2\zeta + 3\zeta^2}{1+\phi_x}$$

$$N_{R,y,1} = 6\zeta\frac{\zeta-1}{l(1+\phi_y)} \qquad N_{R,y,2} = \frac{1 + \phi_y(1-\zeta) - 4\zeta + 3\zeta^2}{1+\phi_y}$$

$$N_{R,y,3} = -6\zeta\frac{\zeta-1}{l(1+\phi_y)} \qquad N_{R,y,4} = \frac{\phi_y\zeta - 2\zeta + 3\zeta^2}{1+\phi_y}$$

$$N_{A,1} = 1-\zeta \qquad N_{A,2} = \zeta$$

$$N_{To,1} = 1-\zeta \qquad N_{To,2} = \zeta$$

are the shape functions for the given beam element. In these shape functions, ϕ_x and ϕ_y are defined as [81]

$$\phi_x = \frac{12EI_x}{\kappa GAl^2}$$
$$\phi_y = \frac{12EI_y}{\kappa GAl^2} \tag{3.21}$$

It should be noted that the shape functions are discriminated by subscripts x and y to address the possible difference between bending stiffnesses around $\bar{x}$ and $\bar{y}$ axes respectively.

3.1.3.5 Modelling of a flexible shaft

The flexible shaft is modelled in rotating reference frame here. For this purpose, the kinetic energy of the rotating beam element that is used to model a flexible shaft should be obtained through expressing the absolute velocity of a point on the cross-section. This is achieved by using the coordinate systems shown in Figure 3.3.

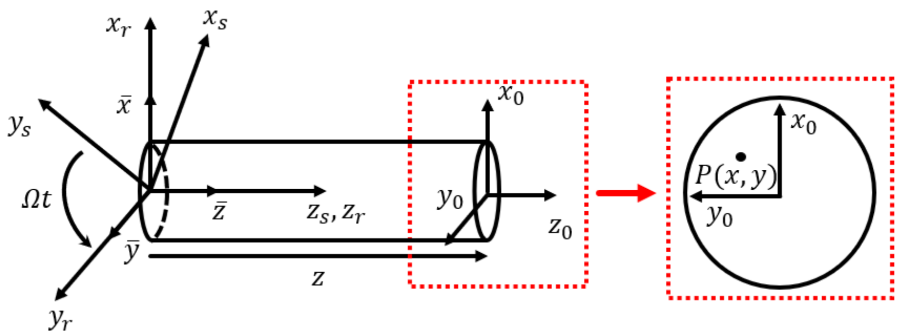

Figure 3.3 : Shaft beam element and coordinate systems.

In Figure 3.3, an undeformed rotating beam element is shown along with several coordinate systems. $x_s y_s z_s$, $x_r y_r z_r$, $\bar{x}\bar{y}\bar{z}$ and $x_0 y_0 z_0$ are stationary coordinate axes, rotating coordinate axes, local coordinate axes, and the coordinate axes on a cross section located at z from the local axes, respectively. For a shaft element in deformed and undeformed case, $x_0 y_0 z_0$, $\bar{x}\bar{y}\bar{z}$ and $x_r y_r z_r$ are in the same orientation and they rotate together with respect to stationary coordinate system $x_s y_s z_s$. $x_0 y_0 z_0$ only performs translational deformations with respect to $\bar{x}\bar{y}\bar{z}$ and for angular deformations of the cross-section new coordinate systems should be defined.

A cross-section may perform three angular displacements (θ, ψ, φ). Therefore, three new coordinate axes are defined on the cross-section as shown in Figure 3.4.

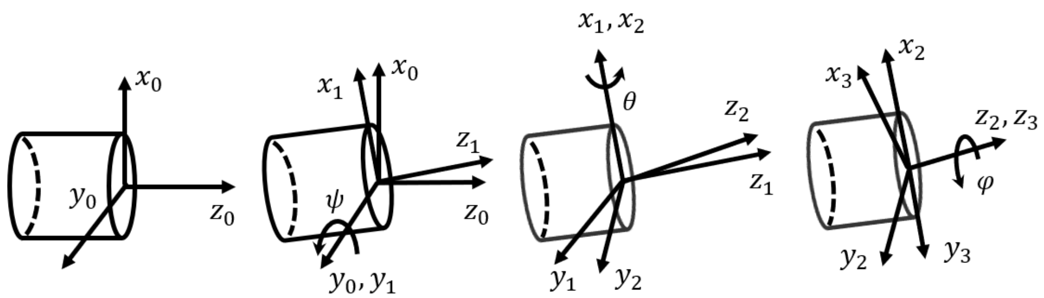

Figure 3.4 : Angular displacements of the beam's cross-section.

In order to express the position of a point on the cross-section with respect to $x_s y_s z_s$, transformation matrices are defined according to Figure 3.3 and Figure 3.4 as

$$[A_1] = \begin{bmatrix} \cos\varphi & \sin\varphi & 0 \\ -\sin\varphi & \cos\varphi & 0 \\ 0 & 0 & 1 \end{bmatrix}$$
$$[A_2] = \begin{bmatrix} 1 & 0 & 0 \\ 0 & \cos\theta & \sin\theta \\ 0 & -\sin\theta & \cos\theta \end{bmatrix} \tag{3.22}$$

$$[A_3] = \begin{bmatrix} \cos\psi & 0 & -\sin\psi \\ 0 & 1 & 0 \\ \sin\psi & 0 & \cos\psi \end{bmatrix}$$

$$[A_4] = \begin{bmatrix} \cos\Omega t & \sin\Omega t & 0 \\ -\sin\Omega t & \cos\Omega t & 0 \\ 0 & 0 & 1 \end{bmatrix}$$

where $[A_1]^T$ performs the transformation from $x_3y_3z_3$ to $x_2y_2z_2$, $[A_2]^T$ performs the transformation from $x_2y_2z_2$ to $x_1y_1z_1$, $[A_3]^T$ performs the transformation from $x_1y_1z_1$ to $x_0y_0z_0$. Lastly, $[A_4]^T$ performs the transformation from $x_ry_rz_r$ to $x_sy_sz_s$. Using these matrices, position vector, $\vec{r}_P$, of the point P located on the cross-section (Figure 3.3) in deformed state is expressed similar to [34,46,48] as

$$\vec{r}_P = [A_4]^T \left(\begin{bmatrix} u \\ v \\ z+w \end{bmatrix} + [A_3]^T[A_2]^T[A_1]^T \begin{bmatrix} x \\ y \\ 0 \end{bmatrix} \right) \tag{3.23}$$

It should be noted that u, v and w are the translational DOFs and defined in rotating reference frame. Here, adopting the small angle approximation [33,34] as

$$\begin{gathered} \cos\theta, \cos\psi, \cos\varphi \approx 1 \\ \sin\theta \approx \theta, \sin\psi \approx \psi, \sin\varphi \approx \varphi \end{gathered} \tag{3.24}$$

and using the equation (3.23), kinetic energy, T, of the whole element is expressed as [33,34]

$$T = \int_0^l \int_A \frac{1}{2} \rho \dot{\vec{r}}_p^T \dot{\vec{r}}_p dA\, dz \tag{3.25}$$

where the over dot represents the derivative with respect to time, ρ is the density, A is the cross section, superscript T represents transpose and l is the length of the element. Let's note here that for finite rotations, the order of rotation is important, normally. However, since the angular deformations are assumed to be infinitesimally small (equation (3.24)), the order of these transformations does not matter [53,82]. As it may be anticipated, the multiplication inside the integral in equation (3.25) will result in many terms some of which are higher order nonlinear terms and thus neglected [46]. It would be appropriate here to introduce the terms that contribute to the dynamics of the system. Equation (3.25) can be more explicitly written as

$$T = \int_0^l \left(\left[\frac{1}{2}\rho A(\dot{u}^2 + \dot{v}^2 + \dot{w}^2) + \frac{1}{2}\rho\left(I_x\dot{\theta}^2 + I_y\dot{\psi}^2 + \left(I_x + I_y\right)\dot{\varphi}^2\right) \right] + \Omega[A\rho(u\dot{v} - v\dot{u})] + \Omega^2 \left[\frac{1}{2}\rho A(u^2 + v^2) + \frac{1}{2}\rho\left(I_x + I_y\right)\varphi^2 \right] \right) dz \tag{3.26}$$

in which $I_x = \int y^2 dA$ and $I_y = \int x^2 dA$ are substituted. In this expression, terms are divided by brackets for the purpose of identification. The terms in the first bracket are used to form the mass matrix. The second term multiplied by Ω is going to form the gyroscopic matrix. It seen that gyroscopic effect couples the vibration in two directions. Finally, the third term multiplied by Ω^2 is going to form the spin softening matrix.

Potential energy of the beam element is obtained from the portion with length dz shown in Figure 3.2. Remembering that the axial and torsional deformations are considered in addition to bending, potential energy of the element, U, now becomes [76]

$$U = \int_0^l \left(\frac{1}{2}E\left[I_y\left(\frac{d\psi}{dz}\right)^2 + I_x\left(\frac{d\theta}{dz}\right)^2 \right] + \frac{1}{2}GA\kappa\left(\gamma_{xz}^2 + \gamma_{yz}^2\right) + \frac{1}{2}GI_p\left(\frac{d\varphi}{dz}\right)^2 + \frac{1}{2}EA\left(\frac{dw}{dz}\right)^2 \right) dz \tag{3.27}$$

where the E is the Young's modulus, I_x and I_y are the area moment of inertia around x and y axes of the cross-section, G is the shear modulus, κ is the shear correction factor and I_p is the polar area moment of inertia. In equation (3.27) the first term in the integral accounts for the potential energy due to normal strain occurring during bending, second term accounts for the shear strain energy, third term is the potential energy caused by the torsional deformation and the last one corresponds to the potential energy contribution from longitudinal deformation.

Substituting the shape functions according to equation (3.19) into kinetic and potential energy equations (3.26) and (3.27) and employing the Lagrange's equation of motion equation (2.27) yield the shaft's beam element's matrices: the mass matrix $[M]$ is

$$[M]=\begin{bmatrix} m_{1,y} & & & & & & & & & & & \\ 0 & m_{1,x} & & & & & & & & sym & & \\ 0 & 0 & 2m_7 & & & & & & & & & \\ 0 & -m_{3,x} & 0 & m_{2,x} & & & & & & & & \\ m_{3,y} & 0 & 0 & 0 & m_{2,y} & & & & & & & \\ 0 & 0 & 0 & 0 & 0 & 2m_8 & & & & & & \\ m_{4,y} & 0 & 0 & 0 & m_{5,y} & 0 & m_{1,y} & & & & & \\ 0 & m_{4,x} & 0 & -m_{5,y} & 0 & 0 & 0 & m_{1,x} & & & & \\ 0 & 0 & m_7 & 0 & 0 & 0 & 0 & 0 & 2m_7 & & & \\ 0 & m_{5,x} & 0 & -m_{6,x} & 0 & 0 & 0 & m_{3,x} & 0 & m_{2,x} & & \\ -m_{5,y} & 0 & 0 & 0 & -m_{6,y} & 0 & -m_{3,y} & 0 & 0 & 0 & m_{2,y} & \\ 0 & 0 & 0 & 0 & 0 & m_8 & 0 & 0 & 0 & 0 & 0 & 2m_8 \end{bmatrix} \tag{3.28}$$

where

$$m_{1,x/y}=\frac{\rho(70A\phi_{x/y}^2l^2+147A\phi_{x/y}l^2+78Al^2+252I_{x/y})}{210l(\phi_{x/y}+1)^2}$$

$$m_{2,x/y}=\frac{l\rho(7A\phi_{x/y}^2l^2+280I_{x/y}\phi_{x/y}^2+14A\phi_{x/y}l^2+140I_{x/y}\phi_{x/y}+8Al^2+112I_{x/y})}{840(\phi_{x/y}+1)^2}$$

$$m_{3,x/y}=\frac{\rho(35A\phi_{x/y}^2l^2+77A\phi_{x/y}l^2-420I_{x/y}\phi_{x/y}+44Al^2+84I_{x/y})}{840(\phi_{x/y}+1)^2}$$

$$m_{4,x/y}=\frac{\rho(35A\phi_{x/y}^2l^2+63A\phi_{x/y}l^2+27Al^2-252I_{x/y})}{210l(\phi_{x/y}+1)^2} \tag{3.29}$$

$$m_{5,x/y}=\frac{\rho(35A\phi_{x/y}^2l^2+63A\phi_{x/y}l^2+420I_{x/y}\phi_{x/y}+26Al^2-84I_{x/y})}{840(\phi_{x/y}+1)^2}$$

$$m_{6,x/y}=\frac{l\rho(7A\phi_{x/y}^2l^2-140I_{x/y}\phi_{x/y}^2+14A\phi_{x/y}l^2+140I_{x/y}\phi_{x/y}+6Al^2+28I_{x/y})}{840(\phi_{x/y}+1)^2}$$

$$m_7=\frac{Al\rho}{6}$$

$$m_8=\frac{l\rho(I_x+I_y)}{6}$$

the structural stiffness matrix $[K]$ is

$$[K]=\begin{bmatrix} k_{1,y} &&&&&&&&&&& \\ 0 & k_{1,x} &&&&&&&& sym && \\ 0 & 0 & k_6 &&&&&&&&& \\ 0 & -k_{3,x} & 0 & k_{2,x} &&&&&&&& \\ k_{3,y} & 0 & 0 & 0 & k_{2,y} &&&&&&& \\ 0 & 0 & 0 & 0 & 0 & k_7 &&&&&& \\ -k_{1,y} & 0 & 0 & 0 & -k_{4,y} & 0 & k_{1,y} &&&&& \\ 0 & -k_{1,x} & 0 & k_{4,x} & 0 & 0 & 0 & k_{1,x} &&&& \\ 0 & 0 & -k_6 & 0 & 0 & 0 & 0 & 0 & k_6 &&& \\ 0 & -k_{3,x} & 0 & k_{5,x} & 0 & 0 & 0 & k_{3,x} & 0 & k_{2,x} && \\ k_{3,y} & 0 & 0 & 0 & k_{5,y} & 0 & -k_{3,y} & 0 & 0 & 0 & k_{2,y} & \\ 0 & 0 & 0 & 0 & 0 & -k_7 & 0 & 0 & 0 & 0 & 0 & k_7 \end{bmatrix} \tag{3.30}$$

where

$$k_{1,x/y}=\frac{AG\kappa\phi_{x/y}^2 l^2+12EI_{x/y}}{l^3\left(\phi_{x/y}+1\right)^2}$$

$$k_{2,x/y}=\frac{EI_{x/y}\left(\frac{6}{\left(\phi_{x/y}+1\right)^2}+2\right)}{2l}+\frac{AG\kappa\phi_{x/y}^2 l}{4\left(\phi_{x/y}+1\right)^2}$$

$$k_{3,x/y}=\frac{AG\kappa\phi_{x/y}^2 l^2+12EI_{x/y}}{2l^2\left(\phi_{x/y}+1\right)^2}$$

$$k_{4,x/y}=\left(\frac{6EI_{x/y}}{l^2\left(\phi_{x/y}+1\right)^2}\right)+\frac{AG\kappa\phi_{x/y}^2}{2\left(\phi_{x/y}+1\right)^2} \tag{3.31}$$

$$k_{5,x/y}=\frac{EI_{x/y}\left(\frac{6}{\left(\phi_{x/y}+1\right)^2}-2\right)}{2l}+\frac{AG\kappa\phi_{x/y}^2 l}{4\left(\phi_{x/y}+1\right)^2}$$

$$k_6=\frac{AE}{l}$$

$$k_7=\frac{G(I_x+I_y)}{l}$$

the gyroscopic matrix $[G(\Omega)]$ is

$$
[G] = \Omega \begin{bmatrix}
0 & & & & & & & & & & & \\
g_1 & 0 & & & & & & & & \mathit{skew} & & \\
0 & 0 & 0 & & & & & & & \mathit{sym} & & \\
g_2 & 0 & 0 & 0 & & & & & & & & \\
0 & g_5 & 0 & g_7 & 0 & & & & & & & \\
0 & 0 & 0 & 0 & 0 & 0 & & & & & & \\
0 & -g_3 & 0 & g_4 & 0 & 0 & 0 & & & & & \\
g_3 & 0 & 0 & 0 & g_6 & 0 & g_1 & 0 & & & & \\
0 & 0 & 0 & 0 & 0 & 0 & 0 & 0 & 0 & & & \\
g_4 & 0 & 0 & 0 & -g_8 & 0 & -g_2 & 0 & 0 & 0 & & \\
0 & g_6 & 0 & g_8 & 0 & 0 & 0 & -g_5 & 0 & g_7 & 0 & \\
0 & 0 & 0 & 0 & 0 & 0 & 0 & 0 & 0 & 0 & 0 & 0
\end{bmatrix} \tag{3.32}
$$

where

$$
\begin{aligned}
g_1 &= \frac{Al\rho(147\phi_x + 147\phi_y + 140\phi_x\phi_y + 156)}{210(\phi_x + 1)(\phi_y + 1)} \\
g_2 &= -\frac{Al^2\rho(35\phi_x + 42\phi_y + 35\phi_x\phi_y + 44)}{420(\phi_x + 1)(\phi_y + 1)} \\
g_3 &= \frac{Al\rho(63\phi_x + 63\phi_y + 70\phi_x\phi_y + 54)}{210(\phi_x + 1)(\phi_y + 1)} \\
g_4 &= \frac{Al^2\rho(35\phi_x + 28\phi_y + 35\phi_x\phi_y + 26)}{420(\phi_x + 1)(\phi_y + 1)} \\
g_5 &= -\frac{Al^2\rho(42\phi_x + 35\phi_y + 35\phi_x\phi_y + 44)}{420(\phi_x + 1)(\phi_y + 1)} \\
g_6 &= \frac{Al^2\rho(28\phi_x + 35\phi_y + 35\phi_x\phi_y + 26)}{420(\phi_x + 1)(\phi_y + 1)} \\
g_7 &= \frac{Al^3\rho(7\phi_x + 7\phi_y + 7\phi_x\phi_y + 8)}{420(\phi_x + 1)(\phi_y + 1)} \\
g_8 &= -\frac{Al^3\rho(7\phi_x + 7\phi_y + 7\phi_x\phi_y + 6)}{420(\phi_x + 1)(\phi_y + 1)}
\end{aligned} \tag{3.33}
$$

and the spin softening matrix $[K_{soft}]$ is

$$[K_{soft}] = \Omega^2 \begin{bmatrix} s_{1,y} & & & & & & & & & & & \\ 0 & s_{1,x} & & & & & & & sym & & & \\ 0 & 0 & 0 & & & & & & & & & \\ 0 & -s_{3,x} & 0 & s_{2,x} & & & & & & & & \\ s_{3,y} & 0 & 0 & 0 & s_{2,y} & & & & & & & \\ 0 & 0 & 0 & 0 & 0 & 2s_7 & & & & & & \\ s_{4,y} & 0 & 0 & 0 & -s_{5,y} & 0 & s_{1,y} & & & & & \\ 0 & s_{4,x} & 0 & s_{5,x} & 0 & 0 & 0 & s_{1,x} & & & & \\ 0 & 0 & 0 & 0 & 0 & 0 & 0 & 0 & 0 & & & \\ 0 & -s_{5,x} & 0 & s_{6,x} & 0 & 0 & 0 & s_{3,x} & 0 & s_{2,x} & & \\ s_{5,y} & 0 & 0 & 0 & s_{6,y} & 0 & -s_{3,y} & 0 & 0 & 0 & s_{2,y} & \\ 0 & 0 & 0 & 0 & 0 & s_7 & 0 & 0 & 0 & 0 & 0 & 2s_7 \end{bmatrix} \tag{3.34}$$

where

$$s_{1,x/y} = -\frac{Al\rho(70\phi_{x/y}^2 + 147\phi_{x/y} + 78)}{210(\phi_{x/y} + 1)^2}$$

$$s_{2,x/y} = -\frac{Al^3\rho(7\phi_{x/y}^2 + 14\phi_{x/y} + 8)}{840(\phi_{x/y} + 1)^2}$$

$$s_{3,x/y} = -\frac{Al^2\rho(35\phi_{x/y}^2 + 77\phi_{x/y} + 44)}{840(\phi_{x/y} + 1)^2}$$

$$s_{4,x/y} = -\frac{Al\rho(35\phi_{x/y}^2 + 63\phi_{x/y} + 27)}{210(\phi_{x/y} + 1)^2} \tag{3.35}$$

$$s_{5,x/y} = \frac{Al^2\rho(35\phi_{x/y}^2 + 63\phi_{x/y} + 26)}{840(\phi_{x/y} + 1)^2}$$

$$s_{6,x/y} = \frac{Al^3\rho(7\phi_{x/y}^2 + 14\phi_{x/y} + 6)}{840(\phi_{x/y} + 1)^2}$$

$$s_7 = -\frac{l\rho(I_x + I_y)}{6}$$

Here, it should be carefully noted that the negative sign in front of the softening matrix given in equation (2.28) is integrated into this softening matrix, $[K_{soft}]$. This means that the $[K_{soft}]$ matrix given above in equation (3.34) is directly added to the structural stiffness matrix $[K]$ to obtain the overall stiffness matrix of the element.

3.1.3.6 Modelling of a flexible blade

In rotor dynamics, the orientation of the body with respect to the axis of rotation is important, since it changes which generalised coordinates play a role in the generation of Coriolis forces. As explained in Chapter 2, only the deformations perpendicular to the axis of rotation generate Coriolis forces acting on the body. It is straightforward to obtain gyroscopic matrices of solid elements which are rotating around different axes of rotation, however, a rather different mathematical model for the gyroscopic effect of rotating beam elements should be derived if the axis of rotation is not along the neutral axis of the beam. Therefore, even though the same beam element is used to discretise both a blade and a shaft, the generation mechanisms of Coriolis forces and spin softening effects are different for blades, and this is what makes the modelling of the beam elements harder than solid elements.

For the purpose of obtaining the governing matrices of a rotating blade, the same approach is followed as the one carried out for the shaft elements. The coordinate axes defined for this purpose is given in Figure 3.5. It should be noted that in this figure, the stationary coordinate system $x_s y_s z_s$ is unique to this element and the orientation should not be confused with the one given in Figure 3.3. This time, the local coordinate system $\bar{x}\bar{y}\bar{z}$ and the rotating coordinate system $x_r y_r z_r$ do not share the same origin but are still in the same orientation during the rotation. Lastly, to prevent a possible confusion, it should be stated that the stationary coordinate system $x_s y_s z_s$ is defined only for the relevant element and does not have to be in the same orientation with the global coordinate system. Depending on the relative orientation of these systems a proper transformation must be carried out for beam elements.

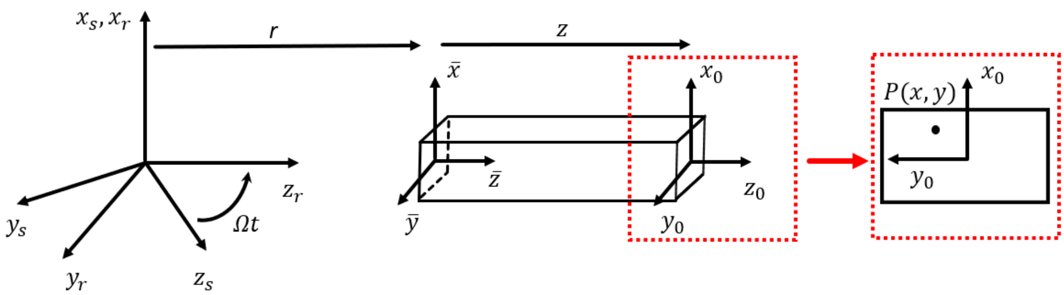

Figure 3.5 : Blade beam element and coordinate systems.

By looking at Figure 3.5, position vector $\vec{r}_P$ of point P on the deformed blade similar to [34,46,48] can be expressed as

$$\vec{r}_P = [A_4]^T \left(\begin{bmatrix} u \\ v \\ r+z+w \end{bmatrix} + [A_3]^T [A_2]^T [A_1]^T \begin{bmatrix} x \\ y \\ 0 \end{bmatrix} \right) \tag{3.36}$$

which resembles the one obtained for a point on the shaft in equation (3.23). All the transformation matrices remain the same except for $[A_4]$ since the element is defined to be rotating around x_s axis as shown in Figure 3.5 and it is now expressed as

$$[A_4] = \begin{bmatrix} 1 & 0 & 0 \\ 0 & \cos\Omega t & \sin\Omega t \\ 0 & -\sin\Omega t & \cos\Omega t \end{bmatrix} \tag{3.37}$$

Kinetic energy of the beam element that is used to discretise a rotating blade can be obtained by taking the derivative of equation (3.36) with respect to time and substituting it into equation (3.25) as [33,34]

$$\begin{aligned} T = \int_0^l \Bigg(& \left[\frac{1}{2}\rho A(\dot{u}^2 + \dot{v}^2 + \dot{w}^2) + \frac{1}{2}\rho\left(I_x\dot{\theta}^2 + I_y\dot{\psi}^2 + \left(I_x + I_y\right)\dot{\varphi}^2\right)\right] \\ & + \Omega\left[A\rho(v\dot{w} - w\dot{v}) + \rho I_y\left(\psi\dot{\varphi} - \varphi\dot{\psi}\right)\right] \\ & + \Omega^2\left[\frac{1}{2}\rho A(v^2 + w^2) + \frac{1}{2}\rho\left(I_y(\varphi^2 + \psi^2) + I_x\theta^2\right)\right]\Bigg) dz \end{aligned} \tag{3.38}$$

where the first term in the bracket is obviously going to form the mass matrix and the formulation is the same with the shaft element. The second term is the gyroscopic term which couples the longitudinal and in-plane bending vibrations as well as the rotational DOFs around the same axes. Finally, the last term is related to the spin softening characteristics of the blade.

The elemental structural stiffness matrix and the elemental mass matrix are the same with the shaft element's matrices (equation (3.28) and (3.30)) hence will not be repeated here. At this point, the gyroscopic and spin softening matrices unique to the blades are obtained through substituting the relevant shape functions and applying Lagrange's equation of motion. The gyroscopic matrix $[G]$ is

$$
[G] = \Omega \begin{bmatrix}
0 & & & & & & & & & & & \\
0 & 0 & & & & & & & & \textit{skew} & & \\
0 & g_2 & 0 & & & & & & & \textit{sym} & & \\
0 & 0 & g_4 & 0 & & & & & & & & \\
0 & 0 & 0 & 0 & 0 & & & & & & & \\
g_1 & 0 & 0 & 0 & g_6 & 0 & & & & & & \\
0 & 0 & 0 & 0 & 0 & g_1 & 0 & & & & & \\
0 & 0 & -g_3 & 0 & 0 & 0 & 0 & 0 & & & & \\
0 & g_3 & 0 & g_5 & 0 & 0 & 0 & g_2 & 0 & & & \\
0 & 0 & g_5 & 0 & 0 & 0 & 0 & 0 & -g_4 & 0 & & \\
0 & 0 & 0 & 0 & 0 & -g_7 & 0 & 0 & 0 & 0 & 0 & \\
g_1 & 0 & 0 & 0 & g_7 & 0 & -g_1 & 0 & 0 & 0 & g_6 & 0
\end{bmatrix} \tag{3.39}
$$

where

$$
g_1 = -\frac{I_y \rho}{\left(\phi_y + 1\right)} \qquad g_2 = \frac{Al\rho(20\phi_x + 21)}{30(\phi_x + 1)}
$$
$$
g_3 = \frac{Al\rho(10\phi_x + 9)}{30(\phi_x + 1)} \qquad g_4 = \frac{Al^2\rho(5\phi_x + 6)}{60(\phi_x + 1)} \tag{3.40}
$$
$$
g_5 = -\frac{Al^2\rho(5\phi_x + 4)}{60(\phi_x + 1)} \qquad g_6 = \frac{I_y l\rho\left(4\phi_y + 1\right)}{6\left(\phi_y + 1\right)}
$$
$$
g_7 = \frac{I_y l\rho\left(2\phi_y - 1\right)}{6\left(\phi_y + 1\right)}
$$

spin softening matrix $\left[K_{soft}\right]$ is

$$
\left[K_{soft}\right] = \Omega^2 \begin{bmatrix}
s_1 & & & & & & & & & & & \\
0 & s_2 & & & & & & & & \textit{sym} & & \\
0 & 0 & 2s_3 & & & & & & & & & \\
0 & s_8 & 0 & s_4 & & & & & & & & \\
s_7 & 0 & 0 & 0 & s_5 & & & & & & & \\
0 & 0 & 0 & 0 & 0 & 2s_6 & & & & & & \\
-s_1 & 0 & 0 & 0 & -s_7 & 0 & s_1 & & & & & \\
0 & s_9 & 0 & -s_{10} & 0 & 0 & 0 & s_2 & & & & \\
0 & 0 & s_3 & 0 & 0 & 0 & 0 & 0 & 2s_3 & & & \\
0 & s_{10} & 0 & s_{11} & 0 & 0 & 0 & -s_8 & 0 & s_4 & & \\
s_7 & 0 & 0 & 0 & s_{12} & 0 & -s_7 & 0 & 0 & 0 & s_5 & \\
0 & 0 & 0 & 0 & 0 & s_6 & 0 & 0 & 0 & 0 & 0 & 2s_6
\end{bmatrix} \tag{3.41}
$$

where

$$s_1 = -\frac{6I_y\rho}{5l(\phi_y + 1)^2}$$

$$s_2 = -\frac{\rho(70A\phi_x^2 l^2 + 147A\phi_x l^2 + 78Al^2 + 252I_x)}{210l(\phi_x + 1)^2}$$

$$s_3 = -\frac{Al\rho}{6}$$

$$s_4 = -\frac{l\rho(7A\phi_x^2 l^2 + 280I_x\phi_x^2 + 14A\phi_x l^2 + 140I_x\phi_x + 8Al^2 + 112I_x)}{840(\phi_x + 1)^2}$$

$$s_5 = -\frac{I_y l\rho(10\phi_y^2 + 5\phi_y + 4)}{30(\phi_y + 1)^2}$$

$$s_6 = -\frac{I_y l\rho}{6}$$

$$s_7 = \frac{I_y\rho(5\phi_y - 1)}{10(\phi_y + 1)^2} \tag{3.42}$$

$$s_8 = \frac{\rho(35A\phi_x^2 l^2 + 77A\phi_x l^2 - 420I_x\phi_x + 44Al^2 + 84I_x)}{840(\phi_x + 1)^2}$$

$$s_9 = -\frac{\rho(35A\phi_x^2 l^2 + 63A\phi_x l^2 + 27Al^2 - 252I_x)}{210l(\phi_x + 1)^2}$$

$$s_{10} = -\frac{\rho(35A\phi_x^2 l^2 + 63A\phi_x^2 l^2 + 420I_x\phi_x + 26Al^2 - 84I_x)}{840(\phi_x + 1)^2}$$

$$s_{11} = \frac{l\rho(7A\phi_x^2 l^2 - 140I_x\phi_x^2 + 14A\phi_x l^2 + 140I_x\phi_x + 6Al^2 + 28I_x)}{840(\phi_x + 1)^2}$$

$$s_{12} = \frac{I_y l\rho(-5\phi_y^2 + 5\phi_y + 1)}{30(\phi_y + 1)^2}$$

3.1.3.7 Modelling of a flexible disc

In the literature, flexible discs are customarily modelled using solid or shell elements. In the textbook [9], a simple model of a rim-with-spokes flywheel modelled using beam elements is shown to represent the dynamics of an axisymmetric structure. Unlike these studies, a special type of disc, in the form of a spiderweb, which can be modelled using beam elements is proposed in this study. An example of the proposed model is given in Figure 3.6. In this figure, black dots represent the nodes and the lines connecting these nodes are the finite beam elements. It is worth stating that this model may not yield very accurate quantitative results, e.g., natural frequencies, of flexible discs. However, such a model can be quite adequate for qualitative investigations of the effects of flexibility and gyroscopic effects of discs on the dynamics of a rotating system. The main advantage of using a spiderweb-like disc model is that it decreases the computational time and memory required for an analysis of a simplified rotating shaft-disc-blade system as the number of DOFs decreases enormously.

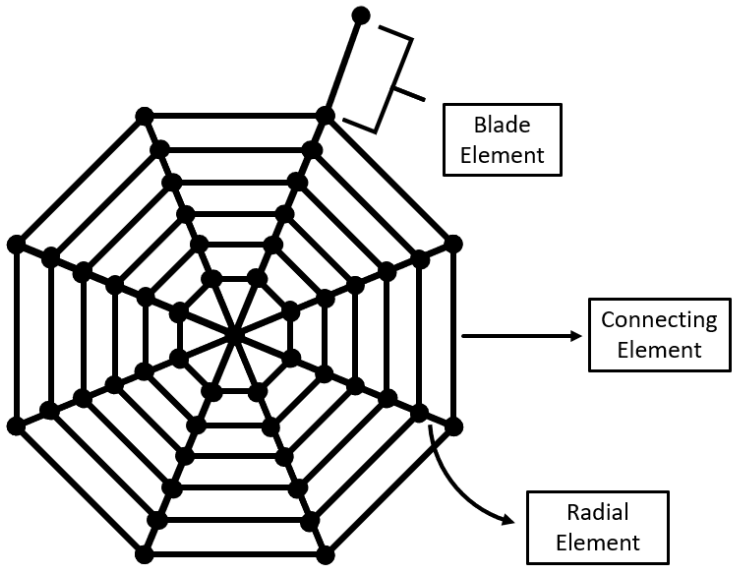

Figure 3.6 : Proposed spiderweb disc model with a blade element attached.

For the disc elements, there are two categories: radial elements and the so-called connecting elements between each branch of radial elements. As the name suggests, radial elements are the ones oriented radially from shaft just like blade elements. Therefore, for the radial elements of the disc, the matrices obtained for a blade are employed. Although the elements of the disc are discriminated as radial and connecting elements, the mathematical model of both element types is the same in the context of this thesis. Accordingly, the matrices of a blade are employed for the connecting elements, as well. Below, the formulation of a connecting element is briefly summarised for further clarification.

One can obtain the kinetic energy of a rotating connecting element by exploiting Figure 3.7. This figure depicts the location and orientation of an arbitrarily chosen connecting beam element on the disc with respect to rotating and stationary coordinate systems. Unlike the blade element, this time, rotating coordinate system's z_r axis is in the same orientation with connecting element's $\bar{y}$ axis. Also, now the position vector of local coordinate system $\bar{x}\bar{y}\bar{z}$ with respect to rotating coordinate system $x_r y_r z_r$ is represented by $\{r\} = \{0, r_y, r_z\}$.

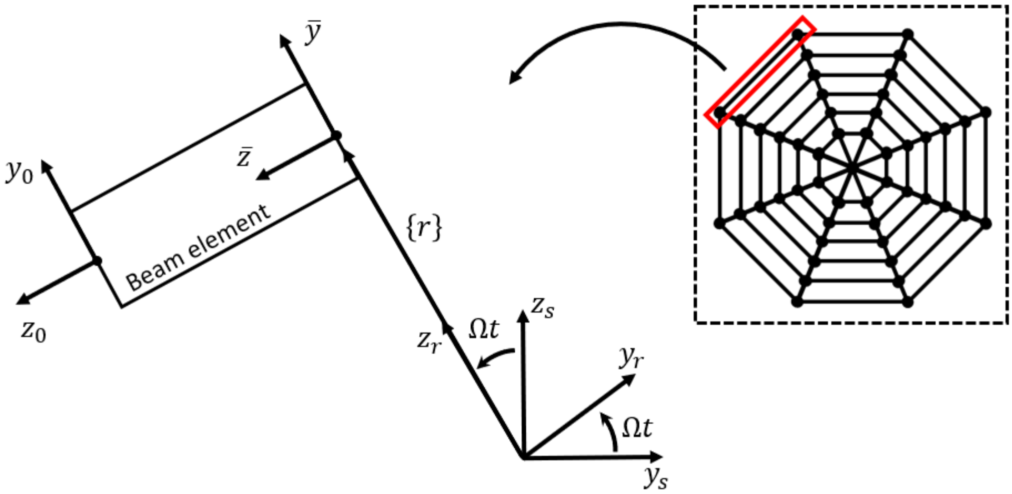

Figure 3.7 : Disc's connecting element and coordinate systems.

In this case, using Figure 3.7, position vector $\vec{r}_P$ of point P on the deformed blade can be expressed as

$$\vec{r}_P = [A_4]^T \left(\begin{bmatrix} 0 \\ r_y \\ r_z \end{bmatrix} + [A_5]^T \left(\begin{bmatrix} u \\ v \\ z + w \end{bmatrix} + [A_3]^T [A_2]^T [A_1]^T \begin{bmatrix} x \\ y \\ 0 \end{bmatrix} \right) \right) \tag{3.43}$$

where a new transformation matrix $[A_5]$ represents the transformation from rotating coordinate system to local coordinate system as

$$[A_5] = \begin{bmatrix} 1 & 0 & 0 \\ 0 & 0 & 1 \\ 0 & -1 & 0 \end{bmatrix} \tag{3.44}$$

Once the equation (3.43) is substituted into kinetic energy expression in (3.25), exactly the same expression given in equation (3.38) is obtained, as expected. Therefore, one can claim that the elements of both groups have the same mathematical model. This is expected since these elements lie in the plane of rotation and this situation is identical to blade elements as well.

Assembling a shaft-disc-blade system with this disc is straightforward. The disc shares one node in the middle with a shaft element when it is assembled. Blade elements are attached to the nodes at the perimeter of the disc as shown in Figure 3.6.

3.2 Modelling With Solid Elements

Due to the complex geometries of rotating structures, solid elements are commonly used in modern rotor dynamics as those elements are capable of representing the details of complex geometries. Although discretising the rotating bodies with solid elements is costly, as it increases the number of DOFs of the system significantly, the modelling procedure is relatively simpler than that of beam elements if the gyroscopic and spin softening effects are to be included. The reason for this is that one needs to deal with the orientation of the beam element with respect to the axis of rotation and depending on the orientation, a proper model should be employed as was shown previously. However, for a solid element, the orientation and the position of the element is known beforehand and defining a rotation matrix (equation (2.20)) depending on the global axis of rotation for all the solid elements of the body is sufficient. This could be the reason that some of the popular FEA programs are still not capable of modelling the gyroscopic effect of rotating beam elements which are not oriented parallel to the axis of rotation.

In the next section, conventional modelling of rotating solid elements that are utilised to discretise a rotating flexible disc and flexible blades is also presented. This made it possible to compare the dynamics of some rotating systems modelled using beam and solid elements.

3.2.1 Finite solid element

For modelling of both flexible disc and blades, isoparametric eight-noded linear hexahedral elements are used. This element and its nodes' coordinates in global and natural coordinate systems are shown in Figure 3.8. Shape functions of this element in natural coordinates are expressed as [72,83]

$$N_i = \frac{(1 + \xi\xi_i)(1 + \eta\eta_i)(1 + \zeta\zeta_i)}{8} \tag{3.45}$$

where the subscript i indicates the i'th node.

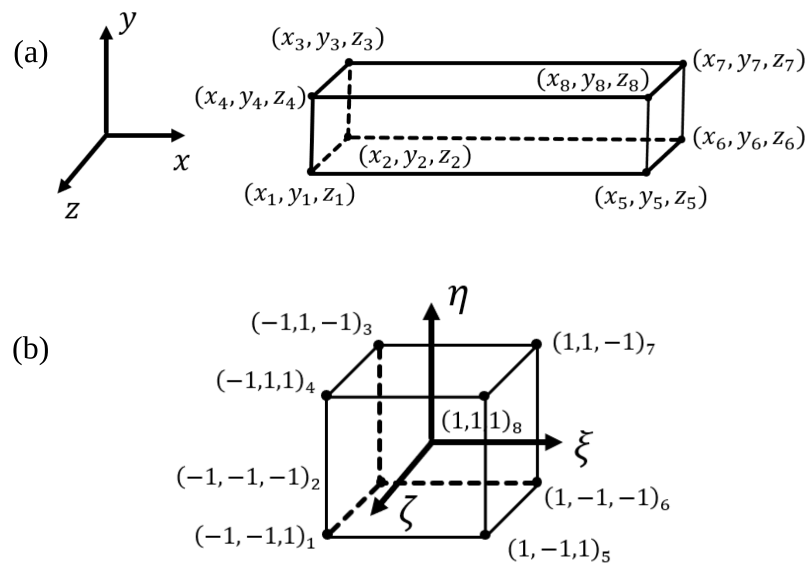

Figure 3.8 : (a) Linear hexahedral element and global coordinate system, (b) isoparametric element in natural coordinate system (adapted from [72]).

Consequently, there appears eight shape functions which are used to obtain the mass, stiffness, gyroscopic and spin softening matrices of the element.

3.2.2 Flexible bladed disc model

For flexible disc-blade model, also known as bladed disc model, the analysis is performed in rotating reference frame here. In Chapter 2, for a rotating general finite element, the derivation of the system matrices is given in global coordinate system. Here, an isoparametric formulation is adopted in order to obtain the system matrices for rotating systems. Before getting into more details, it should be noted that the formulated solid element can be used for modelling both discs and blades. Therefore, separate sub sections are not necessary for blades, discs etc. Actually, this is what makes solid element modelling easier in rotor dynamics.

Recalling the structural stiffness matrix for a general finite element in triple integral form as

$$[K] = \iiint [B(x,y,z)]^T [E][B(x,y,z)] dxdydz \tag{3.46}$$

in which the boundaries are dependent on the coordinates of the nodes. This formulation is obviously given in terms of global coordinates. In order to express the geometry of an isoparametric element, the shape functions in natural coordinates are used as [72,83]

$$x = \sum_{i=1}^{8} N_i(\xi, \eta, \zeta) x_i$$

$$y = \sum_{i=1}^{8} N_i(\xi, \eta, \zeta) y_i \tag{3.47}$$

$$z = \sum_{i=1}^{8} N_i(\xi, \eta, \zeta) z_i$$

The field variables within the element volume, e.g., the displacements, are also expressed, or interpolated, using the same shape functions as [72]

$$\begin{Bmatrix} u \\ v \\ w \end{Bmatrix} = \sum_{i=1}^{8} \left(\begin{bmatrix} N_i & 0 & 0 \\ 0 & N_i & 0 \\ 0 & 0 & N_i \end{bmatrix} \begin{Bmatrix} u_i \\ v_i \\ w_i \end{Bmatrix} \right) \tag{3.48}$$

Now, considering the $[B]$ matrix which contains the derivatives of shape functions with respect to global coordinates (x, y, z) in equation (3.46), a transformation is required between the coordinate systems. For this purpose, using the chain rule, shape function derivatives are expressed as [83]

$$\begin{Bmatrix} \dfrac{\partial N_i}{\partial \xi} \\ \dfrac{\partial N_i}{\partial \eta} \\ \dfrac{\partial N_i}{\partial \zeta} \end{Bmatrix} = \begin{bmatrix} \dfrac{\partial x}{\partial \xi} & \dfrac{\partial y}{\partial \xi} & \dfrac{\partial z}{\partial \xi} \\ \dfrac{\partial x}{\partial \eta} & \dfrac{\partial y}{\partial \eta} & \dfrac{\partial z}{\partial \eta} \\ \dfrac{\partial x}{\partial \zeta} & \dfrac{\partial y}{\partial \zeta} & \dfrac{\partial z}{\partial \zeta} \end{bmatrix} \begin{Bmatrix} \dfrac{\partial N_i}{\partial x} \\ \dfrac{\partial N_i}{\partial y} \\ \dfrac{\partial N_i}{\partial z} \end{Bmatrix} \tag{3.49}$$

in which the matrix on the right-hand side is called Jacobian matrix $[J]$ and can be obtained by using equation (3.47) as

$$[J] = \sum_{i=1}^{8} \begin{bmatrix} \dfrac{\partial N_i}{\partial \xi} x_i & \dfrac{\partial N_i}{\partial \xi} y_i & \dfrac{\partial N_i}{\partial \xi} z_i \\ \dfrac{\partial N_i}{\partial \eta} x_i & \dfrac{\partial N_i}{\partial \eta} y_i & \dfrac{\partial N_i}{\partial \eta} z_i \\ \dfrac{\partial N_i}{\partial \zeta} x_i & \dfrac{\partial N_i}{\partial \zeta} y_i & \dfrac{\partial N_i}{\partial \zeta} z_i \end{bmatrix} \tag{3.50}$$

Using the inverse of the Jacobian matrix and equation (3.49), derivatives of shape functions with respect to global coordinates in $[B]$ matrix are replaced with derivatives of shape functions with respect to natural coordinates.

Lastly, the required integration in global coordinates in equation (3.46) is expressed in natural coordinates using the integration differentials as

$$dxdydz = |J|d\xi d\eta d\zeta \tag{3.51}$$

where $|J|$ is the determinant of the Jacobian matrix. Finally, for an isoparametric hexahedral element, the stiffness matrix can be computed by

$$[K] = \int_{-1}^{1}\int_{-1}^{1}\int_{-1}^{1}[B(\xi,\eta,\zeta)]^T[E][B(\xi,\eta,\zeta)]|J|d\xi d\eta d\zeta \tag{3.52}$$

Similarly, the mass, gyroscopic and spin softening matrices are obtained using equation (2.34), (2.35) and (2.37). Since these matrices do not contain $[B]$, it is more straightforward to transform these expressions to natural coordinates and substituting equation (3.51) is sufficient for this purpose.

As mentioned, solid elements are general elements, which can be used for modelling shafts, discs or blades or any other rotating systems. It is worth stating again that depending on the axis of rotation of the element, the rotation matrix, $[S]$

$$[S] = \begin{bmatrix} 0 & -\Omega_z & \Omega_y \\ \Omega_z & 0 & -\Omega_x \\ -\Omega_y & \Omega_x & 0 \end{bmatrix} \tag{3.53}$$

should be evaluated and substituted in the gyroscopic and spin softening matrices, accordingly.

4. MODELLING AND ANALYSIS OF VARIOUS ROTATING SYSTEMS AND RESULTS

In this chapter, various rotating systems are generated, and discretised using beam and solid elements based on the mathematical models presented in the previous chapter, and their dynamic properties are predicted. Campbell diagrams, frequency split percentages and complex mode shapes are utilised to investigate the dynamics of rotating flexible discs and blades. Also, the spiderweb disc is introduced in this chapter for modelling the gyroscopic effects of flexible discs using beam elements. Moreover, besides the gyroscopic effect, other phenomena such as veering, merging, and coupling vibrations between components are discussed.

4.1 Analyses of Rotating Flexible Shaft-Rigid Disc and Flexible Shaft-Flexible Disc Systems

Literature survey presented before shows that the early models of rotating systems considered rotating discs as rigid members. This assumption can be valid for very thick discs. However, modern engineering structures consist of rotating thin flexible discs and therefore, some of the vibration modes of the discs are likely to be coupled with the shaft's modes. In this section it is aimed to show how a rotating shaft-disc system's natural frequencies change with increasing rotational speed due to the gyroscopic effect, and also to reveal the effect of disc's flexibility by using the mathematical models presented in the previous chapter.

4.1.1 Flexible shaft-rigid disc system

In Section 3.1.2, a well-known model of a flexible shaft-rigid disc system is presented. First, this model is used here to understand the dynamic behaviour of such a system. The results are to be compared with a freely accessible rotor dynamic program named "RotFE" [52]. For this purpose, a system shown in Figure 4.1, is designed. Material and geometric properties of this system are given in Table 4.1.

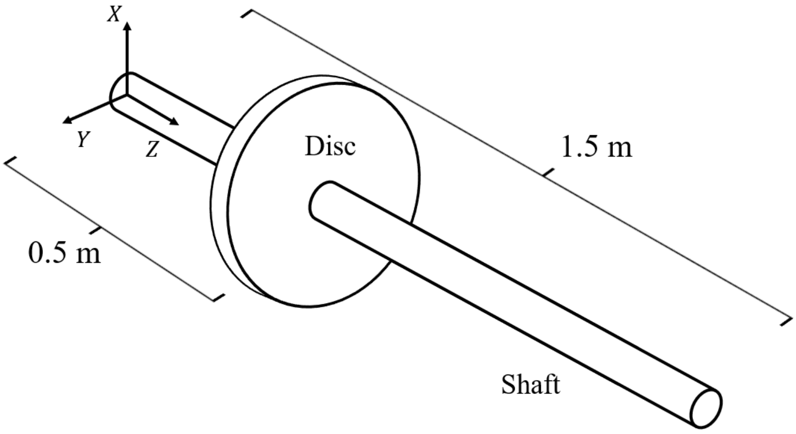

Figure 4.1 : Flexible shaft-rigid disc system.

Table 4.1 : Material and geometric properties.

Component	Property	Value
Shaft	Young's Modulus	210 GPa
	Density	7800 kg/m^3
	Poisson's Ratio	0.3
	Shear Correct. Factor	0.89
	Inner Radius	0
	Outer Radius	0.025 m
	Length	1.5 m
Rigid Disc	Mass	3.45 kg
	Inner Radius	0.025 m
	Outer Radius	0.2 m
	Thickness	0.008 m
Spiderweb Disc	Disc Outer Radius	0.2 m
	# of Radial Elements	10
	# of Connecting Elements	10
	Beams' radius	0.004 m

The natural frequencies and mode shapes of this system are predicted both by the mathematical model presented in this study and by RotFE program in stationary reference frame by the virtue of axisymmetry of the structure. The predicted natural frequencies are compared in Table 4.2. In both models, the system is constrained by fixing the transverse and angular degrees of freedom (u, v, θ, ψ) of the shaft's nodes at both ends. It should be recalled here that axial and torsional DOFs are excluded in the mathematical models. The computed modes are, obviously, the shaft's bending modes and named based on the bending order e.g., “Shaft 1B” represents the first bending mode of the shaft.

Table 4.2 : Natural frequency comparison of the flexible shaft-rigid disc system in stationary reference frame.

Mode	Whirl Direction	Rotational Speed (RPM)					
		0		5000		10000	
		Present Study (Hz)	RotFE [52] (Hz)	Present Study (Hz)	RotFE [52] (Hz)	Present Study (Hz)	RotFE [52] (Hz)
Shaft 1B	BW	91.36	91.36	90.64	90.64	89.90	89.90
	FW	91.36	91.36	92.06	92.06	92.73	92.73
Shaft 2B	BW	248.68	248.67	247.31	247.30	245.80	245.79
	FW	248.68	248.67	249.94	249.93	251.09	251.08
Shaft 3B	BW	496.59	496.57	480.71	480.69	464.12	464.10
	FW	496.59	496.57	511.48	511.45	525.18	525.15
Shaft 4B	BW	789.55	789.48	778.12	778.05	767.17	767.10
	FW	789.55	789.48	801.21	801.14	812.82	812.74
Shaft 5B	BW	1157.77	1157.60	1143.38	1143.21	1128.66	1128.50
	FW	1157.77	1157.60	1171.18	1171.02	1183.15	1182.98

Table 4.2 clearly shows that predicted natural frequencies at each rotational speed obtained from the model presented in this study and RotFE are perfectly in agreement with each other. In order to investigate the dynamics of the system in a rotational speed range, the present work is solved at each 1000 RPM step from 0 to 10000 RPM and a Campbell diagram (Figure 4.2) is plotted. In stationary reference frame analyses, gyroscopic moments cause the double modes to bifurcate. Bifurcated bending modes are visible in Figure 4.2. Frequency splits are used to characterise the influence of the gyroscopic effect. In this case, the Campbell diagram shows that lower modes do not experience a significant gyroscopic effect while higher modes do. This is reasonable since the beam elements experience greater angular displacements at higher modes, which enhances the effects of gyroscopic moments. Additionally, in a shaft-disc system, disc’s position plays an important role on the dynamics of the system [25]. If a disc is mounted at an antinode of a specific mode shape on the shaft, it can be anticipated that the disc will only exhibit translational motion but not a swing motion [25,49]. Obviously, in this situation, since the direction of angular momentum of the disc does not change during vibration, the gyroscopic moments are not generated.

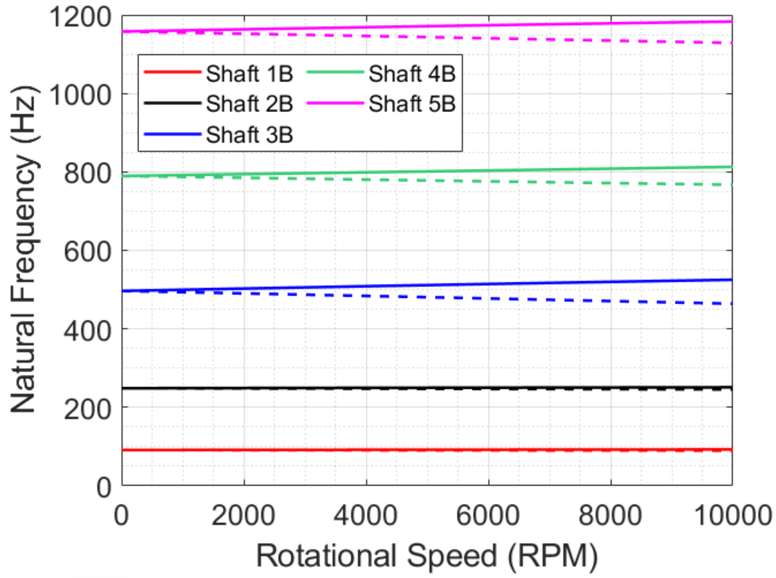

Figure 4.2 : Flexible shaft-rigid disc system's Campbell diagram in stationary reference frame (solid lines: forward, dashed lines: backward).

On the contrary, a disc located at a nodal point of a mode on the shaft is expected to exhibit a strong swing motion, thus strong gyroscopic moments are generated by the disc. In the present system, the disc was shown to be located at one third of the shaft. This results in a distinct frequency split in the third mode than in other modes since the disc's position on the shaft is a node of which the angular displacement is maximum for the third bending mode. This mode shape is illustrated in Figure 4.3. Lastly, it can be noticed that the natural frequencies change as a function of speed almost linearly. As will be shown later, once the flexibilities of the disc and blades are taken into account, this trend may hardly be observed due to the occurrence of interactions between flexible components, and the rotational effects.

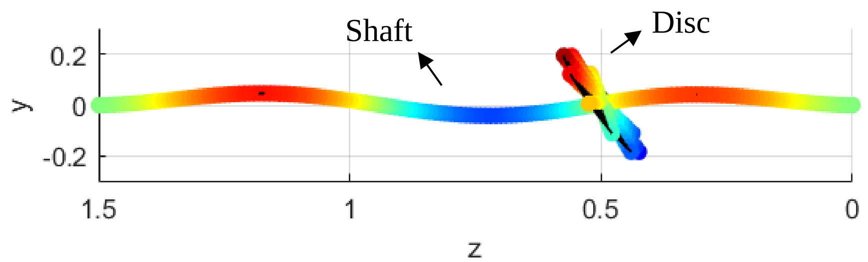

Figure 4.3 : Third bending mode of the flexible shaft-rigid disc system.

So far, the results have shown how a flexible shaft-rigid disc system behaves under the gyroscopic effects. In order to investigate the effect of disc flexibility and the capabilities of spiderweb disc model, new analyses are performed in the forthcoming section.

4.1.2 Flexible shaft-flexible disc system

In this thesis, a flexible shaft-flexible disc system is modelled based on the model given in Chapter 3 in which a spiderweb disc structure was proposed to investigate the effects of a flexible disc. This system is shown in Figure 4.4. The advantage of this approach is that this allows modelling the gyroscopic effects of shaft and disc using relatively simple beam elements. In order to compare the flexible and the rigid disc cases, the rigid disc's mass in the previous problem is matched with the mass of the proposed flexible spiderweb disc's model shown in Figure 4.4. Also, the radius and the thickness of both discs are the same so that the polar and diametral mass moments of inertia are identical. These geometric properties are given in Table 4.1 above. It should be noted that material properties of the disc are the same with the shaft.

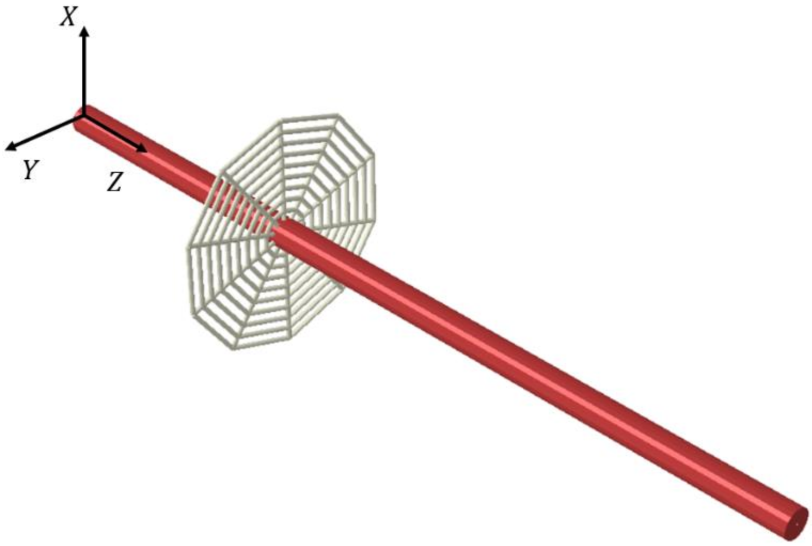

Figure 4.4 : Flexible shaft-flexible disc system proposed in this study (illustrated using Abaqus [84]).

Before performing the analysis for the flexible shaft-flexible spiderweb disc model, it would be appropriate to prove that the flexible spiderweb disc is capable of representing the inertial characteristics of the rigid disc. For this purpose, the Young's modulus of the beam elements of the disc given in Table 4.1 is multiplied with 10^6 in order to numerically force the disc to behave almost as a rigid disc. In other words, the disc is extremely stiffened, thus it will act like a rigid disc within the frequency range of interest. Results of the flexible shaft-rigid disc and the flexible shaft-rigid spiderweb disc are given in Table 4.3. It should be noted that only the shaft bending modes of the rigid spiderweb disc model are included and since the analysis of rigid spiderweb disc is performed in rotating reference frame, to be able to make a comparison, the natural frequencies are converted to stationary reference frame based on the transformation provided in Chapter 2.

Table 4.3 : Natural frequency comparison of the flexible shaft-rigid disc and the flexible shaft-rigid spiderweb disc model in stationary reference frame.

Mode	Whirl Direction	Rotational Speed (RPM)					
		0		5000		10000	
		Rigid Disc (Hz)	Spiderweb Disc (Hz)	Rigid Disc (Hz)	Spiderweb Disc (Hz)	Rigid Disc (Hz)	Spiderweb Disc (Hz)
Shaft 1B	BW	91.36	91.39	90.64	90.40	89.90	88.65
	FW	91.36	91.39	92.06	91.75	92.73	91.51
Shaft 2B	BW	248.68	248.80	247.31	247.29	245.80	245.10
	FW	248.68	248.80	249.94	249.78	251.09	250.34
Shaft 3B	BW	496.59	499.59	480.71	483.55	464.12	463.75
	FW	496.59	499.59	511.48	512.32	525.18	522.21
Shaft 4B	BW	789.55	793.05	778.12	781.62	767.17	769.46
	FW	789.55	793.05	801.21	803.46	812.82	812.70
Shaft 5B	BW	1157.77	1163.80	1143.38	1150.16	1128.66	1134.86
	FW	1157.77	1163.80	1171.18	1175.46	1183.15	1185.14

In Table 4.3 natural frequencies show a good agreement indicating high level of inertial similarity between the spiderweb disc model and a conventional rigid disc. Now, keeping everything related to the geometrical and material properties the same but lowering the Young's Modulus of the beam elements on the disc back to 210 GPa, leads to the flexible shaft-flexible disc model. This model's natural frequencies are determined via eigen solution. The natural frequencies of the system and the relevant Campbell diagram are presented in Table 4.4 and Figure 4.5, respectively. Modes of the system are named based on the mode shapes of the individual components. Shaft's bending modes are represented by "SxB" where x is the order of shaft bending mode. The flexible disc's mode shapes are named depending on the number of NDs occurring on the disc e.g., ND1 indicates a mode shape which exhibits only one ND pattern. Number of NCs are neglected. Additionally, umbrella and torsional modes of the disc are represented by "ND0-U" and "ND0-T" respectively. In order to represent the coupling of some modes, "+" sign is used. Also, a mode shape name written in parentheses indicates a weak coupling.

Table 4.4 : Natural frequencies of flexible shaft-flexible spiderweb disc model at different rotational speeds in rotating reference frame.

Mode Number	Mode Name	Whirl Direction	Natural Frequencies (Hz) 0 RPM	5000 RPM	10000 RPM	Freq. Split (% at 5000 RPM)
1	ND1 +	FW	83.22	8.39	76.15	89.91
2	(S1B)	BW	83.22	84.41	83.17	1.43
3	S1B +	FW	93.25	84.63	81.50	9.24
4	ND1	BW	93.25	175.30	258.43	87.99
5	ND0-U	-	127.82	127.81	127.79	0.01
6	ND2	FW	186.49	186.38	186.22	0.06
7		BW	186.49	186.56	186.59	0.04
8	S2B	FW	250.04	166.92	86.63	33.24
9		BW	250.04	333.10	416.09	33.22
10	ND0-T	-	370.87	361.37	331.26	2.56
11	ND3	FW	430.35	430.18	429.98	0.04
12		BW	430.36	430.49	430.60	0.03
13	ND0-U	-	531.99	531.96	531.89	0.01
14	S3B +	FW	537.24	455.95	373.37	15.13
15	ND1	BW	537.25	577.05	578.47	7.41
16	ND1 +	FW	581.42	579.73	579.04	0.29
17	(S3B)	BW	581.42	624.42	705.69	7.40
18	ND4	FW	753.03	752.81	752.56	0.03
19		BW	753.03	753.23	753.40	0.03
20	S4B +	FW	836.14	753.63	671.20	9.87
21	(ND1)	BW	836.26	918.62	1001.02	9.85

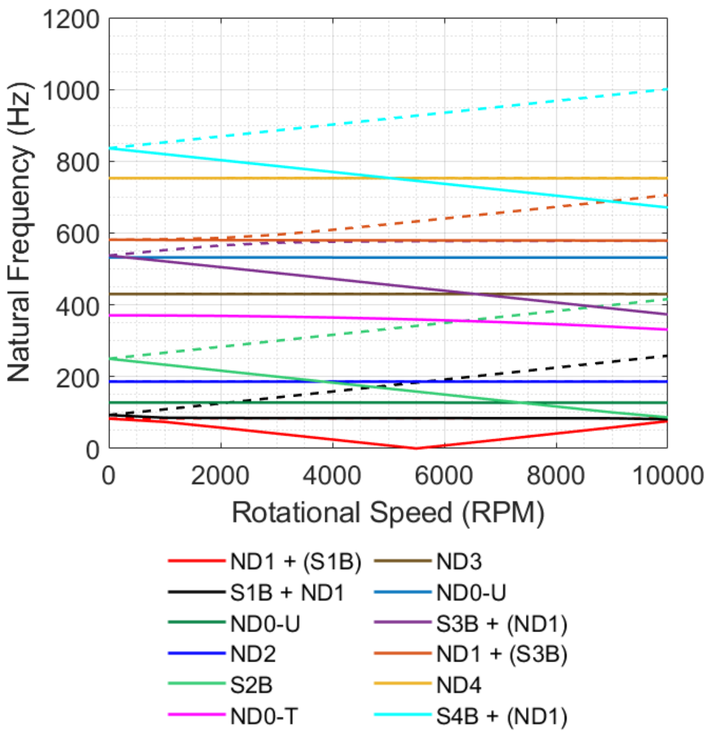

Figure 4.5 : Flexible shaft-flexible spiderweb disc system's Campbell diagram in rotating reference frame (solid lines: forward, dashed lines: backward).

Table 4.4 shows that, as anticipated, there now appears disc modes and shaft-disc coupled modes. It is seen that some of these coupled modes are identified as weak, meaning that a component's vibration is more dominant than the one given in parentheses. This is a crucial point and will be used to make inferences about each component's role in the rotating system's dynamics.

As mentioned earlier, in rotating reference frame, backward modes' frequencies increase, and forward modes' frequencies decrease with increasing rotational speed. This is obvious for every mode. However, the first mode in Table 4.4 is a forward whirl and its natural frequency decreases and eventually reaches zero at a particular rotational speed but then starts to increase. This is a probable case to encounter in analyses performed in rotating reference frame and is an indication of the critical speed of that mode (only for ND1 modes and shaft bending modes). Also, for a rotating observer, the whirl direction, and the travelling wave direction in this mode change from forward to backward after this certain speed.

It is possible to make inferences from Table 4.4 by looking at the frequency split percentages. In our case here, the modes in which the shaft is dominant are highly influenced by the Coriolis forces such that their frequencies seem to change more radically than the disc dominated modes with the increase of rotational speed. The same behaviour of the shaft has also been mentioned in reference [51]. If one recalls from the previous chapters, translational DOFs that are perpendicular to the axis of rotation generates the Coriolis forces and ultimately the gyroscopic effects. In a shaft bending mode, all nodes vibrate along the direction perpendicular to the axis of rotation. Meanwhile, in a disc's ND mode, the nodes substantially vibrate parallel to the axis of rotation. Therefore, it is reasonable to see that the shaft induces gyroscopic effect much more than the disc itself in the rotating reference frame. On the other hand, as the order of the shaft modes increase, some of the nodes along the shaft vibrate less due to the occurrence of nodal points. This, in return, decreases the effects produced by the Coriolis forces resulting in a less frequency split percentage in rotating reference frame. However, it is worth noting that, some modes do not seem to exhibit the behaviour explained so far. This is clearly a sign to show the analysts that these modes require a more detailed investigation as presented later in this section.

Normally, as explained in Chapter 2, for a non-rotating system, each bending mode of a shaft only takes place on a single plane. However, when the gyroscopic effect is present for a rotating body, each point on the shaft traces a circle, or an ellipse if the supports are not isotropic, in space instead of vibrating along a straight line. This whirling motion can be visualised by taking a point on the shaft and plotting its vibration pattern using the mode shape vector of a particular mode. For this purpose, the node where the disc is mounted on the shaft in flexible shaft-flexible spiderweb disc system is chosen and its vibration pattern is plotted. The forward and backward whirling motion of this node in "S2B" mode at 5000 RPM is illustrated in Figure 4.6.

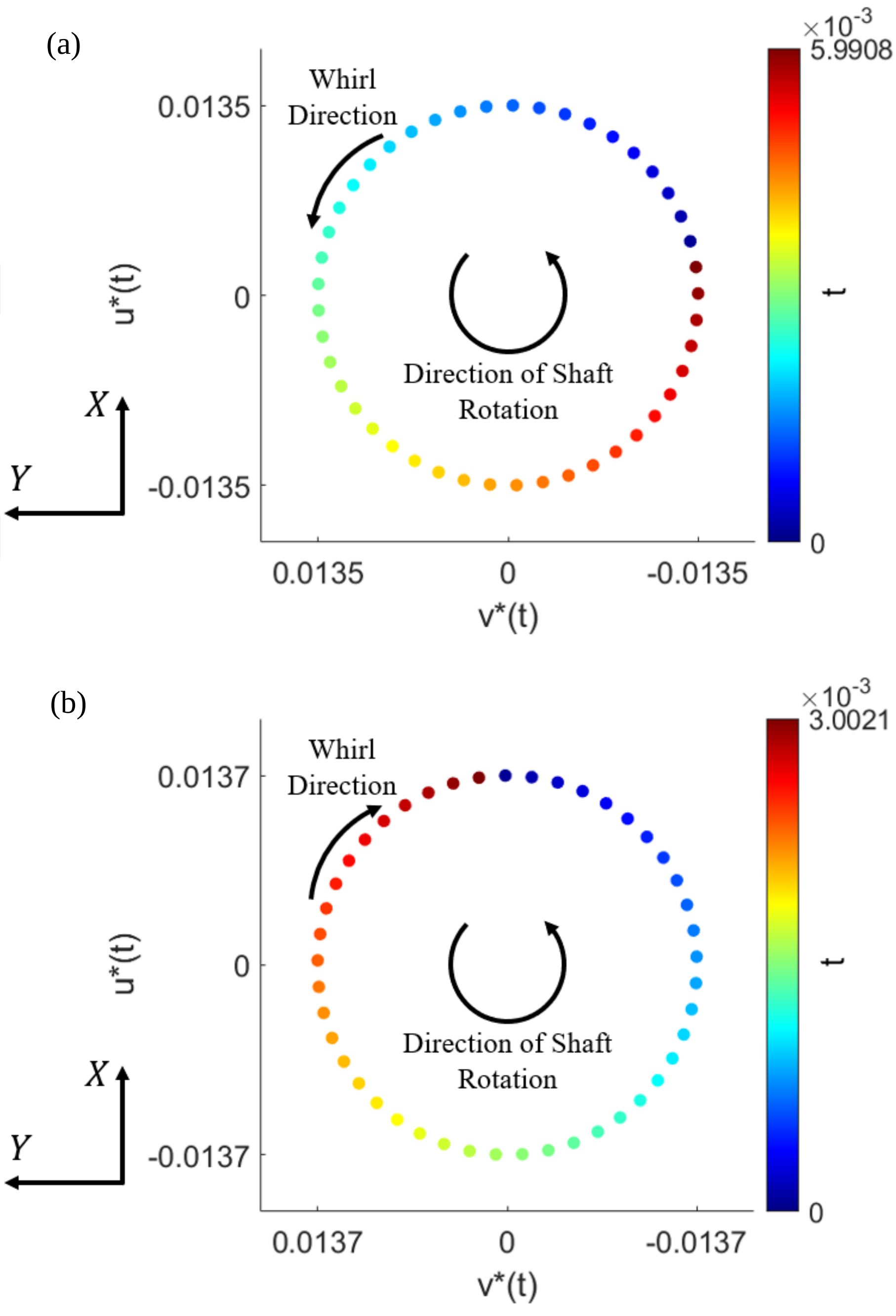

Figure 4.6 : (a) Forward and (b) backward whirl of the node at the disc location of the shaft in "S2B" mode.

A colour bar is utilised in Figure 4.6 to easily compare the whirl direction and the direction of the shaft rotation. It should be noted that throughout this chapter, free vibration patterns of the nodes on the system at a natural frequency in a vibration period, T, are presented using

$$u^*(t) = |u_n| \cdot \cos(\omega_n t + \phi_{u,n})$$
$$v^*(t) = |v_n| \cdot \cos(\omega_n t + \phi_{v,n}) \tag{4.1}$$
$$w^*(t) = |w_n| \cdot \cos(\omega_n t + \phi_{w,n})$$

where $t = [0, T]$ in seconds, ω_n is the n'th mode's natural frequency ($^{rad}/_{s}$); $|u_n|$, $|v_n|$ and $|w_n|$ are the amplitudes of unit normalised complex mode shape of the related node in the global X, Y and Z, respectively and $\phi_{u,n}$, $\phi_{v,n}$, $\phi_{w,n}$ are the phase angles of the related node's translational DOFs in the n'th mode. Obviously; $u^*(t)$, $v^*(t)$ and $w^*(t)$ represent the vibration pattern that the related node undergoes in global X, Y and Z axes in a specific mode shape in a vibration period.

A quick inspection of Figure 4.6 reveals that the node traces a perfect circle, as expected. Also, the direction of the whirl is in the same direction with the shaft rotation in the forward mode and in the opposite direction in the backward mode. This fact holds for all the nodes on rotating shaft systems unless the mode exhibits a mixed whirl which is not the case here.

Now, the unusual behaviour observed in some modes can be discussed. In the light of the information given so far, one may expect to observe higher frequency split in the shaft dominated "S3B + ND1" than the disc dominated "ND1 + (S3B)" mode. Although this is true for the forward whirl modes, the backward whirl modes do not seem to obey this trend and have a different split percentages than their forward pairs (Table 4.4). This phenomenon can also be detected easily when the related modes' frequencies are plotted in a single Campbell diagram apart from the other modes. This diagram is shown in Figure 4.7(a). By looking at this figure, the occurrence of veering phenomenon between the modes is evident. The modes' frequencies get closer with the increase of rotational speed up to a certain speed. After that, they immediately veer away and go on their separate ways. It was stated that, this interaction causes the mode shapes to be exchanged [61,63]. This can be visualised by plotting the mode shapes at different rotational speeds. These mode shapes are provided in Figure 4.7(b-g).

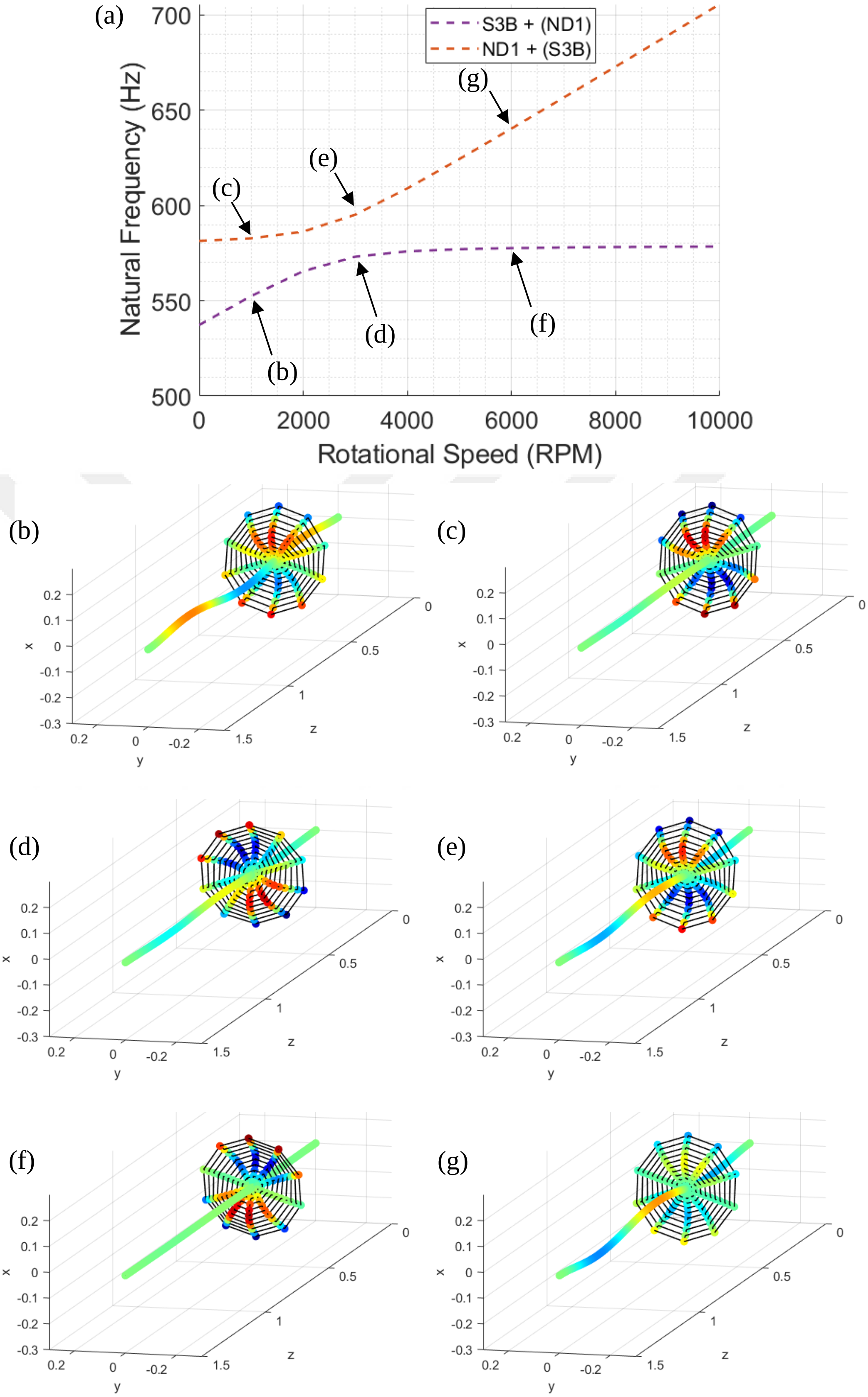

Figure 4.7 : (a) Campbell diagram and (b-g) the complex mode shapes of the veered modes at different rotor speeds (dashed lines in the Campbell diagram represent the backward pairs).

Another occurrence of veering will show that detection of veering may not always be this much easy. During the analysis, a detailed investigation revealed that there exists a “hidden” veering at around 600 RPM between the first and the third modes. This interaction is characterised as hidden because it was stated that the solutions are performed at each 1000 RPM implying that a solution at 1000 RPM is not able to capture this phenomenon since the interaction is already completed until the rotational speed reaches this speed. For a clear understanding, lets visualise this phenomenon from 0 to 1000 RPM by performing the analysis at each 100 RPM step. The Campbell diagram of the interacted modes are shown in Figure 4.8.

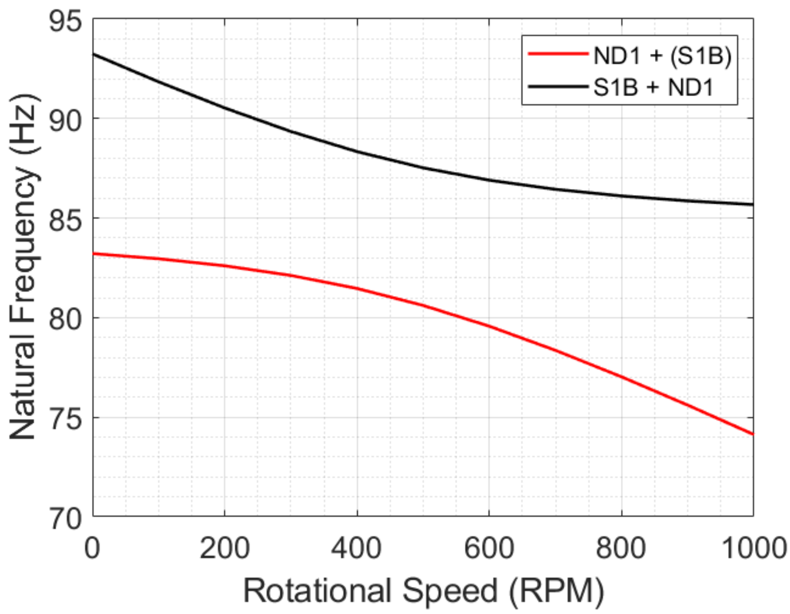

Figure 4.8 : Depiction of veering between forward modes of “ND1 + (S1B)” and “S1B + ND1”.

So far, the results are presented in rotating reference frame. By applying the procedure explained in Chapter 2, the natural frequencies and the Campbell diagram can also be obtained in stationary reference frame as shown in Table 4.5 and Figure 4.9. It should be noted that the natural frequencies of “ND0-U” and “ND0-T”, which are the umbrella and the torsional vibration modes of the disc respectively, are assumed to remain the same as the rotational speed increases since in these mode shapes neither the shaft nor the disc can generate gyroscopic moments in the stationary reference frame [85]. Thus, for a clear visualisation, these modes are excluded from the Campbell diagram in Figure 4.9.

Table 4.5 : Natural frequencies of flexible shaft-flexible spiderweb disc model at different rotational speeds in stationary reference frame.

Mode Number	Mode	Whirl Direction	Natural Frequencies (Hz)			Freq. Split (% at 5000 RPM)
			0 RPM	5000 RPM	10000 RPM	
1	ND1 + (S1B)	FW	83.22	91.73	90.52	10.22
2		BW	83.22	1.07	83.50	98.71
3	S1B + ND1	FW	93.25	167.97	248.16	80.12
4		BW	93.25	91.96	91.76	1.38
5	ND0-U	-	127.82	127.82	127.82	0.00
6	ND2	FW	186.49	353.04	519.56	89.31
7		BW	186.49	19.90	146.74	89.33
8	S2B	FW	250.04	250.25	253.30	0.09
9		BW	250.04	249.77	249.42	0.11
10	ND0-T	-	370.87	370.87	370.87	0.00
11	ND3	FW	430.35	680.18	929.98	58.05
12		BW	430.36	180.49	69.40	58.06
13	ND0-U	-	531.99	531.99	531.99	0.00
14	S3B + ND1	FW	537.24	539.28	540.04	0.38
15		BW	537.25	493.72	411.80	8.10
16	ND1 + (S3B)	FW	581.42	663.06	745.71	14.04
17		BW	581.42	541.09	539.03	6.94
18	ND4	FW	753.03	1086.14	1419.23	44.24
19		BW	753.03	419.89	86.73	44.24
20	S4B + (ND1)	FW	836.14	836.96	837.87	0.10
21		BW	836.26	835.29	834.36	0.12

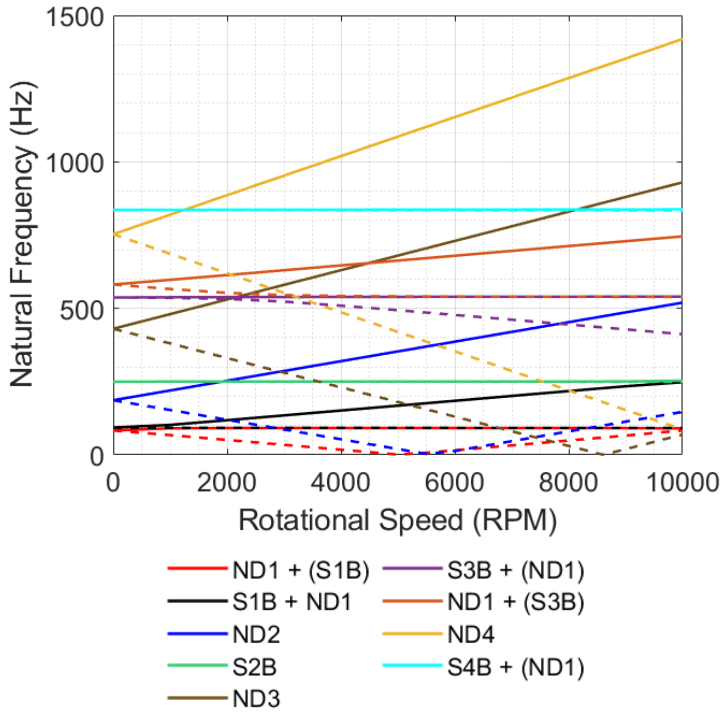

Figure 4.9 : Campbell diagram of the flexible shaft-flexible spiderweb disc system in stationary reference frame (solid lines: forward, dashed lines: backward).

In stationary reference frame, gyroscopic moments are generated by rotational DOFs as opposed to the Coriolis forces generated by the translational DOFs in rotating reference frame. Hence, early modes of the shaft do not generate significant gyroscopic moments due to the relatively lower levels of normalised vibrations of angular DOFs. At the same time, the disc modes are now highly influenced by the gyroscopic effects as each portion between NDs on the disc tries to change the axis of rotation which is known to be the source of gyroscopic moments. However, higher the ND in a mode, the stiffer the mode is. In other words, as the order of the disc modes increases, the disc becomes more rigid, and this reduces the gyroscopic effects of the disc.

It is no surprise that the "S2B" modes do not exhibit a significant bifurcation in stationary reference frame. This situation was the same with the rigid spiderweb disc-flexible shaft model given in Table 4.3 and can be better understood once the forward mode shapes of both cases at 5000 RPM are plotted (Figure 4.10).

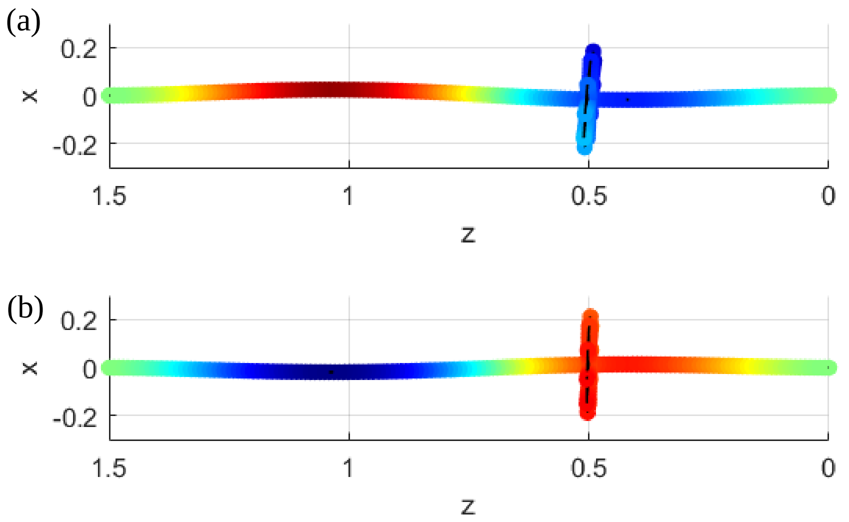

Figure 4.10 : Forward mode shapes of "S2B" at 5000 RPM: (a) rigid spiderweb disc, (b) flexible spiderweb disc.

In Figure 4.10 it is seen that the disc is located close to an antinode, hence it does not precess significantly. Furthermore, approximately the same frequency split percentages of both cases indicate that the flexibility of the disc may not matter if the disc is located near an antinode since it predominantly experiences translational motion. As it can be seen in Table 4.5, the frequency split percentages of "S4B + (ND1)" modes in stationary reference frame are unexpectedly low. To have an insight into these results, the forward mode shape at 5000 RPM is plotted in Figure 4.11.

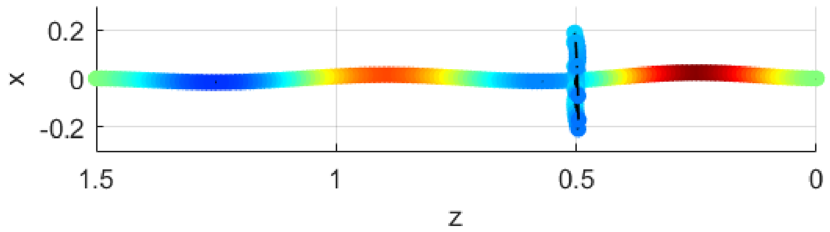

Figure 4.11 : Forward mode shape of “S4B + (ND1)” at 5000 RPM.

Interestingly, unlike the first and second bending modes, there appears a nodal diameter and a nodal circle on the disc. Let’s express these mode shapes with (m, n) where m represents the number of nodal diameters and n represents the number of nodal circles. Although, Figure 4.11, the disc seems to be close to a nodal point, it does not swing like a (1,0) mode. A similar case has been shown in reference [54] in page 444. The mode shapes of a flexible shaft-two flexible discs system provided in this reference showed that tilting motion of the flexible disc induces an evident frequency split in the stationary reference frame. However, despite the discs are located on a nodal point, (1,1) mode of the discs does not cause a strong gyroscopic effect during shaft bending.

So far in this section, the apparent differences between rigid and flexible disc assumptions are presented by investigating the dynamics of systems with rigid and flexible discs. It is seen that besides the strong gyroscopic effects generated by the flexible disc, strong interactions between modes are likely to occur when the rigid disc assumption is put aside. Also, the veering phenomenon occurring between the first and the third mode showed that very careful inspection of the results at as many rotational speeds as possible are required to reveal such phenomenon. The disc’s position and flexibility can be changed parametrically to further analyse the influence of the disc on the system’s dynamics.

4.2 Analysis of a Rotating Flexible Shaft-Disc-Blade System

The dynamics of rotating blades is a focus of interest in the literature. In fact, as referred to in the literature survey, significant amount of studies in the literature focused on isolated rotating blades. This approach is certainly favourable to examine its behaviour under rotational effects. However, it will be insufficient to make comments about rotating blades’ effects on a complete shaft-disc-blade system.

After studying the influence of a flexible disc on a rotating system, one can now take one more step further by adding flexible blades onto the disc. This way, the system becomes more complicated owing to the unique dynamic behaviour of rotating blades. In this context, ten flexible blades are added to the previously analysed flexible shaft-flexible disc system. This system is illustrated in Figure 4.12. The material and geometric properties of the shaft and the disc elements (Table 4.1) are left unchanged. The blades have the same material properties as with the shaft and the disc elements. Also, each blade is assumed to be 0.075 m long and has a rectangular cross-sectional area with dimensions 0.015×0.003 m.

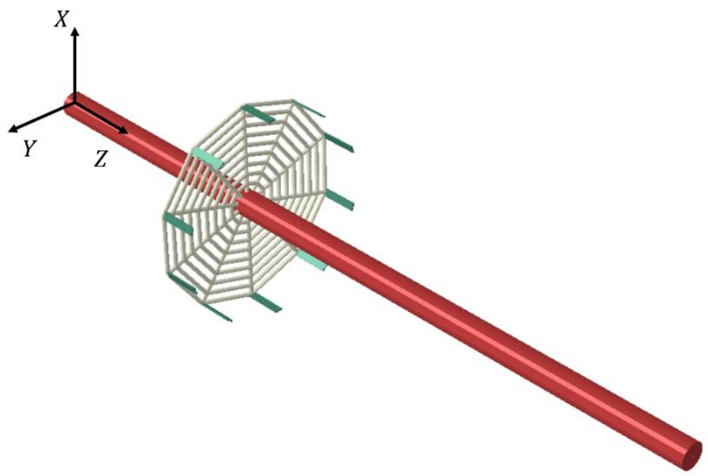

Figure 4.12 : Fully flexible shaft-disc-blade system (illustrated using Abaqus).

Despite the blades in engineering applications are generally oriented radially outwards, in this study, the blades are oriented perpendicular to the disc and parallel to the axis of rotation in order to enhance the Coriolis forces [39,43]. This way, the bifurcation of the double modes will be much more evident.

As before, the natural frequencies and mode shapes of the system is determined via eigen solution at each 1000 RPM step from 0 RPM to 10000 RPM. The frequency split percentage is computed for each mode at 5000 RPM and presented in Table 4.6 along with the natural frequencies of the modes at rest and at different rotational speeds. The Campbell diagram is plotted in Figure 4.13 In addition to the mode shape naming convention explained previously, in order to refer to blade modes, expression “BxB” is used, which represents the x’th bending mode of the blades. It is detected that there appear some modes in which the disc does not exhibit significant or visible vibrations. In such cases, “-Px” extension is used where x represents the nodal diameter pattern of the blades in order to have an understanding of the relative phase of individual blades to each other. For instance, “B1B-P4” mode in Table 4.6 indicates that each blade vibration is described as the first bending mode of vibration, but when all the blades are observed, there appears four NDs between the blades and consequently, a phase angle exists between the blades on both sides of these nodal lines. Correspondingly, the “B1B-P5” mode in Table 4.6 indicates that the blades vibrate in their first bending mode, but out of phase relative to each other since there are ten blades mounted on the disc. Therefore, this mode is not a double mode and travelling waves do not appear.

Table 4.6 : Natural frequencies of flexible shaft-disc-blade system at different rotational speeds in rotating reference frame.

Mode Number	Mode Name	Travelling Wave Dir.	Natural Frequencies (Hz)			Freq. Split (% at 5000 RPM)
			0 RPM	5000 RPM	10000 RPM	
1	ND1	FW	75.96	7.56	76.02	90.05
2		BW	75.96	77.40	76.02	1.90
3	S1B + ND1	FW	92.19	74.66	68.91	19.01
4		BW	92.19	174.61	257.74	89.41
5	ND0-U	-	116.49	116.15	114.62	0.29
6	ND2	FW	162.48	154.62	140.48	4.83
7		BW	162.48	166.51	167.77	2.48
8	S2B + B1B	FW	247.98	164.97	81.88	33.47
9		BW	247.98	329.69	323.24	32.95
10	ND3 + B1B	FW	336.60	309.56	270.04	8.03
11		BW	336.60	354.10	353.95	5.20
12	ND0-U	-	352.16	340.63	306.88	3.28
13	B1B-P1	FW	367.51	356.47	323.80	3.00
14		BW	367.82	359.17	415.02	2.35
15	ND0-T	-	368.09	361.81	340.97	1.71
16	B1B-P4	FW	400.05	375.30	327.18	6.19
17		BW	400.06	393.52	354.62	1.63
18	B1B-P2	FW	401.18	385.36	347.33	3.94
19		BW	401.18	395.80	372.11	1.34
20	B1B-P5	-	406.50	390.64	346.69	3.90
21	B1B + (ND3)	FW	440.74	409.10	372.29	7.18
22		BW	440.74	458.15	464.31	3.95
23	S3B + B1B + (ND1)	FW	538.45	456.73	374.86	15.18
24		BW	538.46[a]	-	-	-

[a]This mode undergoes an interaction with another mode outside of the frequency range of interest. The natural frequencies at other rotational speeds are excluded.

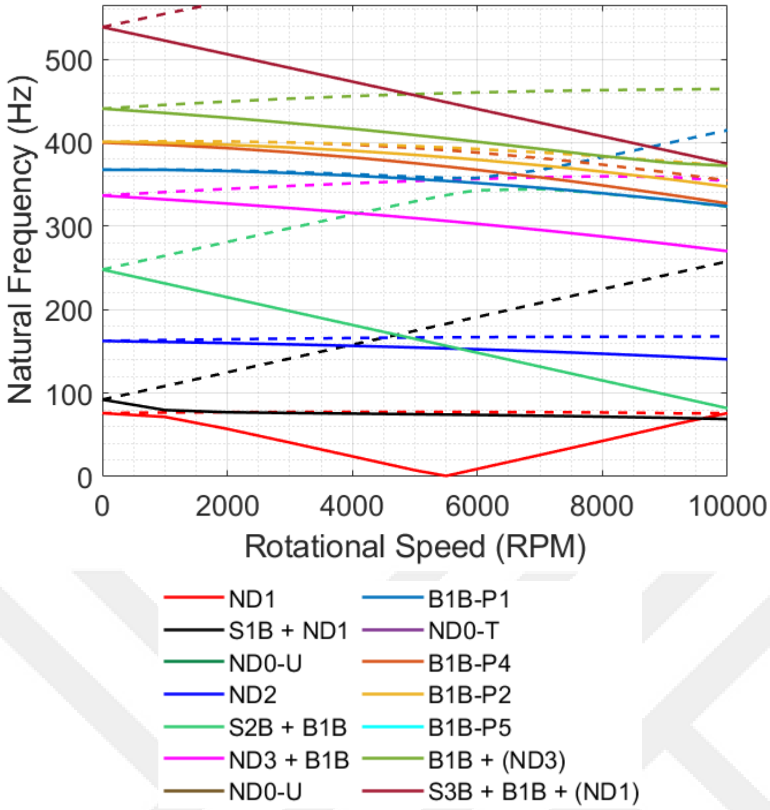

Figure 4.13 : Campbell diagram of the flexible shaft-disc-blade system in rotating reference frame (solid lines: forward, dashed lines: backward).

Unlike the flexible shaft-flexible disc system, the frequency split percentages in Table 4.6 are not the same for each pair of the double modes this time. This is also evident in the Campbell diagram in Figure 4.13. The modes in which the blades actively vibrate relative to other components exhibit a strong softening effect with increasing rotational speed. Therefore, one should be aware that this time, frequency split percentages are strongly influenced by the spin softening effect rather than the gyroscopic effect.

It was shown that the disc dominated modes of flexible shaft-flexible disc system were not strongly influenced by the gyroscopic effects in rotating reference frame. This time, it is seen that there is a significant split percentage for the disc modes. This is the result of rotational effects generated by the blade bending.

Similar to the previous section, “ND1” forward mode and “S1B + ND1” forward mode are interacted through veering and mode shapes are exchanged before the rotational speed reaches 1000 RPM in the current case. This is the reason why “ND1” forward mode quickly decreases to zero and then starts to increase again. Shaft vibration becoming dominant causes this evident change in the forward mode in rotating reference frame. For brevity, this veering is not presented here again.

Obviously, “ND1” forward mode changes whirl direction. Since the analyses are performed at each 1000 RPM step, the speed at which the mode reaches zero is not visible. Therefore, an additional analysis is carried out at 5500 RPM to approximately locate where the line intersects the horizontal axis. By looking at Figure 4.13, one can conclude that there is a critical speed around 5500 RPM.

In Table 4.6, it is seen that “B1B-P4” modes have lower frequency than “B1B-P2” modes at 0 RPM. Normally, one would expect to observe the opposite result. In order to explain this, an investigation on both modes’ shapes should be conducted. In Figure 4.14, vibration pattern of the disc in both mode shapes are presented. It should be noted that the colouring of the nodes is adjusted to only represent the DOF in the global Z direction. It is clearly seen that in “B1B-P4” mode, the roots of the blades exhibit an evident vibration. Meanwhile, in “B1B-P2” mode, the root nodes seem to be more stationary. Therefore, in “B1B-P2” mode, the natural frequency is higher than the “B1B-P4” mode’s natural frequency.

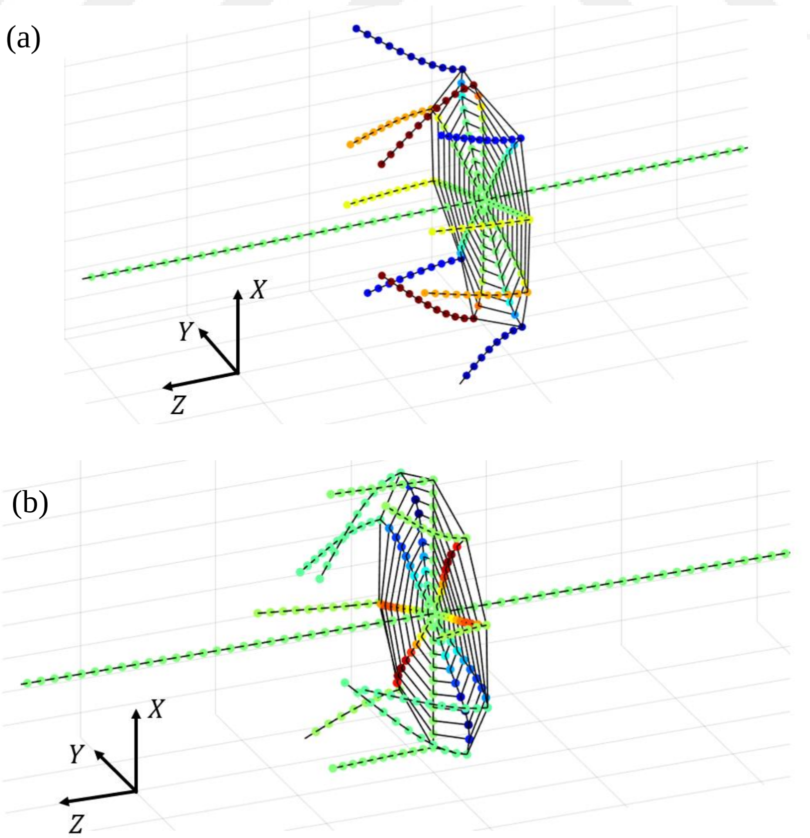

Figure 4.14 : Mode shapes of (a) “B1B-P4” and (b) “B1B-P2” at 0 RPM.

Finally, regarding the mode shapes, for the modes in which the shaft actively plays a role, the splits can be observed easily. This situation is in accordance with the previous case and the gyroscopic effect generation mechanism of a flexible shaft was already mentioned. It should also be noted that disc modes with ND's greater than one do not couple with the shaft modes. Some of the mode shapes at 5000 RPM are given in Figure 4.15.

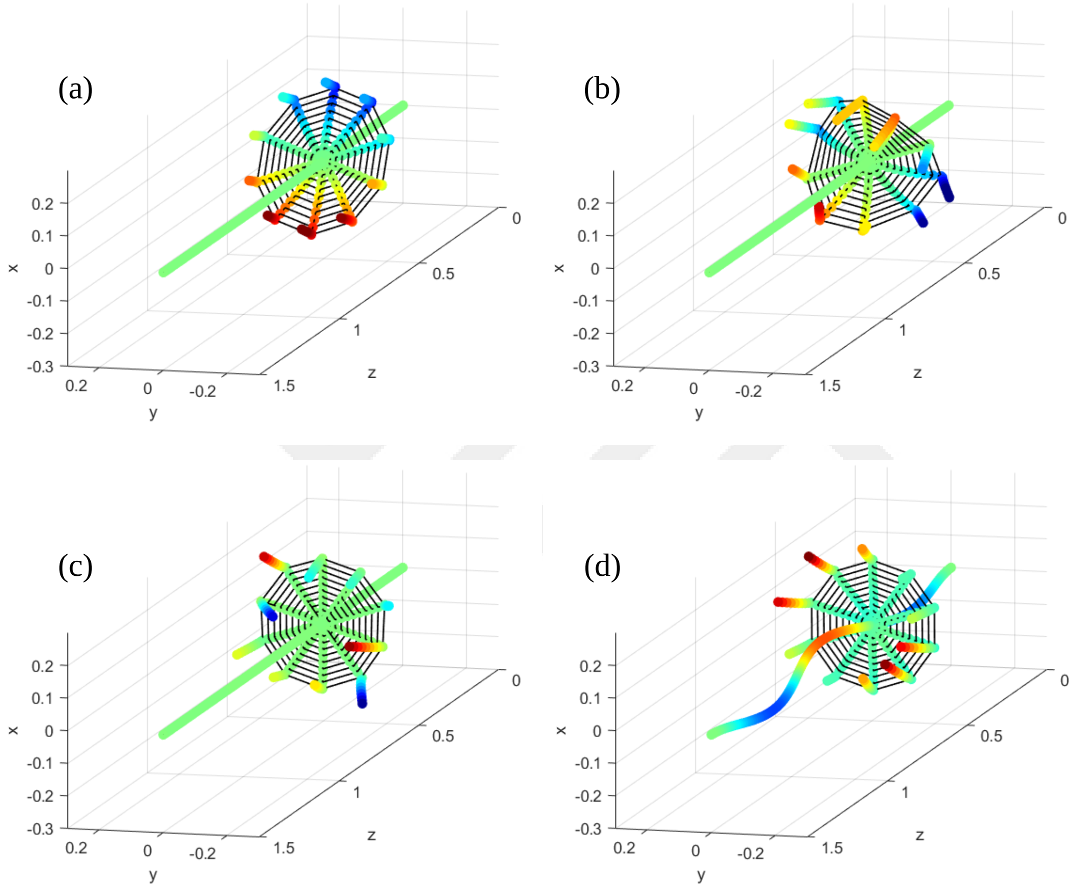

Figure 4.15 : Some of the mode shapes of flexible shaft-disc-blade system at 5000 RPM: (a) ND1, (b) ND2, (c) B1B-P4, (d) S3B + B1B + (ND1).

In Chapter 2, it was mentioned that strict caution is required to identify and keep track of the modes as the rotor speed increases. This is especially important for such cases where modes frequently cross over one another and the veering phenomenon is likely to occur. In the previous case, the difference between frequency split percentages of the two double modes revealed the occurrence of a veering. Unfortunately, in the present case, the given percentages do not help much to detect this critical phenomenon. Therefore, each mode's frequencies and mode shapes should be carefully analysed at each rotor speed in the analysis range. By such an investigation, the present case is determined to be exhibiting two veering interactions. These veered modes are shown in Figure 4.16 and Figure 4.17. As anticipated, mode shape exchanges take place between these interacted modes. Furthermore, an abrupt change in dynamic behaviour as a function of rotor speed is obvious.

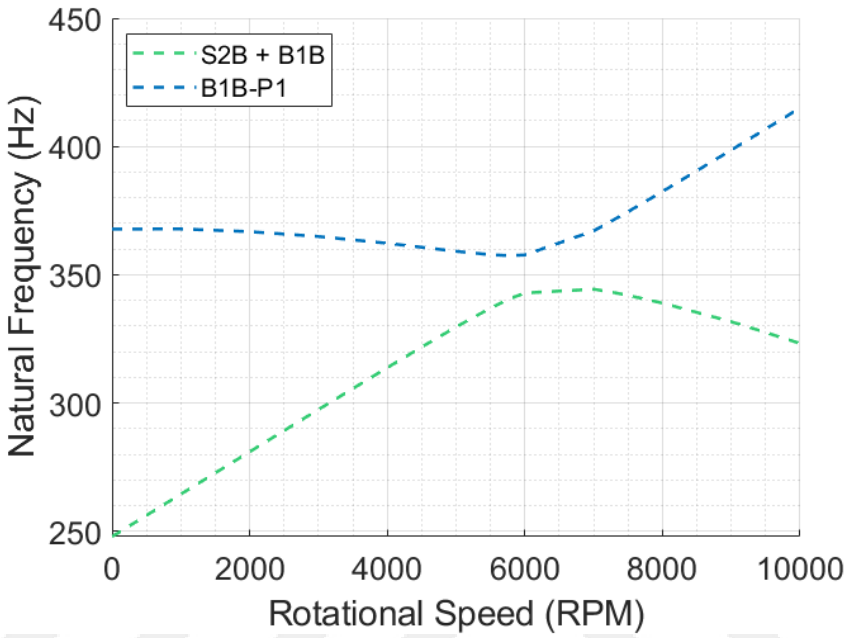

Figure 4.16 : Depiction of the veering between "S2B + B1B" and "B1B-P1" modes.

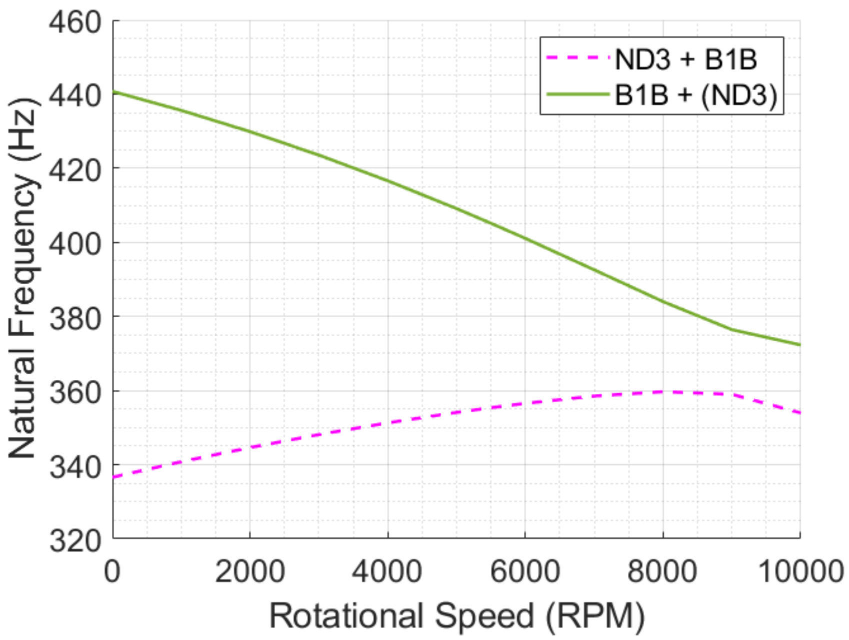

Figure 4.17 : Depiction of the veering between “ND3 + B1B” and “B1B + (ND3)” modes (solid lines: forward, dashed lines: backward).

At 10000 RPM one can see that “ND1” backward and forward modes have unexpectedly the same natural frequencies (Table 4.6). A close investigation of these mode shapes and eigenvalues around this rotor speed reveals a type of “instability”. These two different modes get too close with increasing rotational speed and eventually “merge”. They increase simultaneously in an interval of rotational speed. After the rotational speed passes this interval, the modes are separated again. This type of instability is mentioned in some sources [38,44,48,51,55]. As it was stated in Chapter 2, real parts of eigenvalues are related to the stability condition of the related modes. A positive real part was said to be an indication of an instability. Accordingly, references [38,55] state the fact that the real parts of eigenvalues of the relevant modes arise and change significantly in the merging region although damping is not present in the system. In our case here, the merging of frequencies and the real part of eigenvalues are plotted as a function of rotational speed in the merging region in Figure 4.18 and Figure 4.19, respectively. Here, it should be recalled that forward modes of “ND1” and “S1B + ND1” modes are interacted through veering causing the mode shapes to be exchanged before 1000 RPM. Therefore, obviously, the mode shapes of “ND1” pairs are totally different outside of the instability region. However, in order to prevent a possible confusion, names of modes that undergo veering are not changed in this thesis.

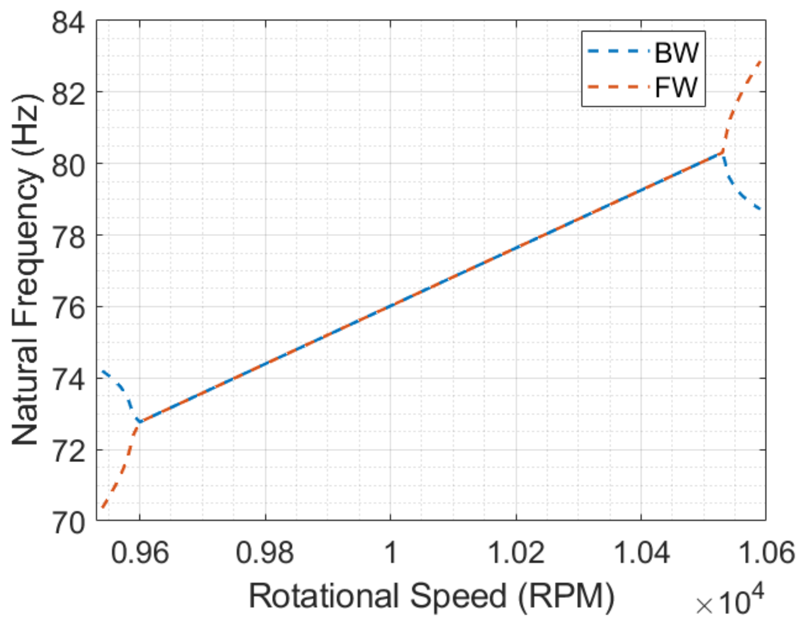

Figure 4.18 : Depiction of the merging between backward and forward modes of “ND1”.

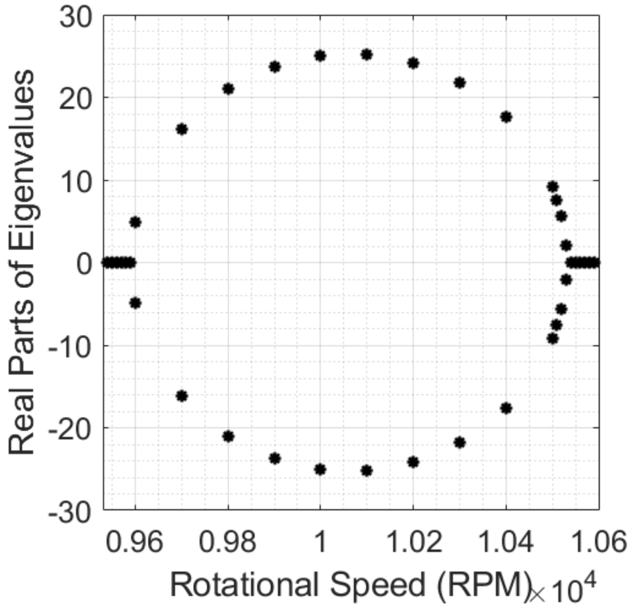

Figure 4.19 : Real parts of eigenvalues of forward and backward “ND1” modes as a function of rotational speed.

It is observed that in the merging region both modes have the same mode shapes. MAC (modal assurance criterion) values are given in Table 4.7 for comparison. Firstly, let’s recall that “ND1” forward mode exchanged its mode shapes with “S1B +ND1” forward mode at around 600 RPM. Since the whirl directions and vibration patterns are different, MAC values are null before 5500 RPM. However, after this speed, forward mode changed its whirl direction in rotating reference frame (Figure 4.13) moreover, the mode shapes started to look alike as shown by the MAC value at 7000 RPM. In the merging region, mode shapes are clearly the same. After passing the merging region, the similarity decreases as indicated by the decreasing MAC values. The mode shape in the merging region resembles an imaginary mode shape “ND1 + (S1B)” (which do not exist in the case here) in which the shaft is weakly coupled to an “ND1” disc mode. Evidently, this indicates that the shaft vibration of backward “ND1” mode becomes more active and the shaft vibration of forward “ND1” mode (interacted with “S1B + ND1” mode through veering) becomes less active in the merging region. This also implies that not only a single mode shape is changed but both modes change to a common mode shape.

Lastly, it is worth mentioning here that reference [48] states that merging phenomenon disappears as the disc in a shaft-disc-blade system gets thicker. This claim, surely, emphasises the influence of disc flexibility in a shaft-disc-blade system.

Table 4.7 : MAC values of the merged modes at different rotational speeds.

Rotational Speed (RPM)	MAC Values (%)	Rotational Speed (RPM)	MAC Values (%)
3000	0	10400	98.85
5000	0	11000	92.25
7000	73.39	12000	62.39
9000	93.81	13000	33.37
9800	98.61	14000	15.36

The results of this system suggest that a fully flexible rotating shaft-disc-blade system has more complicated dynamic characteristics than the model without rotating blades and other conventional flexible shaft-rigid disc systems. Moreover, it can be concluded that the model presented so far is capable of presenting frequency splits due to the gyroscopic effect, strong spin softening effect generated by flexible blades, veering interactions and instabilities which are common, yet critical, phenomena to encounter in rotor dynamics.

4.3 Analyses of Rotating Flexible Bladed Disc Systems

4.3.1 Flexible bladed spiderweb disc

In the previous section, the complicated dynamics of a rotor system was investigated. It was seen that the disc modes with ND's greater than one do not couple with the shaft modes. Therefore, as shown in the literature survey, there are studies which ignore the shaft and focus only on the bladed disc for higher order modes of vibration. Especially the studies which aim to investigate mistuning phenomenon. Thus, modelling and computational effort of the shaft can be avoided in order to minimise the total computational cost.

In this section, only the bladed disc (Figure 4.20) presented in the previous section is investigated to show how a rotating bladed disc behaves under gyroscopic and spin softening influence. The results are given in Table 4.8 and the corresponding Campbell diagram is presented in Figure 4.21.

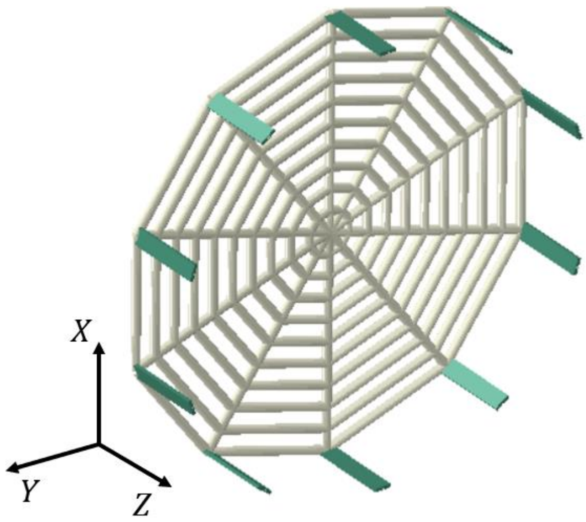

Figure 4.20 : Flexible bladed disc model (illustrated using Abaqus).

Table 4.8 : Natural frequencies of the bladed spiderweb disc system in rotating reference frame.

Mode Number	Mode Name	Travelling Wave Dir.	Natural Frequencies (Hz)			Freq. Split (% at 5000 RPM)
			0 RPM	5000 RPM	10000 RPM	
1	ND1	FW	77.31	74.67	68.96	3.41
2		BW	77.31	78.00	76.84	0.90
3	ND0-T	-	115.91	100.57	37.55	13.23
4	ND0-U	-	116.56	116.87	115.57	0.27
5	ND2	FW	162.48	154.61	140.43	4.84
6		BW	162.48	166.50	167.71	2.48
7	ND3 + B1B	FW	336.60	309.55	270.01	8.04
8		BW	336.60	354.09	353.95	5.20
9	ND0-U	-	352.32	345.65	324.58	1.89
10	B1B + (ND1)	FW	366.21	354.24	321.64	3.27
11		BW	366.21	356.50	323.40	2.65
12	B1B-P4	FW	400.05	375.30	327.18	6.19
13		BW	400.05	393.52	354.62	1.63
14	B1B-P2	FW	401.18	385.36	347.34	3.94
15		BW	401.18	395.80	372.11	1.34
16	B1B-P5	-	406.49	390.64	346.69	3.90
17	B1B + (ND3)	FW	440.74	409.09	372.24	7.18
18		BW	440.74	458.15	464.29	3.95
19	ND0-U	-	563.88	562.20	557.86	0.30
20	ND1 + B1B	Mixed	593.21	588.30	582.22	0.83
21			593.21	595.21	594.19	0.34
22	ND4 + B1B	FW	614.26	604.39	606.46	1.61
23		BW	614.26	633.60	653.46	3.15

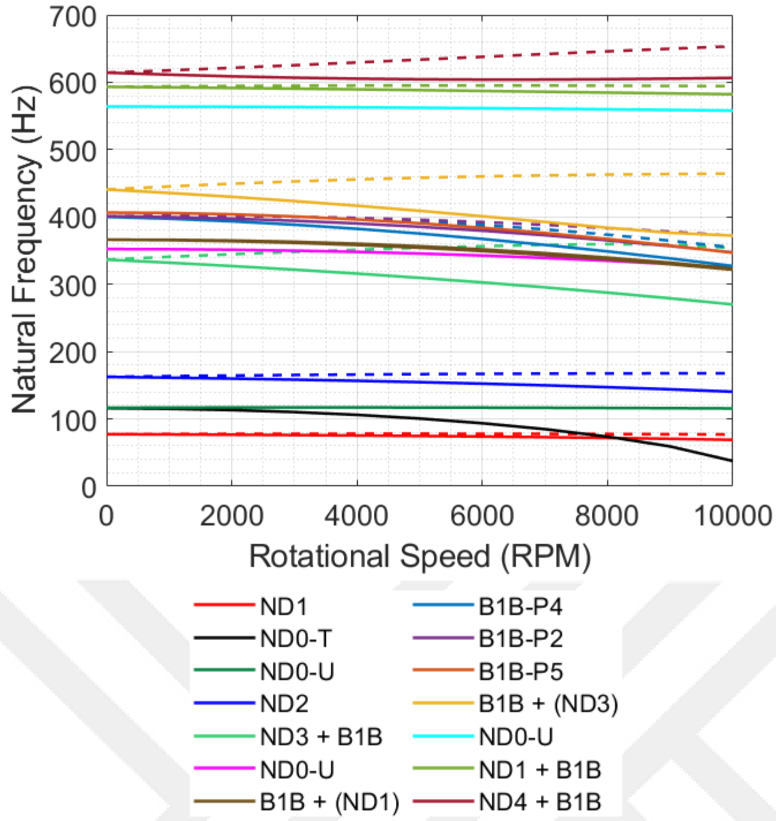

Figure 4.21 : Flexible bladed spiderweb disc system's Campbell diagram in rotating reference frame (solid lines: forward, dashed lines: backward).

The results show that the dissimilarity of the frequency split percentages between the double modes caused by the existence of the blades applies here, as well. The blade dominated modes are highly influenced by the spin softening. In fact, the backward modes' frequencies of these mode shapes which are expected to be increasing due to Coriolis forces, decreases with increasing speed. Meanwhile, the modes with remarkable disc vibration exhibits an evident split between backward and forward modes. This behaviour can be explained by investigating the mode shapes of these modes. For this purpose, let's plot the backward modes' frequencies of "B1B-P2" and "B1B + (ND3)" as a function of rotational speed (Figure 4.22).

It is seen that both backward frequencies increase at lower rotational speeds. Although this trend continues for the "B1B + (ND3)" mode, the spin softening effect takes over in the "B1B-P2" mode at approximately 1000 RPM. Nikolic et al. [39] states that the Coriolis forces affect the amount of coupling between tangential and radial displacements of the blades. In other words, if the Coriolis forces are strong, so is the coupling between the displacements in both direction and ultimately the gyroscopic effect in rotating reference frame.

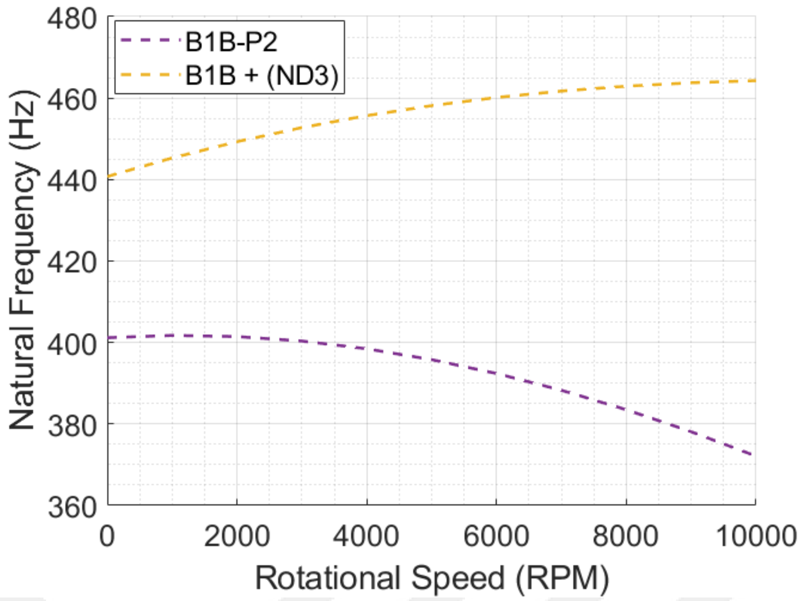

Figure 4.22 : Natural frequencies of “B1B-P2” and “B1B + (ND3)” as a function of rotational speed.

In order to examine the coupling between radial and tangential motions of blades in the aforementioned modes, orbital motion of the tip of a blade (the farthest one in the global X direction in Figure 4.20) in both modes at 1000 and 5000 RPM is plotted in Figure 4.23. The related vibration patterns are computed by using equation (4.1). However, the amplitude, $|u_n|$, in both modes are normalised to 1 to have an accurate comparison of the coupling. It should be noted that for the relevant blade, the radial motion and the tangential motion is represented by $u^*(t)$ and $v^*(t)$, respectively.

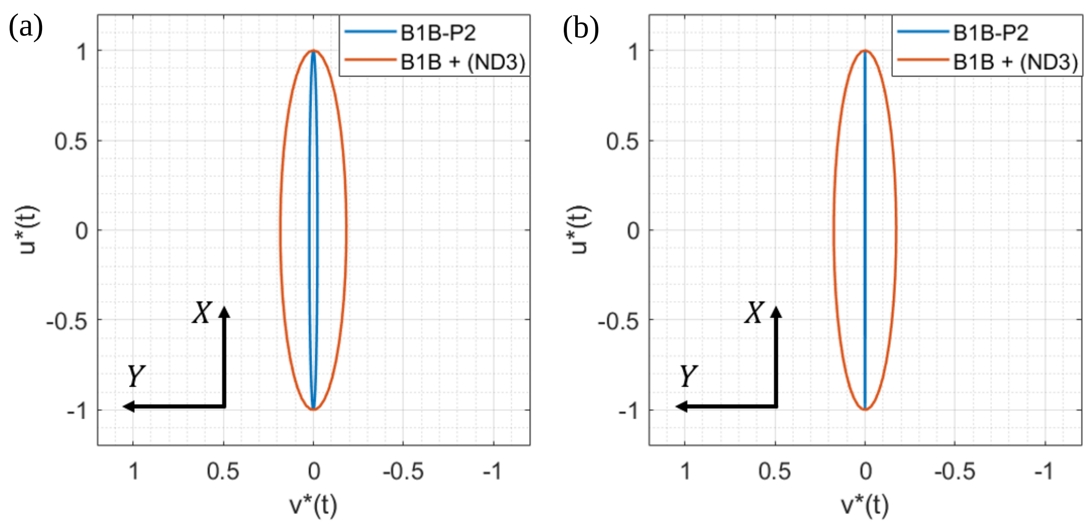

Figure 4.23 : Blade tip orbit in “B1B-P2” and “B1B + (ND3)” modes at (a) 1000 RPM and (b) 5000 RPM.

From Figure 4.23 it is clearly seen that the there is almost no coupling between the radial and the tangential displacement components in “B1B-P2” mode. At the same time, an elliptic orbital motion of the blade tip is clearly visible in “B1B + (ND3)” mode indicating the source of apparent gyroscopic effect in Figure 4.21. It should be noted that this behaviour is the same for other modes, but the blade tip orbits are not provided here for brevity.

This model can be used to demonstrate the occurrence of travelling waves on the disc and the whirling behaviour of the blades. For this purpose, the nodes at the perimeter on the disc, shown in Figure 4.24, are taken into account.

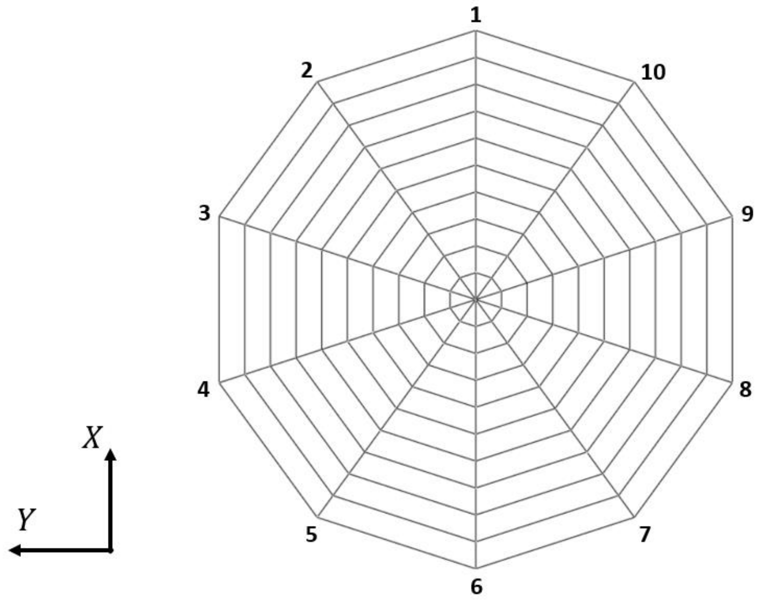

Figure 4.24 : Enumeration of the nodes at the perimeter of the disc.

The normalised displacements of these nodes for one period along global Z direction for two different modes (“ND1” and “ND2”) at 5000 RPM are illustrated in Figure 4.25 and Figure 4.26. It should be noted that all amplitudes, $|w_n|$, of nodes 2-10 (Figure 4.24) are normalised with the amplitude of node 1 for visual purposes. These results allow one to determine the travelling wave direction and compare it with the direction of rotation in order to determine whether a mode is a forward or a backward mode. As expected, the opposite nodes on the disc have the same phase in “ND2” mode therefore, the solid lines are overlapping with their dashed line pairs in Figure 4.26.

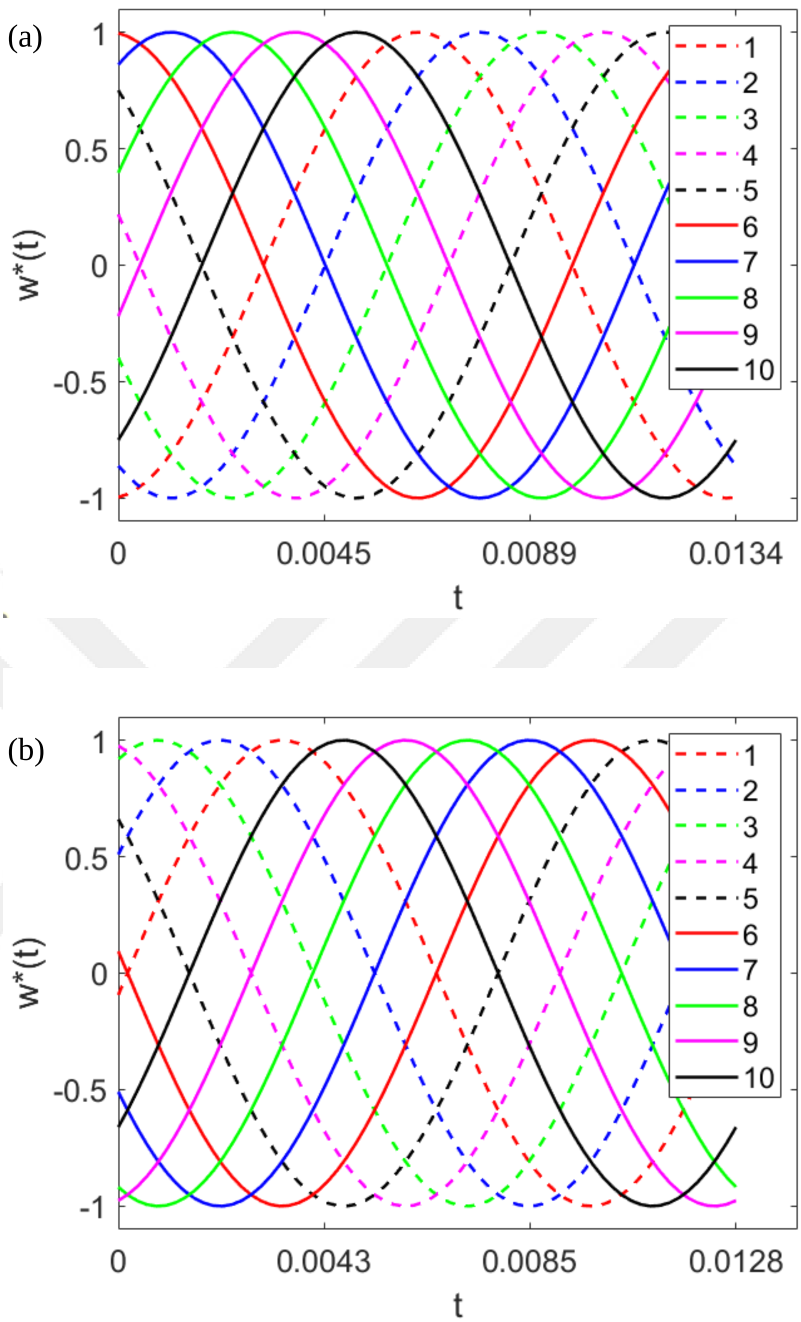

Figure 4.25 : The normalised displacements of the nodes on the disc for a period along the global Z direction in ND1 mode, (a) forward mode, (b) backward mode.

A mode can be designated forward or backward provided that the whole system exhibits the same wave/whirl direction. In Table 4.8, the double modes of "ND1 + B1B" are designated as "mixed" because both modes are observed to exhibit both forward and backward wave/whirl directions, simultaneously. In order to prove this, the related lower frequency mode at 5000 RPM is chosen. The normalised displacements ($w^*(t)$) on the disc along the global Z direction in this mode is plotted in Figure 4.27(a). Additionally, the orbital motion of the tip of the blade that is connected to the node 1 (Figure 4.24) in the same mode shape is plotted in Figure 4.27(b).

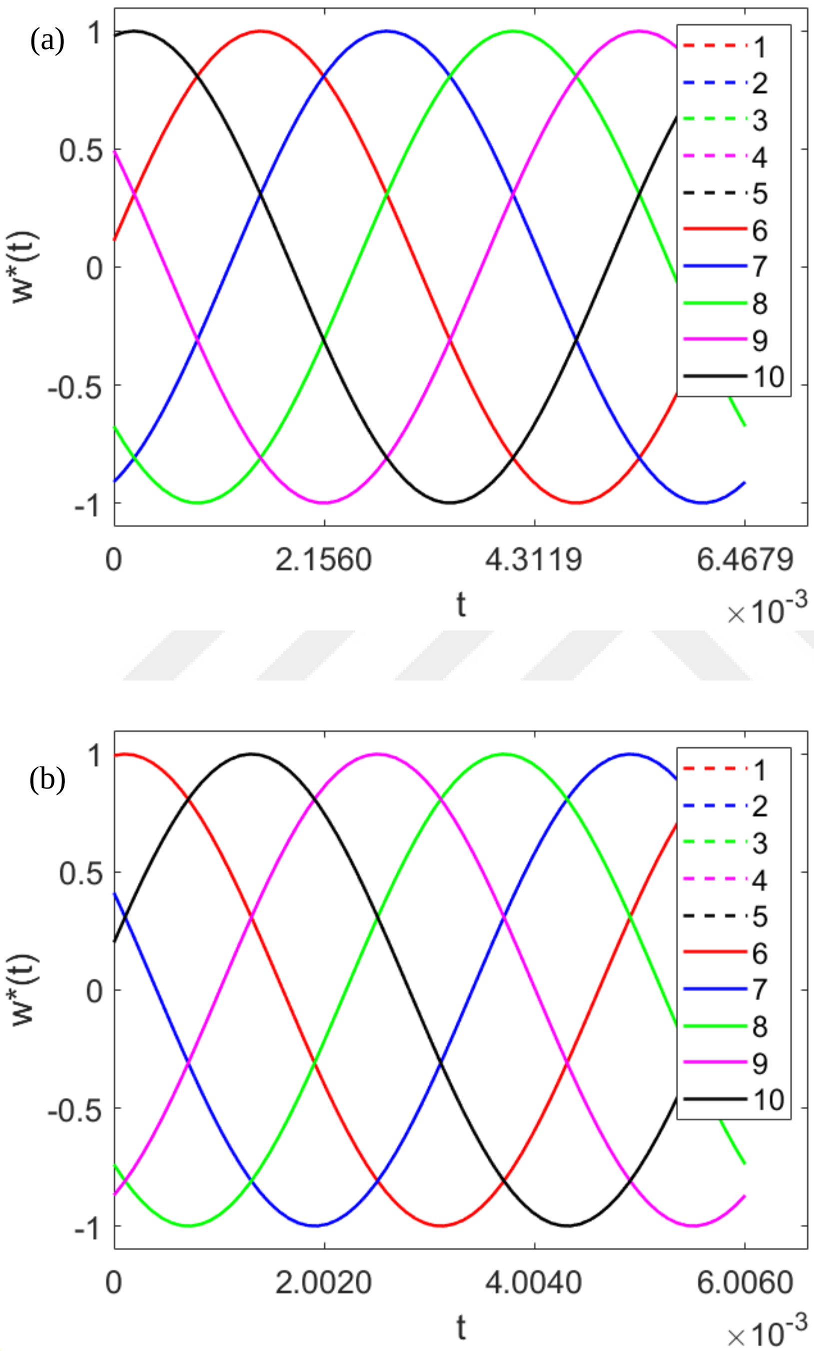

Figure 4.26 : The normalised displacements of the nodes on the disc for a period along the global *Z* direction in ND2 mode, (a) forward mode, (b) backward mode.

It can be seen in Figure 4.27(a) that there appears a travelling wave on the disc in backward direction while in Figure 4.27(b) the blade elliptically whirls in the forward direction. Therefore, a certain direction cannot be assigned to this mode [86].

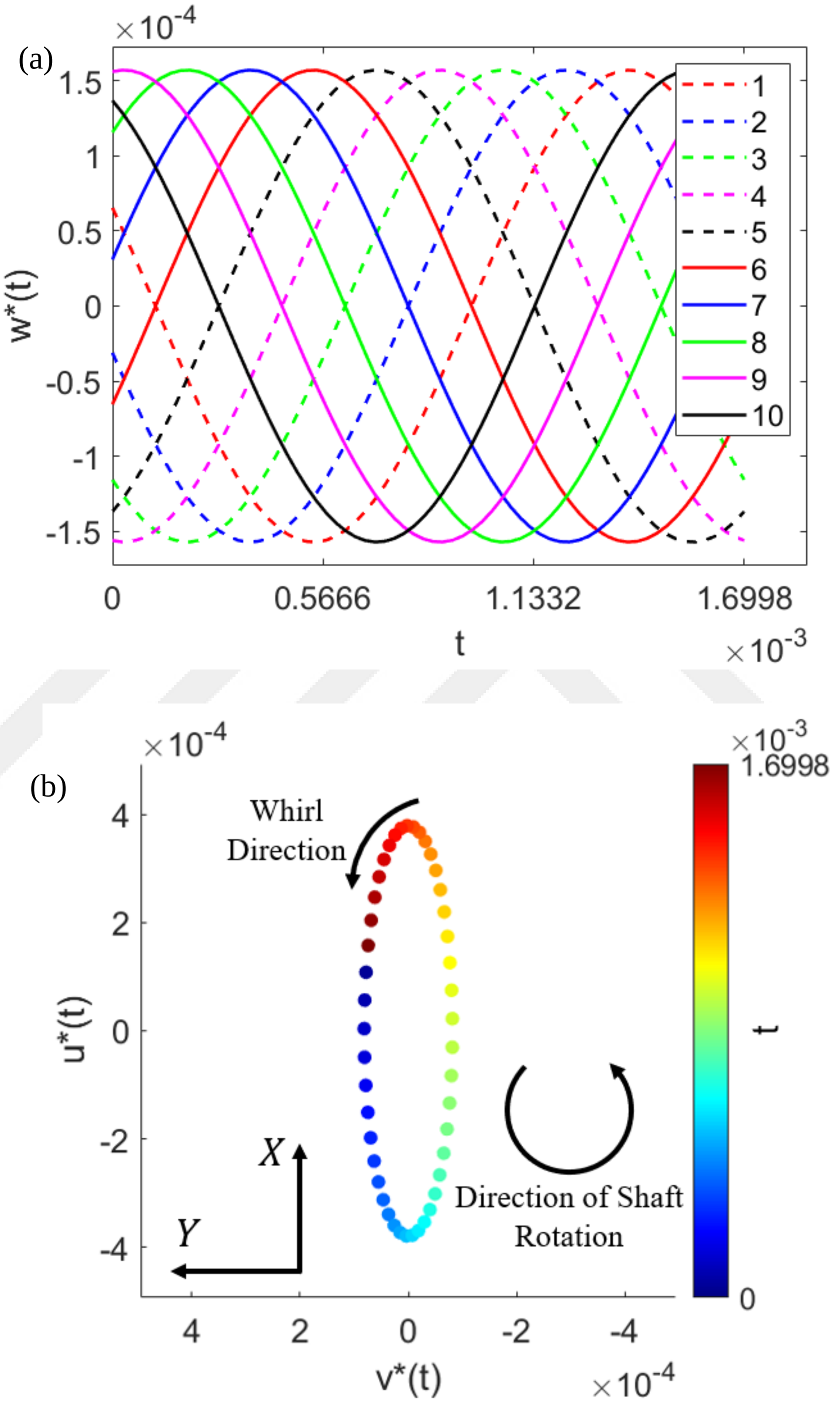

Figure 4.27 : Illustration of (a) backward travelling wave on the disc and (b) forward blade tip whirling in “ND1 + B1B” mode.

4.3.2 Flexible solid bladed disc

So far, systems modelled using beam elements have been presented. These models were substantially simplified models of rotating systems. However, in modern engineering applications, systems are much more complicated in terms of geometry. Thus, analysts refer to solid and shell elements for more accurate modelling. Popular FEM programs, such as ANSYS, are found to be satisfactorily capable of representing gyroscopic effects using solid elements [60]. Therefore, in the literature, it is possible to encounter studies [42,87] which are analysing complex rotating systems by FE programs using solid elements.

In this section, dynamics of a solid element model of a bladed disc is discussed. This way, it is aimed to (i) demonstrate that the gyroscopic effects can be included using the solid element with gyroscopic matrices developed in this study, and (ii) show how similarly a beam element model and a solid element model behave under rotational effects. The disc with bent blades and its mesh is shown in Figure 4.28. A similar model has been studied by Ruffini [43]. However, it must be stated at the outset that the beam element model presented in the previous section and solid elements model presented here are models for different bladed discs, hence quantitative comparisons are not aimed here.

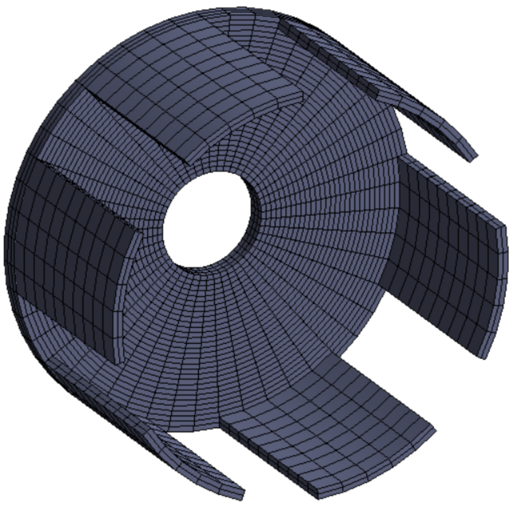

Figure 4.28 : Solid element model of the bent bladed disc (illustrated in ANSYS Workbench [88]).

The system is discretised using isoparametric hexahedral elements presented in Chapter 3. The same model is also generated in ANSYS Workbench with identical mesh properties (SOLID 185 with full integration) for verification purposes. The mesh is shown in Figure 4.28. Unfortunately, due to lack of computational capacity, mesh quality and convergence are overlooked. Nonetheless, similar results are expected since the same mesh is employed in ANSYS and in the program developed in this thesis. Additionally, the same model in nonrotating state is analysed in FINES [89]. The geometrical and material properties of the system are given in Table 4.9.

Table 4.9 : Material and geometric properties of the solid bladed disc.

Property	Value
Young's Modulus	210 GPa
Poisson's ratio	0.3
Density	7800 $^{kg}/_{m^3}$
Disc Outer Radius	0.1 m
Disc Inner Radius	0.025 m
Disc Thickness	0.01 m
Blade Length	0.1 m

First, the system is solved at 0 RPM at which the rotational effects are absent. The results from FINES and ANSYS along with the results of this study and the percentage errors between the present study and ANSYS are listed in Table 4.10. Some of these mode shapes are illustrated and can be compared with the mode shapes obtained from ANSYS in Figure 4.29.

Table 4.10 : Natural frequencies of the solid bladed disc model at rest.

Mode Number	Mode	Present Study (Hz)	FINES (Hz)	ANSYS (Hz)	Error-ANSYS (%)
1	B1B + (ND1)	504.48	504.48	484.32	4.16
2		504.48	504.48	484.32	4.16
3	B1B + (ND2)	509.96	509.96	496.82	2.64
4		509.96	509.96	496.82	2.64
5	ND0-U	544.73	544.73	521.95	4.36
6	B1B-P3	564.27	564.27	546.83	3.19
7	ND2 + B1B	875.76	875.76	859.08	1.94
8		875.76	875.76	859.08	1.94
9	ND3 + B1B	941.86	941.86	935.78	0.65
10	ND1 + B1B	943.60	943.60	909.30	3.77
11		943.60	943.60	909.30	3.77

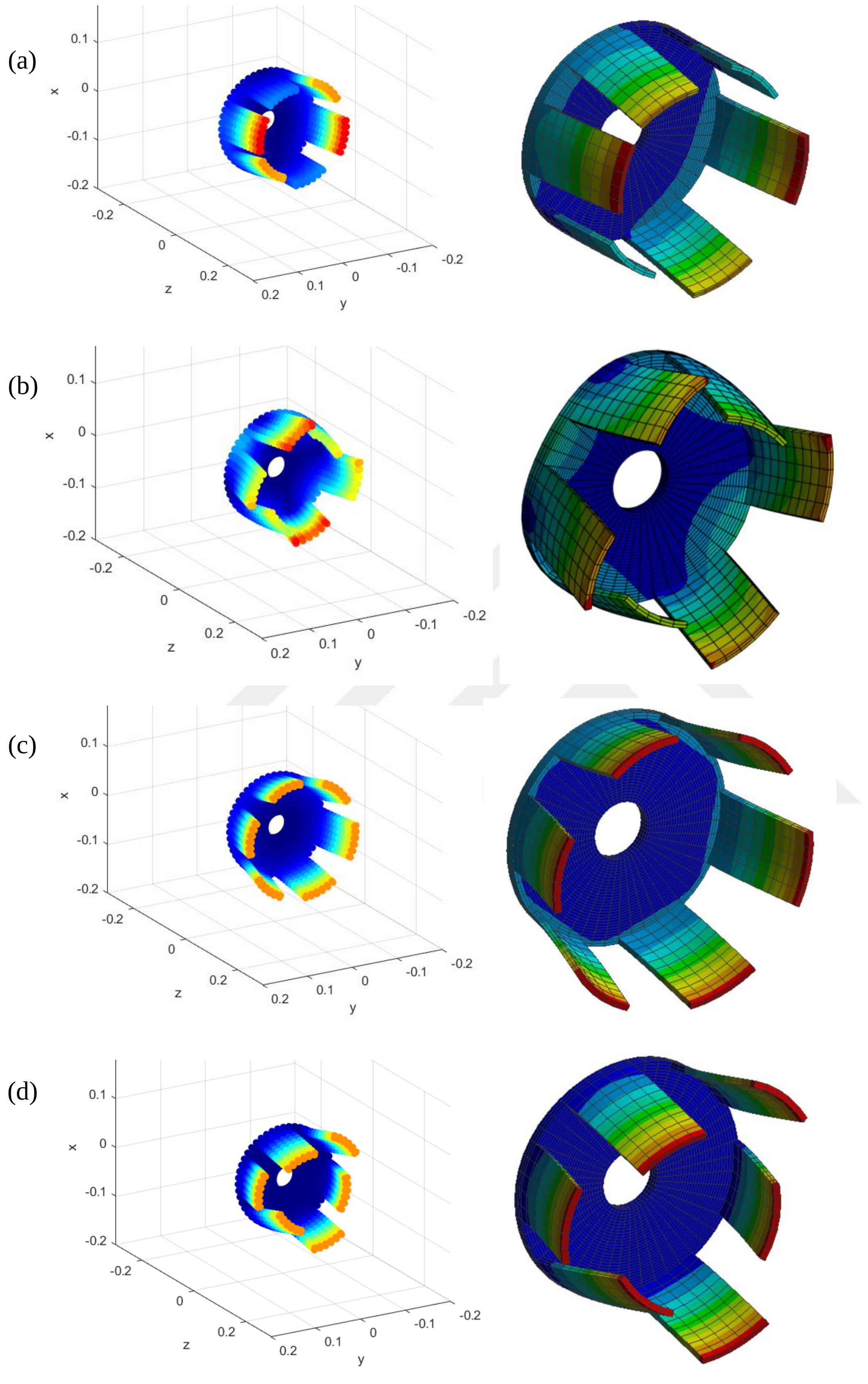

Figure 4.29 : Comparison of mode shapes (a) B1B + (ND1), (b) ND2 + B1B, (c) ND0-U, (d) B1B-P3 obtained in this study (left) and ANSYS (right).

In Table 4.10, although the percentage errors in all modes are less than 5%, they are still significantly high. Yet, present study shows a perfect agreement with FINES. This discrepancy can be explained by referring to the ANSYS documentation [90]. ANSYS employs a method called “B-bar method” to deal with volumetric locking. The reference [90] states that the average volumetric strain of the elements is substituted for the volumetric strain at the Gauss integration point. Therefore, this presents a more flexible hexahedral element in ANSYS than the standard 8-noded hexahedral element in this thesis.

Nevertheless, exploiting the rotor dynamics capability of ANSYS with solid element modelling, the same system is analysed at 5000 RPM in rotating reference frame. The frequency split percentage is utilised again to examine the capability of this study to model the gyroscopic effects by comparing it with the one computed from ANSYS. Results of the rotating system is given in Table 4.11 and the Campbell diagram of the present study in the speed range from 0 to 10000 RPM is given in Figure 4.30.

Table 4.11 : Predicted natural frequencies of the bladed disc using solid elements with gyroscopic capability.

Mode Number	Mode	Travelling Wave Direction	Rotational Speed (RPM)				Freq. Split at 5000 RPM (Present Study-%)	Freq. Split at 5000 RPM (Ansys-%)
			0		5000			
			Present Study (Hz)	Ansys (Hz)	Present Study (Hz)	Ansys (Hz)		
1	B1B + (ND1)	FW	504.48	484.32	470.60	450.27	6.72	7.03
2		BW	504.48	484.32	523.57	503.80	3.78	4.02
3	B1B + (ND2)	FW	509.96	496.82	459.98	448.04	9.80	9.82
4		BW	509.96	496.82	540.59	525.49	6.01	5.77
5	ND0-U	-	544.73	521.95	537.08	514.15	1.40	1.49
6	B1B-P3	-	564.27	546.83	547.68	530.46	2.94	2.99
7	ND2 + B1B	Mixed	875.76	859.08	835.29	821.01	4.62	4.43
8			875.76	859.08	929.69	911.67	6.16	6.12
9	ND3 + B1B	-	941.86	935.78	956.44	950.11	1.55	1.53
10	ND1 + B1B	Mixed	943.60	909.30	910.65	876.60	3.49	3.60
11			943.60	909.30	979.88	945.45	3.84	3.98

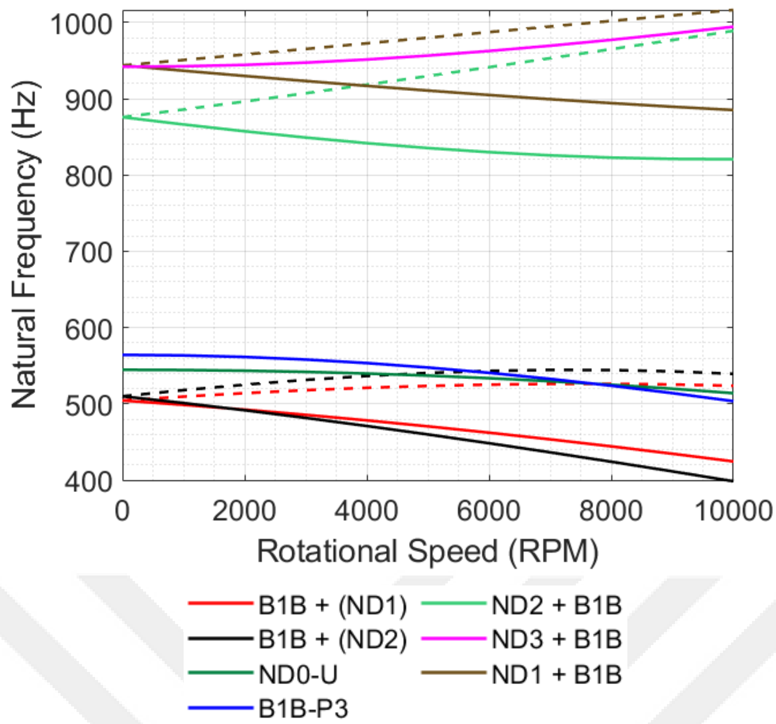

Figure 4.30 : Solid bladed disc system's Campbell diagram in rotating reference frame.

Naturally, since the problem is analysed in rotating reference frame, forward modes tend to decrease, and backward modes tend to increase from 0 to 5000 RPM. However, the Campbell diagram (Figure 4.30) reveals that for the first two mode pairs, the spin softening effect becomes dominant and starts to supress the gyroscopic effect at approximately 7000 RPM, thus backward modes begin to decrease as well. As it might be anticipated, these modes are blade bending dominated modes. At this point, a similarity can be established with the previous models. In the previous cases, it was noted that, the modes with significant blade vibration exhibited a strong softening with increasing rotational speed. This is clearly an indication of agreement between the dynamic behaviour of beam and solid element models. Meanwhile, bifurcation of the higher modes due to gyroscopic effect is evident due to the disc-blade coupling.

Regarding the mode shapes, besides the ND0 modes, owing to the existence of six identical blades, "ND3" modes appear to be single modes and do not exhibit travelling wave behaviour. Naturally, other modes exhibit the forward and backward whirling except the last two modes. Similar to the bladed disc model in the previous section, these modes do not have a certain whirl/travelling wave direction because of the opposite behaviour of the disc and the blades.

The frequency split percentages (Table 4.11) of present study and ANSYS are found to be satisfactorily close. Therefore, if one puts the apparent error between the natural frequencies of both models aside, the agreement of frequency split percentages between these models indicates the accuracy of modelling the gyroscopic effects on the solid bladed disc model presented in this study.

In the light of the results obtained in this chapter, unlike flexible shaft-rigid disc and flexible shaft-flexible disc systems, a bladed system, whether modelled with beam elements or solid elements, presents a nonlinear change of natural frequencies and nonidentical frequency splits of the double modes with the increase of rotational speed. This causes the bladed systems' natural frequencies to be unpredictable and the dynamic behaviour rather complicated especially when veering and instability is present. Therefore, it can be concluded that proper modelling, solutions at different rotational speeds, close examination of mode shapes and deep knowledge about rotor dynamics are required for such systems during analyses.

5. CONCLUSIONS AND SUGGESTIONS FOR FUTURE WORK

5.1 Conclusions

The main aim of this thesis was to include the gyroscopic effects in the models of rotating systems using FEM and investigate the gyroscopic effects on the dynamics of such systems. In the literature on rotor dynamics, it was seen that simpler structures, such as flexible shaft-rigid disc and rotating isolated blades, are discretised using finite beam elements. On the other hand, more complex systems, consisting of flexible discs and blades, are discretised using solid and shell elements. Obviously, using solid or shell elements increases the accuracy of the solutions of complex structures at the expense of more modelling effort and higher computational cost. In this study, besides the shaft and the blades, a disc model in the form of a spiderweb discretised using finite beam elements is proposed to investigate the gyroscopic effects in flexible shaft-disc-blade systems and analyse each flexible component's role in the dynamics of such systems. Using finite beam elements only, a cost-effective model of a simplified shaft-disc-blade system is obtained thanks to the relatively lower number of DOFs in the model. On the other hand, it is also aimed to form a basis for the development of additional capabilities in FEA programs to analyse non-axisymmetric rotating beam element models.

By comparing the traditional flexible shaft-rigid disc and flexible shaft-flexible spiderweb disc systems, the effect of disc's flexibility is investigated. These models showed that some modes of the flexible disc are likely to couple with shaft bending modes resulting in a different dynamic behaviour than that of flexible shaft-rigid disc system. It is seen that the disc flexibility introduces a rather complicated phenomenon called veering. The exchange of mode shapes and radical changes in frequency split percentages caused by the veering interaction emphasises the importance of disc flexibility. Also, the whirling behaviour which is a unique phenomenon of rotating shafts is investigated by illustrating the orbital displacement of the shaft in both forward and backward mode pairs. Unlike many studies in the literature, results are examined both in rotating and stationary reference frames in this thesis. In this way, the change of natural frequencies in both frames are explained by the virtue of establishing the relationship between gyroscopic moments and the Coriolis forces.

A fully flexible shaft-disc-blade system is assembled by adding blades that are oriented parallel to the shaft, but perpendicularly to the flexible disc. The reason for selecting such orientation for the blades instead of mounting them radially is to enhance the gyroscopic effect in rotating reference frame. Otherwise, as known in the literature, blades are known to be generating strong spin softening effects which may overshadow the gyroscopic effects. Due to the non-axisymmetrical geometry of the system, analyses are performed in rotating reference frame. The frequency splits caused by the gyroscopic effects, evident decreases of frequencies of blade dominated modes due to spin softening effect, mode shape exchanges due to veering and occurrence of merging type instability regions showed how complicated the dynamics of a rotating shaft-disc-blade system can get.

Since the disc modes with the number of NDs greater than one are not coupled with shaft bending, it is possible to see many studies focused on isolated bladed disc models. The same bladed disc structure in the previous cases apart from the shaft is dealt with to examine not only the frequency split characteristic but also peculiar results of the gyroscopic effects on a flexible disc in detail. Additionally, based on the finite solid element model presented in Chapter 3, a simplified bladed disc model is analysed to investigate the dynamics of a conventional bladed disc structure. The occurrence of travelling waves on the spiderweb disc, strong spin softening effect in blade-dominated modes and the enhancement of the gyroscopic frequency splits due to the coupled vibrations of both the disc and the blades confirmed the success of the developed model to accurately address the dynamics of such systems.

In accordance with the objectives of the thesis, Campbell diagrams, complex mode shapes and frequency split percentages are utilised to investigate the dynamics of different rotating structures under the influence of the gyroscopic effect. The investigations revealed that the simplified rotating systems discretised using finite beam elements presented in this study are capable of representing the gyroscopic effects generated by the Coriolis forces/gyroscopic moments on the dynamics of the system accurately. Besides achieving this main objective, the veering phenomena, merging type instability and the influence of spin softening effect are clearly observed using very cost-effective models and analyses. On the other hand, this study emphasised the high level of complexity of the dynamics of a rotating shaft-disc-blade system despite the simplified geometry and the discretisation using finite beam elements. This complexity manifests that the investigation of the dynamics of rotating structures under the gyroscopic influence requires serious caution and deep knowledge and experience about rotating body dynamics.

Finally, it is believed that this thesis can be a preliminary work for improving the rotor dynamic capabilities of FEA programs on rotating beam elements.

5.2 Suggestions for Future Work

Owing to the sophisticated nature of rotor dynamics, this study can be further improved. Suggestions for future work are as follows:

- It is known that damping in rotors is related to the stability of the rotating systems. However, since the aim was not to examine the stability, damping was ignored in this thesis. A model with damping can be studied to analyse the stability of rotating systems in details in the future.
- The centrifugal stiffening was excluded in order to avoid strong stiffening effects generated by the blades, which overshadows the gyroscopic effect. However, a model including this effect will be more realistic, hence worth understanding. Moreover, since the proposed disc model has also radial beam elements, an investigation seems to be necessary to determine if this spiderweb model is as accurate as a solid disc model in terms of representing the centrifugal stiffening effect.
- The spiderweb disc model proposed in this thesis may not be accurate enough to represent a flexible solid disc. A further study can be conducted to obtain an improved version of the proposed disc model that can more effectively simulate the free vibrational characteristics of solid discs.
- In this thesis, beam elements oriented in particular configurations are modelled and used in specific rotating systems A general beam element, arbitrarily oriented in space, including gyroscopic and spin softening effects, can be developed for general-purpose FEA programs for rotor dynamics applications.

REFERENCES

[1] **Rankine, W. M.** (1869). On the centrifugal force of rotating shafts. *Van Nostrand's Eclectic Engineering Magazine (1869-1879)*, *1*(7), 598.

[2] **Rao, J. S.** (2011). *History of rotating machinery dynamics* (Vol. 20). Springer Science & Business Media.

[3] **Tiwari, R.** (2017). *Rotor systems: analysis and identification*. CRC press.

[4] **Dunkerley, S.** (1894). VIII. On the whirling and vibration of shafts. *Philosophical Transactions of the Royal Society of London.(A.)*, (185), 279-360.

[5] **Ishida, Y., & Yamamoto, T.** (2012). *Linear And Nonlinear Rotordynamics: a modern treatment with applications*. Weinheim, Germany: Wiley-VCH Verlag & Co. KGaA.

[6] **Jeffcott, H. H.** (1919). XXVII. The lateral vibration of loaded shafts in the neighbourhood of a whirling speed. The effect of want of balance. *The London, Edinburgh, and Dublin Philosophical Magazine and Journal of Science*, *37*(219), 304-314.

[7] **Nelson, F. C.** (2007). Rotor dynamics without equations. *International Journal of COMADEM*, *10*(3), 2.

[8] **Kramer, E.** (1993). *Dynamics of Rotors and Foundations*. Springer-Verlag Berlin Heidelberg.

[9] **Genta, G.** (2005). *Dynamics of rotating systems*. Springer Science & Business Media.

[10] **Eshleman, R. L., & Eubanks, R. A.** (1967). On the critical speeds of a continuous shaft-disk system. *Journal of Manufacturing Science and Engineering, Transactions of the ASME*, *89*(4), 645–652. https://doi.org/10.1115/1.3610126

[11] **Eshleman, R. L., & Eubanks, R. A.** (1969). On the critical speeds of a continuous rotor. *Journal of Manufacturing Science and Engineering, Transactions of the ASME*, *91*(4), 1180–1188. https://doi.org/10.1115/1.3591768

[12] **Nelson, H. D., & McVaugh, J. M.** (1976). The Dynamics of Rotor-Bearing Systems Using Finite Elements. *Journal of Engineering for Industry*, *98*(2), 593–600. https://doi.org/10.1115/1.3438942

[13] **Zorzi, E. S., & Nelson, H. D.** (1977). Finite Element Simulation of Rotor-Bearing Systems with Internal Damping. *Journal of Engineering for Power*, *99*(1), 71–76. https://doi.org/10.1115/1.3446254

[14] **Nelson, H. D.** (1980). A finite rotating shaft element using Timoshenko beam theory. *Journal of Mechanical Design*, *102*(4), 793–803.

[15] **Özgüven, H. N., & Özkan, Z. L.** (1984). Whirl speeds and unbalance response of multibearing rotors using finite elements. *Journal of Vibration and Acoustics, Transactions of the ASME, 106*(1), 72–79. https://doi.org/10.1115/1.3269158

[16] **Gasch, R.** (1976). Vibration of large turbo-rotors in fluid-film bearings on an elastic foundation. *Journal of Sound and Vibration*, *47*(1), 53–73. https://doi.org/10.1016/0022-460X(76)90407-7

[17] **Sauer, G., & Wolf, M.** (1989). Finite element analysis of gyroscopic effects. *Finite Elements in Analysis and Design*, *5*(2), 131–140. https://doi.org/10.1016/0168-874X(89)90018-8

[18] **Yu, J., Craggs, A., & Mioduchowski, A.** (1999). Modelling of shaft orbiting with 3-D solid finite elements. *International Journal of Rotating Machinery*, *5*(1), 53–65. https://doi.org/10.1155/S1023621X99000056

[19] **Yu, J. J.** (1997). *Dynamic Analysis of Rotor-Bearing Systems Using Three-Dimensional Solid Finite Elements*. (PhD thesis). University of Alberta, Faculty of Graduate Studies and Research. https://doi.org/10.7939/R32R3P56M

[20] **Nandi, A., & Neogy, S.** (2001). Modelling of rotors with three-dimensional solid finite elements. *Journal of Strain Analysis for Engineering Design*, *36*(4), 359–371. https://doi.org/10.1243/0309324011514539

[21] **Loewy, R. G., & Khader, N.** (1984). Structural dynamics of rotating bladed-disk assemblies coupled with flexible shaft motions. *AIAA Journal*, *22*(9), 1319–1327. https://doi.org/10.2514/3.48567

[22] **Jacquet-Richardet, G., Ferraris, G., & Rieutord, P.** (1996). Frequencies and modes of rotating flexible bladed disc-shaft assemblies: A global cyclic symmetry approach. *Journal of Sound and Vibration*, *191*(5), 901–915. https://doi.org/10.1006/jsvi.1996.0162

[23] **Irretier, H., Jacquet-Richardet, G., & Reuter, F.** (1999). Numerical and Experimental Investigations of Coupling Effects in Anisotropic Elastic Rotors. *International Journal of Rotating Machinery*, *5*(4), 263–271.

[24] **Combescure, D., & Lazarus, A.** (2008). Refined finite element modelling for the vibration analysis of large rotating machines: Application to the gas turbine modular helium reactor power conversion unit. *Journal of Sound and Vibration*, *318*(4–5), 1262–1280. https://doi.org/10.1016/j.jsv.2008.04.025

[25] **Heydari, H., & Khorram, A.** (2019). Effects of location and aspect ratio of a flexible disk on natural frequencies and critical speeds of a rotating shaft-disk system. *International Journal of Mechanical Sciences*, *152*, 596–612. https://doi.org/10.1016/j.ijmecsci.2019.01.022

[26] **Zhao, S., Zhang, X., Zhang, S., Safaei, B., Qin, Z., & Chu, F.** (2022). A unified modeling approach for rotating flexible shaft-disk systems with general boundary and coupling conditions. *International Journal of Mechanical Sciences*, *218*, 107073. https://doi.org/10.1016/j.ijmecsci.2022.107073

[27] **Yokoyama, T.** (1988). Free vibration characteristics of rotating Timoshenko beams. *International Journal of Mechanical Sciences*, *30*(10), 743–755. https://doi.org/10.1016/0020-7403(88)90039-2

[28] **Bazoune, A., & Khulief, Y. A.** (1992). A finite beam element for vibration analysis of rotating tapered Timoshenko beams. *Journal of Sound and Vibration*, *156*(1), 141-164.

[29] **Yoo, H. H., & Shin, S. H.** (1998). Vibration analysis of rotating cantilever beams. *Journal of Sound and Vibration*, *212*(5), 807–828.

[30] **Lin, S. C., & Hsiao, K. M.** (2001). Vibration analysis of a rotating Timoshenko beam. *Journal of Sound and Vibration*, *240*(2), 303–322. https://doi.org/10.1006/jsvi.2000.3234

[31] **Chung, J., & Yoo, H. H.** (2002). Dynamic analysis of a rotating cantilever beam by using the finite element method. *Journal of Sound and Vibration*, *249*(1), 147–164. https://doi.org/10.1006/jsvi.2001.3856

[32] **Zohoor, H., & Kakavand, F.** (2012). Vibration of Euler-Bernoulli and Timoshenko beams in large overall motion on flying support using finite element method. *Scientia Iranica*, *19*(4), 1105–1116. https://doi.org/10.1016/j.scient.2012.06.019

[33] **Yang, X. D., Wang, S. W., Zhang, W., Yang, T. Z., & Lim, C. W.** (2018). Model formulation and modal analysis of a rotating elastic uniform Timoshenko beam with setting angle. *European Journal of Mechanics /A Solids*, *72*, 209–222. https://doi.org/10.1016/j.euromechsol.2018.05.014

[34] **Zeng, J., Ma, H., Yu, K., Xu, Z., & Wen, B.** (2019). Coupled flapwise-chordwise-axial-torsional dynamic responses of rotating pre-twisted and inclined cantilever beams subject to the base excitation. *Applied Mathematics and Mechanics (English Edition)*, *40*(8), 1053–1082. https://doi.org/10.1007/s10483-019-2506-6

[35] **Yang, X. D., Li, Z., Zhang, W., Yang, T. Z., & Lim, C. W.** (2019). On the gyroscopic and centrifugal effects in the free vibration of rotating beams. *Journal of Vibration and Control*, *25*(1), 219–227. https://doi.org/10.1177/1077546318774246

[36] **Chen, Y., Zhou, S., Cai, C., Wang, W., Hao, Y., Zhou, T., Wang X. & Li, Q.** (2023). Study on the Rotation Effect on the Modal Performance of Wind Turbine Blades. *Energies*, *16*(3). 1036. https://doi.org/10.3390/en16031036

[37] **Hsieh, S. H., & Abel, J. F.** (1995). Comparison of two finite element approaches for analysis of rotating bladed-disk assemblies. *Journal of Sound and Vibration*, *182*(1), 91–107. https://doi.org/10.1006/jsvi.1995.0184

[38] **Genta, G.** (2004). On the stability of rotating blade arrays. *Journal of Sound and Vibration*, *273*(4–5), 805–836. https://doi.org/10.1016/S0022-460X(03)00784-3

[39] **Nikolic, M., Petrov, E. P., & Ewins, D. J.** (2006). Coriolis forces in forced response analysis of mistuned bladed disks. *Journal of Turbomachinery*, *129*(4), 730–739. https://doi.org/10.1115/1.2720866

[40] **Nikolic, M.** (2006). *New Insights into the Blade Mistuning Problem.* (PhD thesis). Imperial College London.

[41] **Kan, X., & Xu, Z.** (2019). Vibration localization for a rotating mistuning bladed disk with the Coriolis effect by a state-space decoupling method. *Proceedings of the Institution of Mechanical Engineers, Part G: Journal of Aerospace Engineering*, *233*(3), 1011–1020. https://doi.org/10.1177/0954410017744238

[42] **Xin, J., & Wang, J.** (2011). Investigation of Coriolis effect on vibration characteristics of a realistic mistuned bladed disk. *Proceedings of ASME Turbo Expo 2011*, 993–1005.

[43] **Ruffini, V.** (2016). *Coriolis effects in bladed discs.* (PhD thesis). Imperial College London.

[44] **Huang, S. C., & Ho, K. B.** (1996). Coupled shaft-torsion and blade-bending vibrations of a rotating shaft-disk-blade unit. *Journal of Engineering for Gas Turbines and Power*, *118*(1), 100–106. https://doi.org/10.1115/1.2816524

[45] **Yang, C. H., & Huang, S. C.** (2005). The coupled vibration in a shaft-disk-blades system. *Journal of the Chinese Institute of Engineers*, *28*(1), 89–99. https://doi.org/10.1080/02533839.2005.9670975

[46] **Ma, H., Lu, Y., Wu, Z., Tai, X., Li, H., & Wen, B.** (2015). A new dynamic model of rotor-blade systems. *Journal of Sound and Vibration*, *357*, 168–194. https://doi.org/10.1016/j.jsv.2015.07.036

[47] **Chatelet, E., D'ambrosio, F., & Jacquet-Richardet, G.** (2005). Toward global modelling approaches for dynamic analyses of rotating assemblies of turbomachines. *Journal of Sound and Vibration*, *282*(1-2), 163-178.

[48] **She, H., Li, C., Tang, Q., & Wen, B.** (2018). The investigation of the coupled vibration in a flexible-disk blades system considering the influence of shaft bending vibration. *Mechanical Systems and Signal Processing*, *111*, 545–569. https://doi.org/10.1016/j.ymssp.2018.03.044

[49] **She, H., Li, C., Tang, Q., & Wen, B.** (2020). Effects of blade's interconnection on the modal characteristics of a shaft-disk-blade system. *Mechanical Systems and Signal Processing*, *146*. https://doi.org/10.1016/j.ymssp.2020.106955

[50] **Yang, L., Mao, Z., Chen, X., Yan, R., Xie, J., & Hu, H.** (2022). Dynamic coupling vibration of rotating shaft–disc–blade system — Modeling, mechanism analysis and numerical study. *Mechanism and Machine Theory*, *167*. https://doi.org/10.1016/j.mechmachtheory.2021.104542

[51] **Lesaffre, N., Sinou, J. J., & Thouverez, F.** (2007). Contact analysis of a flexible bladed-rotor. *European Journal of Mechanics, A/Solids*, *26*(3), 541–557. https://doi.org/10.1016/j.euromechsol.2006.11.002

[52] **Bucher I.** (2010). Rotor Dynamics toolbox (RotFE). Retrieved October 21, 2021. Available at https://www.mathworks.com/matlabcentral/fileexchange/28563-rotor-dynamics-toolbox-rotfe.

[53] **Meriam, J. L., & Kraige, L. G.** (2012). *Engineering mechanics: dynamics*. John Wiley & Sons.

[54] **Friswell, M. I., Penny, J. E., Garvey, S. D., & Lees, A. W.** (2010). *Dynamics of rotating machines*. Cambridge university press.

[55] **Vollan, A., & Komzsik, L.** (2012). *Computational techniques of rotor dynamics with the finite element method*. CRC Press.

[56] **Géradin, M., & Rixen, D. J.** (2014). *Mechanical vibrations: theory and application to structural dynamics*. John Wiley & Sons.

[57] **Marion, J. B.** (1965). Dynamics of Rigid Bodies. In *Classical Dynamics of Particles and Systems* (pp. 361–415). https://doi.org/10.1016/b978-1-4832-5676-4.50017-2

[58] **Price, R. H.** (2020). Gyroscopes simply explained with Coriolis pseudotorques. *American Journal of Physics*, *88*(12), 1145–1146. https://doi.org/10.1119/10.0002141

[59] **Ewins, D. J.** (2009). *Modal testing: theory, practice and application*. Research Studies Press.

[60] **Ruffini, V., Schwingshackl, C. W., & Green, J. S.** (2015). Prediction capabilities of Coriolis and gyroscopic effects in current finite element software. In *Proceedings of the 9th IFToMM International Conference on Rotor Dynamics* (pp. 1853-1862). Springer International Publishing.

[61] **Manconi, E., & Mace, B.** (2017). Veering and Strong Coupling Effects in Structural Dynamics. *Journal of Vibration and Acoustics*, *139*(2).

[62] **Jei, Y. G., & Lee, C. W.** (1990). Curve veering in the eigenvalue problem of rotor-bearing systems. *KSME Journal*, *4*, 128–135. https://doi.org/10.1007/BF02954034

[63] **Kenyon, J. A., Griffin, J. H., & Kim, N. E.** (2004). Sensitivity of tuned bladed disk response to frequency veering. In *Turbo Expo: Power for Land, Sea, and Air* (Vol. 41715, pp. 247-256).

[64] **Nguyen-Schäfer, H.** (2012). *Rotordynamics of Automotive Turbochargers*. Springer Berlin Heidelberg.

[65] **Lee, C. W., Jia, H. S., Kim, C. S., & Chun, S. B.** (1997). Tuning of simulated natural frequencies for a flexible shaft-multiple flexible disk system. *Journal of Sound and Vibration*, *207*(4), 435–451. https://doi.org/10.1006/jsvi.1997.1199

[66] **Rządkowski, R., & Drewczynski, M.** (2004). Natural frequencies and modes shapes of two mistuned bladed discs on the shaft. *Proceedings of the ASME Turbo Expo 2004*, *6*, 447–455. https://doi.org/10.1115/gt2004-54265

[67] **Rządkowski, R., & Drewczynski, M.** (2006). Forced vibration of several bladed discs on the shaft. *Proceedings of the ASME Turbo Expo 2006*, 789–800. https://doi.org/10.1115/GT2006-90158

[68] **Matsushita, O., Tanaka, M., Kanki, H., Kobayashi, M., & Keogh, P.** (2017). *Vibrations of rotating machinery*. Berlin: Springer.

[69] **Ehrich, F. F.** (1992). *Handbook of rotordynamics*. Krieger Publishing Company.

[70] **Kirchgäßner, B.** (2016). Finite elements in rotordynamics. *Procedia Engineering*, *144*, 736-750.

[71] **Geradin, M., & Kill, N.** (1984). A new approach to finite element modelling of flexible rotors. *Engineering Computations*, *1*(1), 52–64. https://doi.org/10.1108/eb023560

[72] **Logan, D. L.** (2017). *A First Course in the Finite Element Method* (6th ed.). Cengage Learning.

[73] **Schmiechen, P.** (1997). *Travelling Wave Speed Coincidence*. (PhD thesis). Imperial College London.

[74] **Kim, K. T.** (2015). Whirl speeds of mistuned bladed rotors supported by isotropic stator. *Journal of Sound and Vibration*, *357*, 409–426. https://doi.org/10.1016/j.jsv.2015.07.009

[75] **Hohlrieder, M., & Irretier, H.** (1997). Comparison of the rotor dynamic and structure dynamic calculation of compressors. *Journal of Engineering for Gas Turbines and Power*, *119*(2), 425–429. https://doi.org/10.1115/1.2815592

[76] **Petyt, M.** (1990). *Introduction to finite element vibration analysis*. Cambridge University Press.

[77] **Thomas, D. L., Wilson, J. M., & Wilson, R. R.** (1973). Timoshenko beam finite elements. *Journal of Sound and Vibration*, *31*(3), 315–330. https://doi.org/10.1016/S0022-460X(73)80276-7

[78] **Carrer, J. A. M., Mansur, W. J., Scuciato, R. F., & Fleischfresser, S. A.** (2014). Analysis of Euler-Bernoulli and Timoshenko beams by the boundary element method. *Proceedings of 10th World Congress on Computational Mechanics*, *1*(1), 2333–2349. https://doi.org/10.5151/meceng-wccm2012-18818

[79] **Timoshenko, S.** (1937). *Vibration problems in engineering* (2nd ed.). D. Van Nostrand Company, Inc

[80] **Kapur, K. K.** (1966). Vibrations of a Timoshenko Beam Using Finite-Element Approach. *The Journal of the Acoustical Society of America*, *40*(5), 1058–1063.

[81] **Bazoune, A., Khulief, Y. A., & Stephen, N. G.** (2003). Shape functions of three-dimensional Timoshenko beam element. *Journal of Sound and Vibration*, *259*(2), 473–480. https://doi.org/10.1006/jsvi.2002.5122

[82] **Greenwood, D. T.** (2006). *Advanced Dynamics*. New York: Cambridge University Press.

[83] **Hutton, D. V.** (2004). *Fundamentals of finite element analysis*. McGraw-Hill Science Engineering.

[84] **ABAQUS** (2014). Abaqus (Version 6.14) [Computer software]. Dassault Systèmes Simulia Corp.

[85] **Lee, C. W., Jia, H. S., Kim, C. S., & Chun, S. B.** (1997). Tuning of simulated natural frequencies for a flexible shaft-multiple flexible disk system.

Journal of Sound and Vibration, *207*(4), 435–451. https://doi.org/10.1006/jsvi.1997.1199

[86] **COMSOL** (2018), Rotordynamics Module User's Guide (Version 5.4) [Software user guide].

[87] **Kumar, D.** (2016). Rotordynamic Analysis Using 3D Elements in Fixed and Rotating. *International Mechanical Engineering Congress and Exposition*, 1–10.

[88] **ANSYS Inc.** (2022). Ansys Workbench (Version 2022 R2) [Computer software]. Ansys Inc.

[89] **Sanliturk, K.Y.** (2023). FINES: Finite element for structures [Computer software]. Istanbul Technical University Mechanical Engineering Department.

[90] **ANSYS Inc.** (2021). Element Reference (Version 2021 R2) [Software documentation].

CURRICULUM VITAE

Name Surname **:** Abdülsamet ERKAN

EDUCATION **:**

- **B.Sc.** **:** 2020, MEF University, Engineering Faculty, Mechanical Engineering Department

PROFESSIONAL EXPERIENCE AND REWARDS:

- September 2021- August 2022, MEF University, Teaching Assistant
- July 2020 - February 2021, Baykar Technologies, Mechanical Engineer

PUBLICATIONS, PRESENTATIONS AND PATENTS ON THE THESIS:

- **Erkan A.**, **Koruk H., Sanliturk K. Y.** 2022. Modelling and analysis of gyroscopic effects in rotating systems. *Proceedings of 4th International Conference on Applied Engineering and Natural Sciences*, November 10-13, 2022, Konya, Turkey